Programa de Doctorado en Biociencias Moleculares, Facultad Medicina.

Universidad Autónoma de Madrid

ROLE OF EMILIN1 DURING MELANOMA PROGRESSION AND LYMPH NODE PRE-METASTATIC NICHE FORMATION

Ana Isabel Amor López

Madrid, 2019

Role of EMILIN1 during melanoma progression and lymph node pre-metastatic niche formation

Doctoral Thesis submitted to the Universidad Autónoma de Madrid for the degree of Doctor of Philosophy by M.Sci. in Molecular Biomedicine,

Ana Isabel Amor López

Universidad Autónoma de Madrid,

Department of Biochemistry, Faculty of Medicine

Thesis Director

Héctor Peinado Selgas

Microenvironment and Metastasis Group,

Spanish National Cancer Research Centre (CNIO)

Madrid, 2019

Dr. Héctor Peinado Selgas, head of Microenvironment and Metastasis Group in the Spanish National Cancer Research Centre (CNIO)

CERTIFIES:

That Ms. Ana Isabel Amor López, Master in Neuroimaging from King´s College of London has completed her Doctoral Thesis **"Role of EMILIN1 during melanoma progression and lymph node pre-metastatic niche formation"** and meets the necessary requirements to obtain the PhD Degree in Molecular Biosciences. To this purpose, she will defend her Doctoral Thesis at the Universidad Autónoma de Madrid. The Doctoral Thesis has been carried out under my direction and hereby I authorize it to be defended to the appropriate Thesis Tribunal.

I hereby issue this certificate in Madrid, on 23th of October 2019.

Héctor Peinado Selgas

PhD Thesis Director

cnio stop cancer

This Thesis, submitted for degree of Doctor of Philosophy at the Universidad Autónoma de Madrid, has been completed in the Microenvironment and Metastasis Laboratory at the Spanish National Cancer Research Centre (CNIO), under the supervision of Dr. Héctor Peinado Selgas.

This work was supported by the following grants and fellowships:

- Beca Excelencia Severo Ochoa PhD Fellowship, 2014 call- Ana Isabel Amor López. Ministerio de Ciencia, Innovación y Universidades.
- Proyecto GRUPOS COORDINADOS ESTABLES DE INVESTIGACIÓN, Asociación Española contra el cáncer (AECC). SAF2014 54541-R. MINECO

A mi familia

SUMMARY

It has been described that melanoma-derived exosomes have a role in lymph node metastasis reinforcing lymphangiogenesis and extracellular matrix remodeling. Several studies have demonstrated that melanoma-derived exosomes home in sentinel lymph nodes promoting gene expression changes that favor metastasis. Recent data from our laboratory support a role for melanoma-derived exosomes in establishing the lymph node pre-metastatic niche formation due to specific cargo. In this thesis, we postulated that lymph node microenvironment acts as a selective pressure selecting specific phenotypes for metastasis. As such, we wanted to analyze if lymph node metastatic melanoma cells present a specific signature that may favor their survival in lymph nodes. In our analysis, we have found a specific signature of genes over-expressed and proteins hyper-secreted in exosomes from a mouse melanoma lymph node metastatic model. Out of these candidates, EMILIN1 was selected due to its relevance in lymphatic vessel functionality. We have found that EMILIN1 impacts negatively on cell proliferation and migration of melanoma cells. Overall, our data support that EMILIN1 acts as a *tumour suppressor-like* protein both intrinsically and extrinsically and its function is inactivated by its degradation and secretion in exosomes. Importantly, our *in vivo* studies demonstrate that its overexpression reduced primary tumour growth and metastasis in mouse melanoma models. Analysis in human melanoma showed that its expression is maintained along melanoma progression but cells expressing high levels of EMILIN1 are reduced in metastatic lesions. Overall, our analysis suggests a novel mechanism involved in the inactivation of EMILIN1 in melanoma favouring tumour progression.

RESUMEN

Se ha descrito que los exosomas derivados del melanoma tienen un papel en la metástasis a los ganglios linfáticos, reforzando tanto la linfangiogénesis como la remodelación de la matriz extracelular. Varios estudios han demostrado que los exosomas de melanoma anidan en los ganglios linfáticos centinelas, promoviendo cambios en la expresión génica favoreciendo la metástasis del melanoma. Datos recientes obtenidos en nuestro laboratorio, respaldan que los exosomas derivados de células de melanoma participan activamente en la formación del nicho pre-metastásico en los ganglios linfáticos debido a una firma molecular específica. En esta tesis, postulamos que el microambiente de los ganglios linfáticos actúa como una presión selectiva, que selecciona fenotipos específicos que están favorecidos para metastatizar eficientemente. Por ello, en esta tesis hemos analizado si células de melanoma murino derivadas de metástasis en los ganglios linfáticos, presentan una firma molecular específica que favorece su metástasis. En nuestro análisis hemos seleccionado genes sobre-expresados y proteínas hiper-secretadas en un modelo derivado de metástasis a ganglios linfáticos. De estos candidatos, se seleccionó EMILIN1 debido a su relevancia en la funcionalidad de los vasos linfáticos. En nuestros estudios, hemos podido ver que EMILIN1 reduce la proliferación celular y la migración de células de melanoma. En resumen, nuestros datos respaldan que EMILIN1 actúa como una proteína con propiedades similares a los supresores tumorales, tanto intrínseca como extrínsecamente, y su función se inactiva por su degradación y secreción en los exosomas. Es importante destacar que nuestros estudios *in vivo* demuestran que su sobre-expresión conduce tanto a una reducción del tamaño tumoral como de la metástasis. El análisis inmunohistoquímico llevado a cabo en muestras de pacientes de melanoma, mostró que su expresión se mantiene a lo largo de la progresión del melanoma, pero las células que expresan altos niveles de EMILIN1 se reducen en las lesiones metastásicas. En general, nuestro estudio demuestra un nuevo mecanismo implicado en la inactivación de EMILIN1 en el melanoma que favorece la progresión tumoral.

INDEX

Index

ABBREVIATIONS

Agrn	Agrin
Akt	Alpha serine/threonine-protein kinase
ATP	Adenosine triphosphate
BMDC	Bone marrow-derived cells
BRAF	B-Raf Proto-Oncogene
Bv8	Prokineticin-2
CD169	Sialic acid binding Ig like lectin 1
CD31	Platelet and endothelial cell adhesion molecule
Cd37	Cell differentiation antigen 37
CD44	CD44 molecule (Indian blood group)
Cdh17	Cadherin-17
cDNA	Complementary deoxyribonucleic acid
Col5a1	Collagen type V alpha 1 chain
CSD	Chronically sun-damaged
CTCs	Circulating tumor cells
Cx	Connexin
CXCL1	C-X-C Motif chemokine ligand 1
CXCR2	C-X-C Motif chemokine Receptor 2
DMSO	Dimethyl sulfoxide
DNA	Deoxyribonucleic acid
E1-E933A	Emilin1 mutant E993A
E1-R914W	Emilin1 mutant R914W
EC	Endothelial cell
ECM	Extracellular matrix
Edu	5-ethynyl-2′-deoxyuridine
EMI	EMI domain
EMILIN1	Elastin microfibril interface-located protein 1
EMILIN2	Elastin microfibril interface-located protein 2
Erk1/2	Extracellular signal-regulated protein kinases 1 and 2
EV	Extracellular vesicle
FDR	False discovery rate
FN	Fibronectin
gC1q	Binding protein domain
GSEA	Gene Set Enrichment Analysis
GW4869	N N,N′-Bis[4-(4,5-dihydro-1H-imidazol-2-yl)phenyl]-3,3′-p-phenylene-bis-acrylamide dihydrochloride
HMB45	Mouse Monoclonal antibody against melanoma glycoprotein 100
Hspg2	Heparan Sulfate Proteoglycan 2
Icam2	Intercellular adhesion molecule 2
ITGA2B	Integrin alpha2 beta
IVIS	In Vivo Imaging spectrum
KEEG	Kyoto Encyclopedia of Genes and Genomes
KIT	c-kit proto-oncogene
KO	Knock out
LEC	Lymphatic endothelial cell

LN	Lymph node
LOX	Lyxil oxidase
Lyve-1	Lymphatic vessel endothelial hyaluronan receptor 1
MC1R	Melanocortin 1 receptor
MDK	Midkine
MDSC	Myeloid-derived suppressor cells
MET	MET proto-oncogene
MG-132	Proteasome inhibitor
miR	MicroRNA
MMP	Matrix metallopeptidases
MMP2	Matrix metallopeptidases2
MMP9	Matrix metallopeptidases9
MMRN2	Multimerin 2
mRNA	Messenger RNA
MVB	Multivesicular body
NE	Neutrophil elastase
NF1	Neurofibromatosis-1
Nid1	Nidogen 1
Nid2	Nidogen 2
NIR815	Near-infrared fluorescent cell labelling reagent
NRAS	NRAS proto-oncogen
NRP1	Neuropilin 1
NSCLC	Non-small-cell lung carcinoma
PBS	Phosphate-buffered saline
PCA	Principal component analysis
PG	PROTEOGLYCAN
PI	Propidium
PI3K	Phosphoinositide 3-kinases
PIGF	Placental-derived Growth Factor
PMN	Pre-metastatic niche
PTEN	Phosphatase and tensin homolog
PVDF	Polyvinylidene difluoride
qPCR	Puantitative polymerase chain reaction
RNA	Ribonucleic acid
S100A8	S100 calcium-binding protein A8
S100A9	S100 calcium-binding protein A9
SCS	Lymph node subcapsular sinus
SDF-1	Stromal cell-derived factor 1
SEMA3A	Semaphorin-3A
Slc40a1	Solute Carrier Family 40 Member 1
sLN	Sentinel lymph node
TCGA	The Cancer Genome Atlas
TGF-β1	Transforming growth factor beta 1
TGFBR2	Transforming growth factor receptor 2
TIMP-1	Tissue inhibitor of Metallopeptidase 1
TLR3	Toll-like receptor 3
TMA	Tissue microarray

TNC	Tenascin C
TNF	Tumour necrosis factor
TNFα	Tumour necrosis factor alpha
uPA	Urokinase-type plasminogen activator
UV-R	Ultraviolet radiation
VCAM-1	Vascular cell adhesion molecule 1
VEGF	Vascular endothelial growth factor
VEGFR-1	Vascular endothelial growth receptor 1
WT	Wild type
αMSH	α-Melanocyte stimulating hormone

1. INTRODUCTION

1.1. The term “metastasis”

Metastasis is a significant contributor to morbidity and mortality among cancer patients. For over a century, cancer biologists have intensely explored the mechanisms underlying the emergence and spread of tumor cells, but how cancer cells acquire the competence to colonize distant organs remains as a central question in cancer biology. The most remarkable fact about this process is that a minority of cells from the primary tumour are able to infiltrate and survive in distant organs.

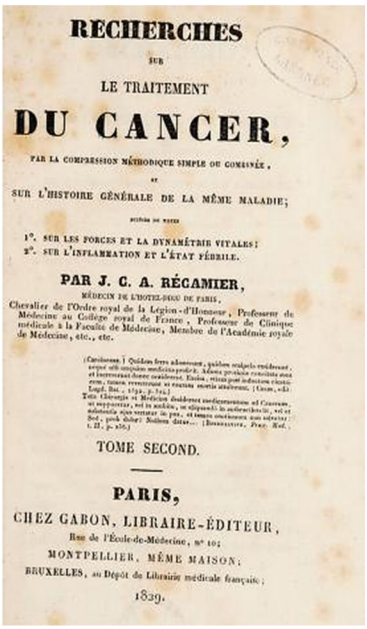
RECHERCHES
SUR
LE TRAITEMENT
DU CANCER,
PAR LA COMPRESSION MÉTHODIQUE SIMPLE OU COMBINÉE,
ET
SUR L'HISTOIRE GÉNÉRALE DE LA MÊME MALADIE;
1°. SUR LES FORCES ET LA DYNAMÉTRIE VITALES;
2°. SUR L'INFLAMMATION ET L'ÉTAT FÉBRILE.
PAR J. C. A. RÉCAMIER,
MÉDECIN DE L'HOTEL-DIEU DE PARIS,
TOME SECOND.
PARIS,
CHEZ GABON, LIBRAIRE-ÉDITEUR,
MONTPELLIER, MÊME MAISON;
BRUXELLES, au Dépôt de Librairie médicale française;
1829.

The term “metastasis” was originally coined in 1829 by ***Jean Claude Recamier*** in an important historical work called *“Recherches sur le Traitement du Cancer, Vol. 1: Par la Compression Méthodique Simple ou Combinée, Et sur l'Histoire Générale de la Même Maladie”.* Récamier’s book was one of the earliest medical texts on oncology and his discussion of cancer concludes with this statement: “***I will be happy if my work, imperfect as it is, may aid only one other observer, to discover the best way to cure the appalling disease which has been my particular concern for many years.”*** Despite recognizing the devastating consequences of metastasis from so long and knowing the low possibilities of this process to success, we are not yet able to effectively treat cancer that has spread to vital organs.

The pathogenesis of metastasis is the end result of a series of stochastic events that first allow cancer cells to spread out and survive in distant sites and later to grow as secondary tumours [1] . A continuous evolution of tumour cell phenotype and the heterogeneity across cancer types and patients are important factors to bear in mind in the pathogenesis of metastasis [2, 3].

1.1.1. Main steps involved in metastasis

Metastasis is a complex process that has been categorized into different biological mechanisms for its better understanding. This stepwise classification has helped researchers to identify and target the different steps involved in metastasis at different points [4] .

The first step is tumour cell invasion, understood as the migration of individual cells that detach from the primary tumour; this process involves changes in both intrinsic and extrinsic mechanisms such as remodelling of the surrounding stroma with the participation of extracellular proteases, etc. [5]. Next, tumour cells intravasate into the lymphatic and hematogenous vasculature by an active process where different cells and molecular factors are involved [6-8]. Multiple factors extrinsic and intrinsic to tumour cells (including epithelial-to-mesenchymal transition, production of proteases and migratory capacity) are involved in these two first steps. Of note, most tumour cells that enter the vasculature die as a result of hydrodynamic physical damage or leukocyte attack [9]. As a consequence, several mechanisms have been identified to promote tumour cell survival in the circulation. For example, tumour-platelet interaction has been described as a mechanism favouring homing and survival in secondary sites [10] **(Fig.1)**. The next steps are the extravasation and homing of newly arrived tumour cells in metastatic organs **(Fig.1).**

Metastasis is currently considered as a "selective" process where tumour cell interactions with metastatic organs are considered crucial for it success [11]. In 1889, the English surgeon, ***Stephen Paget*** postulated a hypothesis to understand metastatic organotropism: ***"What is that decides what organs shall suffer in the case of disseminated cancer?"***, also known as ***"The seed and soil"*** hypothesis. He postulated that metastasis is dependent on the interactions between "seeds", (the cancer cells), and the "soil" (the host microenvironment) [12] **(Fig.1)**. Later in 1928***, James Ewing*** *postulated* that cancer cells were directed to that site by the direction of lymphatic and circulatory systems [3]. In the late 1970s and early 1980s, studies by **Isaiah Fidler** and co-workers conclusively demonstrated that, although tumour cells traffic through the vasculature of all organs, metastases selectively develop in congenial organs [13].

Nowadays, the most accepted model is that although the mechanical properties of blood flow were important, successful metastatic colonization occurs at certain organ sites more efficiently than in others **(Fig.1).** Even if we are more than a 100 years apart of the first observation by Dr. Paget, our knowledge of how metastasis is driven is still a matter of study.

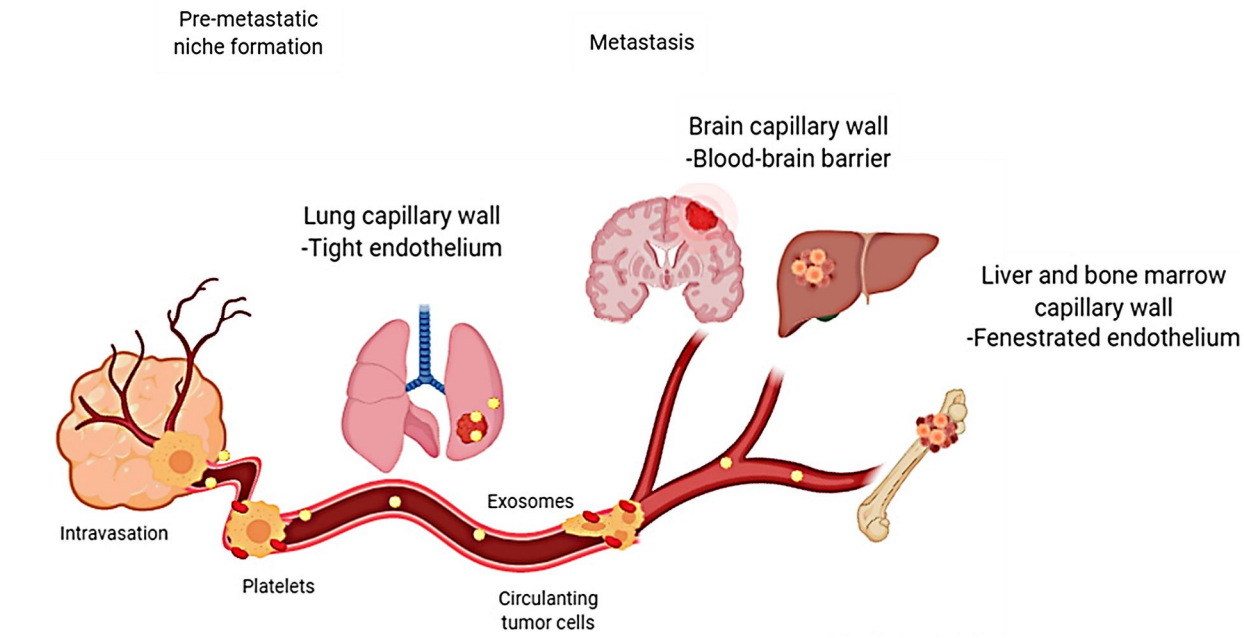

Fig.1 "The seed and soil" hypothesis. Metastasis is dependent on the interactions between tumour cells (seeds), and the host microenvironment (soil). Primary tumour-secreted factors promote tumour formation and formation of pre-metastatic niches, once cells leave the primary tumour home in metastatic organs more favorable for metastasis (e.g. lung, liver, brain, bone marrow). While distal organs such as the brain are more difficult to penetrate, due to the blood brain barrier, other organs such as bones and liver present fenestrated capillaries permissive to tumour cell homing and metastasis [11].

1.2. Pre-metastatic niche concept

Historically, primary tumours have been the main focus of analysis by cancer researchers. However, the complex interaction that exists between tumour cells with the surrounding non-malignant cells and the extracellular matrix (ECM) is an active and constant event. Indeed, the tumour microenvironment has been found to have an active role in the regulation of malignant cell behaviour [4] . In this context, malignant cancer cells gradually acquire mutations in oncogenes or tumour suppressor genes that confer the ability to egress from the tissue of origin, survive in the haematogenous or lymphatic circulation, and survive at distant sites. Metastatic organs have characteristics that allow the metastatic cell to adhere, proliferate and survive, whereas other microenvironments would be considered as "hostile".

Fundamental discoveries by Dr. Lyden and colleagues have revealed that tumours induce the formation of microenvironments at distant organs that are conducive to the survival and outgrowth of tumour cells prior to their arrival at these sites. These microenvironments were termed "pre metastatic niches" (PMNs) [14-16]. This unique concept proposes the ability of primary tumour cells to pre-condition for future metastatic disease before the arrival of circulating tumour cells

(CTCs) *via* tumour-derived factors. Therefore, PMN represents an abnormal and favourable microenvironment for metastasis [14] .

1.2.1. Pre-metastatic niche formation

Many factors are involved in the PMN formation, for example secretion of soluble factors by the primary tumour, such as VEGF-A, TNFα, and TGFβ, induces the expression of the inflammatory chemo-attractants S100A8 and S100A9 [17]. Similarly, bone marrow-derived cells (BMDCs) expressing the vascular endothelial growth factor receptor 1 (VEGFR-1) precede to the arrival of metastatic tumour cells and macrometastatic disease at distant sites [15]. More recently, it has been found that proteins involved in ECM remodelling such as the lysyl oxidase (LOX) are also involved in the formation of PMNs [18]. Moreover, in colorectal cancer it has been described the first evidence about primary malignant cell-secreted VEGF-A stimulates tumour-associated macrophages to produce CXCL1, which recruits CXCR2-positive myeloid-derived suppressor cells (MDSCs) to form a PMN to promote liver metastases [19] **(Fig.2)**.

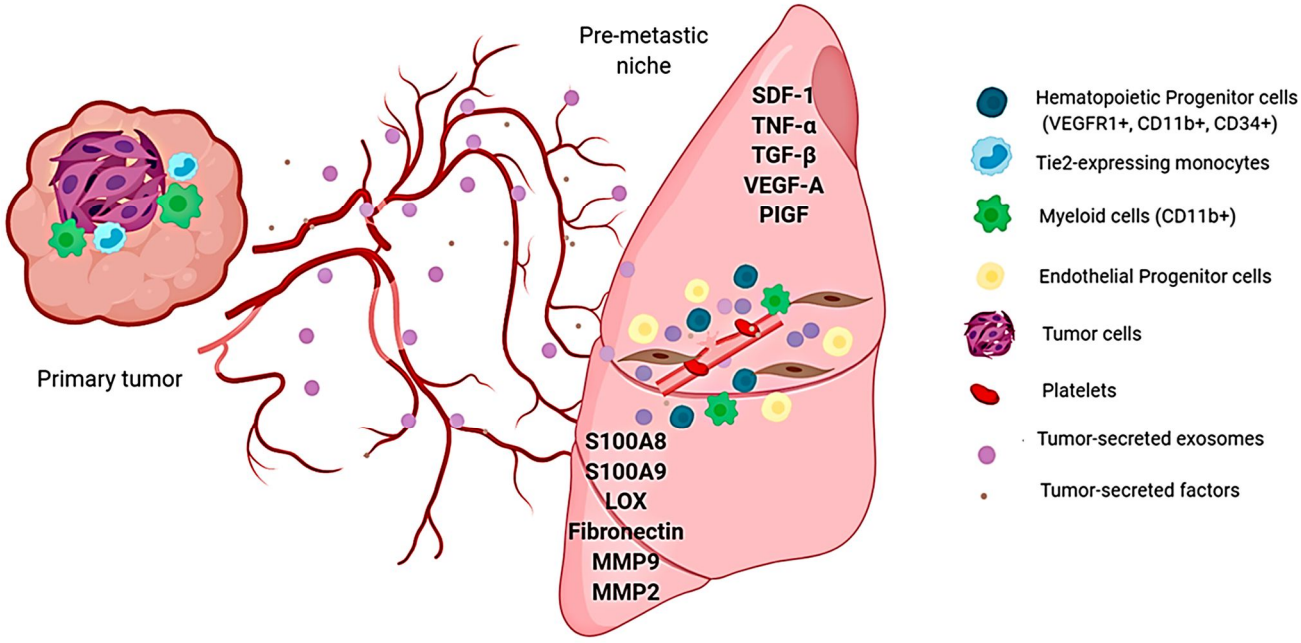

Fig.2 Setting a fertile soil: The pre-metastatic niche and the main secreted factors and cells populations involved in. Tumour-secreted factors such as SDF-1, TNF-α, TGF-β, VEGF-A, and PIGF have been involved in the recruitment of different cell types to pre-metastatic sites upregulating the expression of specific molecules as S100A8, S100A9, LOX, fibronectin, MMP9, MMP2. Then, these molecules promote the recruitment of specific bone marrow-derived cells involved in pre-metastatic niche formation such as hematopoietic progenitor and myeloid cells. Platelets also help to pre-metastatic niche formation by secretion of pro-angiogenic and extracellular matrix-remodelling factors [16]. The release of extracellular vesicles (EVs), has recently become a subject of increasing interest during PMN formation [14, 23]

Another hallmark in cancer is the result of an increased glucose metabolism [20]. A recent study has found that high *miR-122* levels in the circulation have been associated with metastasis in breast cancer patients, and they demonstrate that cancer-cell-secreted *miR-122* facilitates metastasis by increasing nutrient availability in the PMN [20]. Also, it has been described a new role for perivascular cells in PMN formation. Perivascular phenotypic switch has been studied in inflammation and vascular diseases [21] but very recently it has been determine how the disruption of perivascular-cell-specific Klf4 expression inhibited perivascular phenotypic switching which contribute to fibronectin protein production that promoted tumour cell metastatic behaviour and decreased metastasis of melanoma (B16-F10 cell line) or metastatic rhabdomyosarcoma (M3-9M cell line) models [22]. A novel cell-cell communication mechanism, the release of extracellular vesicles (EVs), has recently become a subject of increasing interest during PMN formation [14, 23] **(Fig.2).**

1.3. Involvement of extracellular vesicles in metastasis

In the 1980s, exosomes (a subtype of EV) were described as vesicles of endosomal origin secreted from reticulocytes. However, the interest around EVs has increased during the last years due to their participation in several cellular processes [24] **(Fig.3)**.

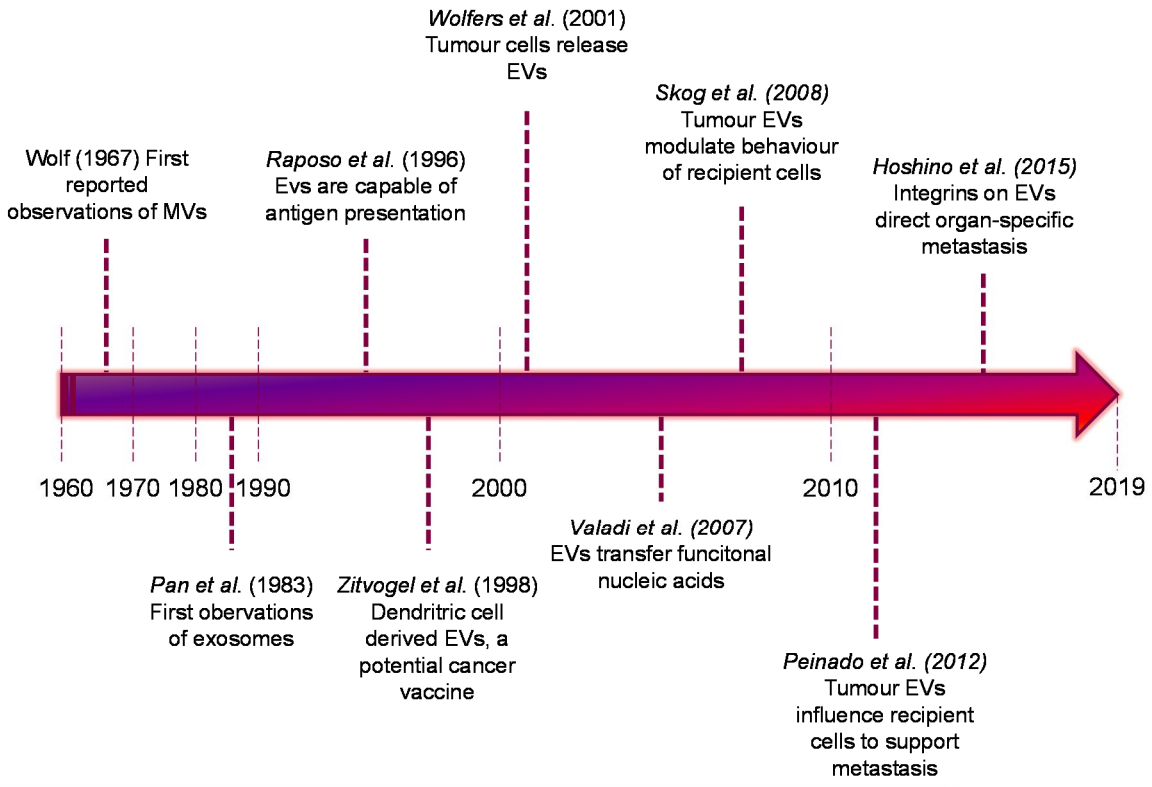

Fig.3 Timeline of key discoveries in extracellular vesicle research. Several key works have highlighted the role of tumour-derived EVs in promoting cancer growth and metastasis and their potential utility as biomarkers [24].

EVs are composed of a lipid bilayer that contains molecular cargo representative from the cell of origin (e.g. proteins, RNA, DNA, etc…) [23]. EVs have been shown to regulate the physiology of neighboring recipient cells by several mechanisms, from inducing intracellular signaling following binding to receptors, to conferring new properties after the acquisition of new receptors, enzymes or even genetic material from the vesicles [25]. So far, the main types of EVs are microvesicles and exosomes [25]. Microvesicles represent a heterogeneous population of EVs (<1000 nm), which are secreted by blebbing from the cell membrane after activation by different stimuli [25] . Exosomes are smaller membrane vesicles (30-100 nm) derived from the luminal membranes of multivesicular bodies that are secreted by cells through fusion of the MVB with the cell membrane [25, 26]. It has been shown that tumor cells secrete large amounts of EVs not only in the surrounding microenvironment, but also, and perhaps more importantly, in the blood stream [25]. Exosomes serve as a vehicle for horizontal transfer of molecules such as RNAs, DNA and proteins which, once in the target cell, can exert their function [23]. Therefore, EVs can be considered as a cell-cell communication system that horizontally transfers information between cells [25, 27, 28] **(Fig.4).**

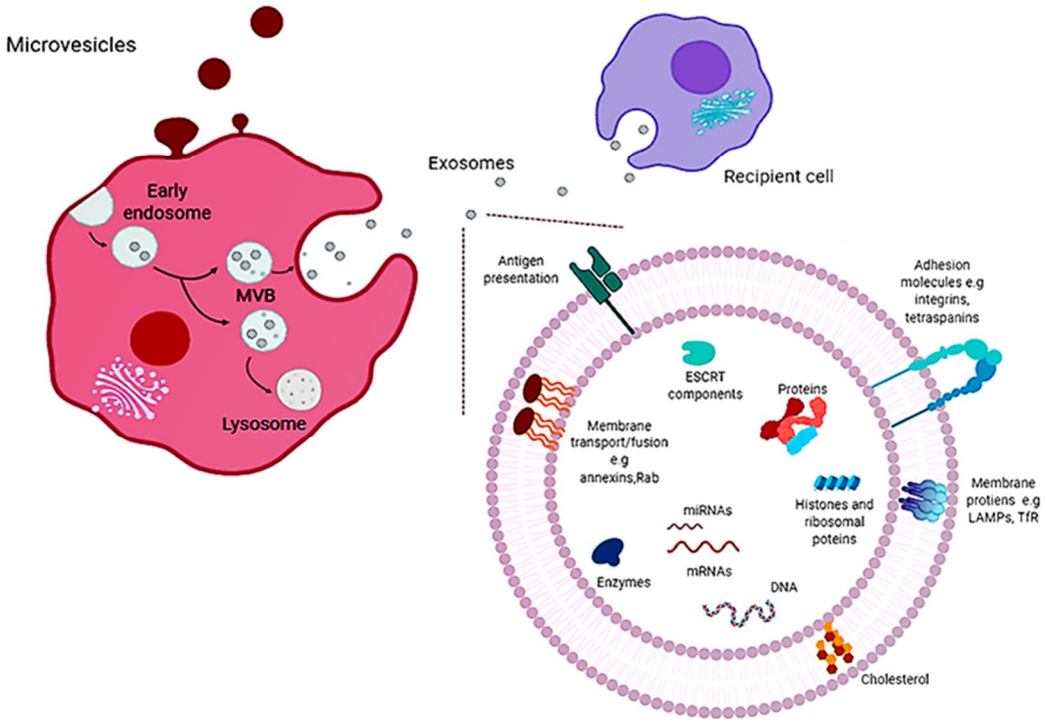

Fig.4 Exosome biogenesis and composition. Schematic representation of the different types of extracellular vesicles released by cells, either by direct budding from the plasma membrane (microvesicles) or by fusion of the multivesicular bodies (MVB) with the plasma membrane (exosomes) [23,26].

1.3.1. Exosomes in PMN initiation and evolution

2009 was the year when the role of tumor-secreted factors and EVs in PMN initiation started to have recognition [29]. It was published that the combined effects of soluble factors and exosomes derived from CD44 variant isoform (CD44v)-positive pancreatic cancer cells mediated the formation of a PMN in lymph nodes and lungs [29]. More recently, it has been shown that tumor-secreted exosomes play a crucial role in the PMN formation in the lung and horizontal transfer of molecules between tumor cells and bone marrow progenitors, resulting in increased metastasis [30]. This process was defined as "education"; involving the release of tumour-derived cargo (specifically, the oncoprotein c-MET) in exosomes that promote systemic changes in the host favoring PMN formation and metastasis [30]. Latterly, tumour-secreted exosomes have been shown to promote the PMN in distal organs including pancreatic and breast cancer favoring metastasis [31-33]. Importantly, exosome proteomics revealed that integrins expressed in tumour-derived exosomes are involved in the metastatic organotropism of breast and pancreatic cancer by helping exosome homing in distal sites and preparing PMN in specific organs. Exosomal α6β4 and α6β1 integrins have been associated with lung metastasis, while exosomal integrin αvβ5 was linked to liver metastasis. Targeting β4 and β5 integrins decreased tumour exosome uptake in distal organs, as well as lung and liver metastasis, respectively. These authors showed that analysis of these integrins in plasma could help to predict organ-specific metastasis [32].

1.3.2. Exosomes in lymph node metastasis

Adjacent lymph nodes (LNs) to the primary tumor are often the first site of metastasis (termed as sentinel lymph nodes) [34]. LN metastases have been intensively studied in the last years finding that carcinomas and melanomas tend to metastasize more frequently in LNs than sarcomas for example [8, 35, 36]. Although LN metastases are themselves rarely life threatening, they could be considered as the first step of metastasis in many cancer types and are associated with poor prognosis in cancer patients [36, 37]. It has been also proposed that LN metastases can be a source of cancer cells for distant metastases [38, 39]. Therefore, defining the mechanisms involved in LN metastasis and PMN formation could bring the clue to block the metastatic process from the beginning.

Since EVs mimic features of their tumours of origin and their size is within the range for lymphatic transport, their participation in lymphatic pathways to settle PMN at both local (LNs) or a distal sites have been analysed in the past years [40]. Moreover, the knowledge about their presence in different body fluids, including blood, urine, saliva, breast milk, semen and cerebrospinal fluid and

the techniques of their isolation [26], have been critical for the use as a diagnostic and prognostic tool in melanoma progression.

It has been described that exosomes derived from melanoma cells have a role in preparing the LNs supporting processes such as lymphangiogenesis, ECM remodeling or immunosuppression [41, 42] **(Fig.5)**. *In vivo* studies showed that homing of melanoma-derived exosomes to sentinel LNs reinforce melanoma cell recruitment, ECM deposition, and lymph(angio)genesis in the LNs [41]. These changes facilitate tumor cell homing and metastases in LNs [41, 42]. However, the molecular mechanisms underlying are far for being totally uncovered. Recent data from our laboratory support that specific factors secreted in melanoma-derived exosomes are transferred and influenced lymphangiogenesis in lymphatic endothelial cells (LECs) preparing PMN formation in LNs reinforcing metastasis (Garcia-Silva et al, 2019, submitted)

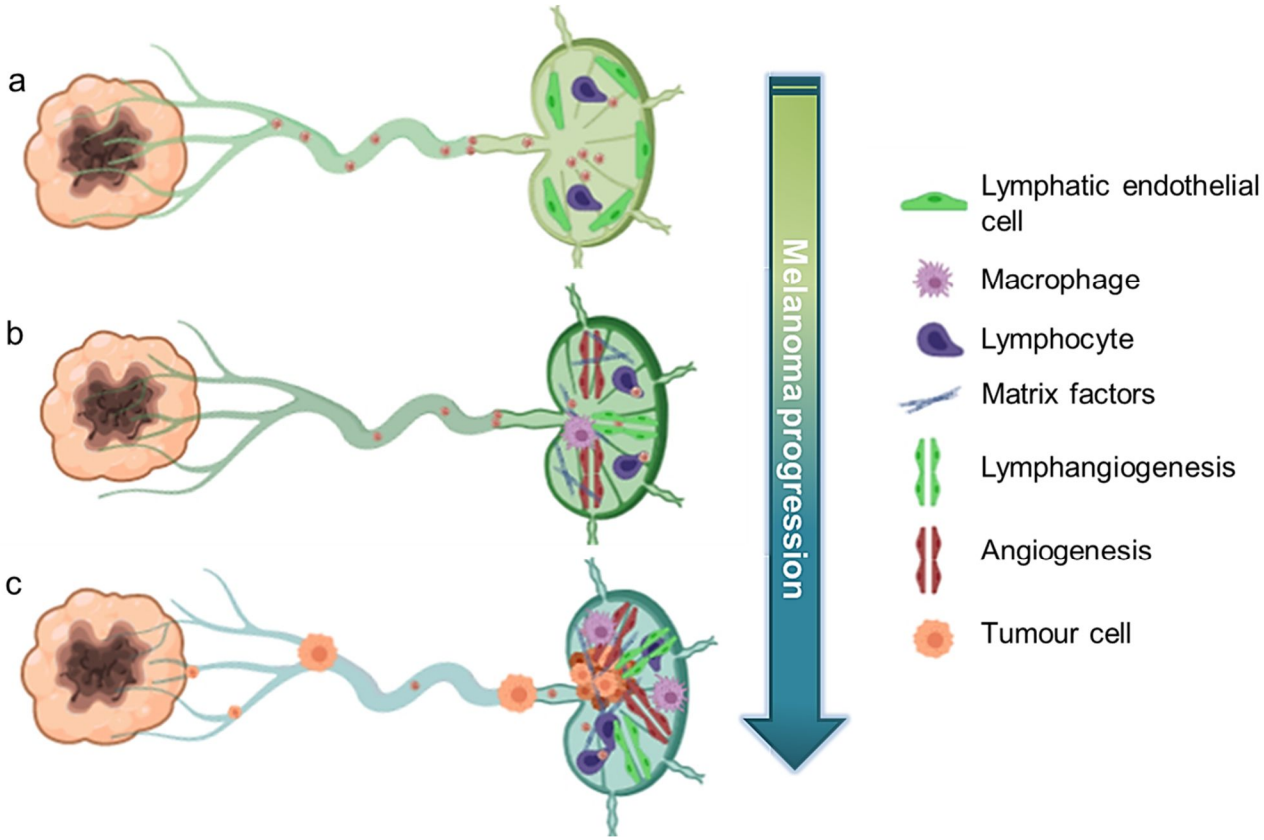

Fig.5 Tumour-derived exosomes reinforce lymph node metastasis. **(a)** Melanoma-derived exosomes reach sentinel lymph nodes, **(b)** within sentinel nodes; melanoma exosomes induce PMN by inducing lymphangiogenesis, tumour cell recruitment, matrix remodelling, angiogenesis and immunosuppression, **(c)** metastatic melanoma cells home in LNs where they find a microenvironment favouring their survival and metastasis [41].

1.4. Melanoma

An estimated 132,000 new melanoma cases are diagnosed worldwide each year [43]. In the United States melanoma represents nearly 5 percent of all cases of cancer [43]. Melanoma is a deadly disease; it is responsible for nearly three-quarters of all skin cancer deaths and is increasing in frequency [43]. Unlike other skin tumours, melanoma is always malignant [44, 45]. It was not until 1806, when ***René Laennec*** described "*la melanose*" to the Faculté de Médecine in Paris, where the disease was characterized in detail and named [46]. Melanoma is a recurring cancer of specialized skin cells (melanocytes) that produce the protective skin-darkening pigment melanin [47]

1.4.1. From melanocytes to melanoma

Melanocytes are neural crest-derived cells that colonize during development the skin [48] and although divide infrequently, less twice per year [49], is the cell population where melanoma arises. The melanocyte-keratinocyte complex responds quickly to a wide range of environmental stimuli. The main function of melanocytes is to provide melanin pigment to the keratinocytes through melanosomes. The melanin granules accumulate above the nuclei and absorb harmful UV-R before it can reach the nucleus and damage the DNA. When melanin is produced and distributed properly in the skin, dividing cells are protected at least in part from mutations that might otherwise be caused by harmful UV [50]. For the induction of this process, melanocyte stimulating hormone (αMSH) in a p53-dependent manner is secreted by keratinocytes to its receptor in the melanocytes, melanocortin 1 receptor (MC1R) [51] **(Fig.6)**.

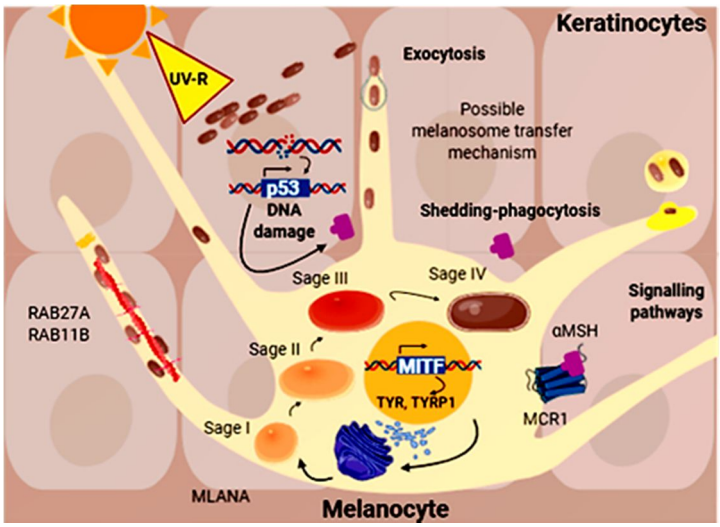

Fig.6 Melanogenesis. Differentiated melanocyte showing its typical cellular processes and some of the most frequently associated genes and biochemical synthesis of melanin, which occurs inside specialised organelles called melanosomes [51].

However, repeated exposures to UV-R during an individual's lifetime are responsible not only for skin aging, but also for the appearance of skin cancer [47]. Cumulative levels of exposure to ultraviolet (UV) radiation cause melanocytic neoplasms. These neoplasms are staged by how far it has progressed, ranging from a benign neoplasm, such as a nevus, to a malignant neoplasm, such as a metastatic melanoma.

1.4.2. Melanoma subtypes

The classification of melanoma may be based in the chronically sun-damaged (CSD). Based in this, there are two categories: CSD and non-CDS that differ in their anatomical site of origin, degree of cumulative exposure to ultraviolet radiation (UV-R), host age, mutation burden and oncogenic alterations [47, 52].

- **CSD melanomas** are macroscopic and microscopic signs of long-term exposure to UV radiation that appears in the skin of the head, neck and the dorsal surfaces of the distal extremities of older individuals (<55 years of age). Molecular alterations are associated with *neurofibromin 1 (NF1), NRAS, BRAF*^{nonV600E} or *KIT* mutations [53].
- **Non-CDS melanomas** arise on more intermittently sun-exposed areas as trunk and proximal extremities of younger individuals. This type of melanoma is associated with a moderate mutation burden characterize by *BRAF*^{V600E} mutations [54, 55].

1.4.3. Metastasis in melanoma

The most dangerous characteristic of melanoma is its ability for early dissemination [56]. Metastases from melanoma usually appear first in the LNs of the draining area of primary tumour [56]. Lymphatic remodelling in cancer is has been considered as one of the main contributor for melanoma metastasis [57, 58]. The influence of LN remodelling together with morphological and functional changes in the tumour microenvironment are important aspects influenced by melanoma cells [59, 60]. It has been demonstrated a correlation between patient outcomes with lymphagiogenesis and lymphatic remodelling in cutaneous melanoma metastasis [57, 58]. These data support that tumour lymphangiogenesis is a prognostic indicator for the risk of LN metastasis in cutaneous melanoma. Most of the studies have been related with the lymphatic remodelling at the primary tumour and have focused on the capacity of lymphatics to facilitate the entry and transport of tumour cells [61]. Lymphatic remodelling has been shown to occur in several types of primary tumours including melanoma [58]. LEC proliferation and migration is the main mechanism involved in the sprouting and enlargement of lymphatic vessels along tumour progression [58]. Importantly, tumour proximity to lymphatics also influences metastatic outcome. For example proximity of a VEGF-D (+) primary tumour to small lymphatics is an important determinant of metastasis [62]. To analyse the relevance of lymphatics in PMN formation and metastasis a recent

work has described a mouse model for live imaging of lymphangiogenesis. This mouse model, called “lymphoreporter”, allows tracking of lymphatic vessels improving the visualization of metastatic routes involving the lymphatic vasculature [63]. This strategy has revealed early induction of distal PMNs uncoupled from lymphangiogenesis at primary lesions. In this work, they described that the heparin-binding factor midkine (MDK) as a systemic inducer of neo-lymphangiogenesis in melanoma secretome [63].

In the past decades it has been described new findings about the potential extrinsic mechanisms involved in LN PMN formation. The homing of melanoma-derived exosomes to sentinel LNs promotes changes that affect melanoma cell recruitment, vascular proliferation and ECM deposition [41]. Interestingly, critical and important changes in the ECM have been proposed as key factors involved in the creation of the PMN [14, 64, 65]. Tumour models of melanoma and breast cancer has been used for the analysis and characterization of tumour-induced lymphatic network remodelling [66]. Multiple cell adhesion molecules are affected in tumour-draining LN LECs along tumour progression [66-69]. For example, integrin αIIb (ITGA2B) is upregulated in LECs of tumor-draining LNs mediating adhesion of tumor cells to fibrinogen *in vitro* [66]. Interestingly, expression or plasma levels of fibrinogen correlate with LN metastasis in mouse cancer models and in gastric cancer patients [67], in colon cancer growth [68] or in spontaneous metastasis of Lewis lung carcinoma [69], indicating that its deposition in draining LNs might contribute to the formation of pre-metastatic niches. Based on these studies, LN and ECM remodelling seems crucial in facilitating lymph node metastasis.

1.5. Extracellular matrix remodelling during metastasis

The function of connective tissues depends on the physical and biochemical properties of their ECM [70]. ECM composition and remodelling is essential for biological and mechanical processes such as providing support, segregating tissues from one another, and regulating intercellular communication [70]. The composition of the ECM can be broadly summarized as a combination of water, protein, and polysaccharide, although each tissue has an ECM with a unique composition and topology that is generated during tissue development through a dynamic and reciprocal, biochemical and biophysical dialogue between the various cellular components and the surrounded microenvironment [70].

1.5.1. Molecular composition of ECM and its role in tissue homeostasis

Two main classes of macromolecules are involved in the ECM composition, proteoglycans (PGs) and fibrous proteins (collagens, elastins, fibronectins and laminins) [70]. The principal function of proteoglycans is binding due to theirs force-resistance properties. The chemical composition of the

polysaccharide chains are very rigid and hydrophilic, so they tend to occupy large volumes in relation to their mass forming gels. Also the high negative charge causes them to attract a large amount of cations, causes large amounts of water to be retained in the ECM, producing a turgor pressure that enables the matrix to oppose compression forces [70]. On the other hand, collagens are the responsible of providing tensile strength [71], cell adhesion regulation and migration [72], chemotaxis and participate in direct tissue development [73]. Moreover, collagen associates with elastin, another major ECM fibre that provides recoil to tissues that importantly undergo repeated stretch [74]. Other important protein is fibronectin (FN) which is intimately involved in directing the organization of the interstitial ECM. Additionally, fibronectin is capable of interacting with biologically relevant molecules, including heparin, collagen, gelatin, fibrin and tenascin that interfering with the remodelling of the ECM by regulating cell adhesion, migration, growth and differentiation [75-77].

ECM is considered a dynamic structure which is in constant degradation and secretion [78]. The balance between this two phenomena orchestrated by ECM-modifying activities, is responsible for tensional homeostasis and the properties of each organ, such as elasticity and compressive/tensile strength [78]. This tissue homeostasis is mediated by the coordinated secretion of metalloproteases (MMPs) [79] and their inhibitors (TIMPs) [80] and the activity of other enzymes such as lysyl oxidases (LOX) [81, 82] and transglutaminases, which participate in the proper formation of this three-dimensional network. Thus, the tissue ECM is a highly dynamic whose precise orchestration is crucial to the maintenance of normal function.

1.5.2. ECM changes in PMN

During the last years it has been described that in the formation of the PMN many matrix proteins participate, as a whole known as “metastatic matrisome” [83, 84] among those important ones are fibronectin, lysyl oxidases [17], tenascin-C (TNC) [85], periostin, collagen IV [86], and different metalloproteases [87, 88]. Although little is known about the mechanisms by which the accumulation of these proteins and microenvironment modifications occur in tissues distant from the primary tumour, different studies point to the role of exosomes. For example, tumour exosomal *miR-494* and *miR-542p* were transferred to lymph node stromal cells and lung fibroblasts, leading to cadherin-17 (Cdh17) downregulation and matrix metalloproteinase upregulation (Mmp2, Mmp3, and Mmp14) [89]. Also, TLR3 activation in lung epithelial cells by tumour exosomal noncoding small nuclear RNA (snRNA) enhances expression of S100a8, S100a9, Mmp9, Bv8, and fibronectin, which, in turn, contributes to lung PMN formation [90].

1.5.2.1. ECM changes in Lymph nodes

In melanoma, was described how melanoma-derived exosomes promote tumour cell recruitment, ECM deposition, remodelling and vascular proliferation in the lymph nodes [41, 91]. Analysis of gene expression profile after a single dose of melanoma-derived exosomes showed differential gene expression within sentinel lymph nodes. Authors observed the induction of angiogenic growth factors, as VEGF-B necessary for melanoma growth and the survival of neovasculature [41]. Their data further show that induction of sentinel nodes by melanoma exosomes increase the expression of a network of interconnected ECM factors as MAPK, urokinase plasminogen activator (uPA) protease, collagen 18, and laminin 5 that may promote trapping of melanoma cells within sentinel node niches [41]. The role played by the ECM, in which lymphatics are embedded, is considered important for lymphatic network function **(Fig.7).** In the quest to identify new lymphatic molecules, several ones have been identified in the maturation of lymphatic vessels, including Cx26, Cx37, and Cx43 [92], Reelin [93], semaphorin 3A (SEMA3A)-NRP1 [94, 95], or transforming growth factor beta receptor II (TGFBR2) [96]. Among all of them, Emilin1 was described also as an important component of the lymphatic perivascular elastic apparatus and its involvement in the structure-function relationship of lymphatic vessels, as well as in lymphangiogenesis [97, 98].

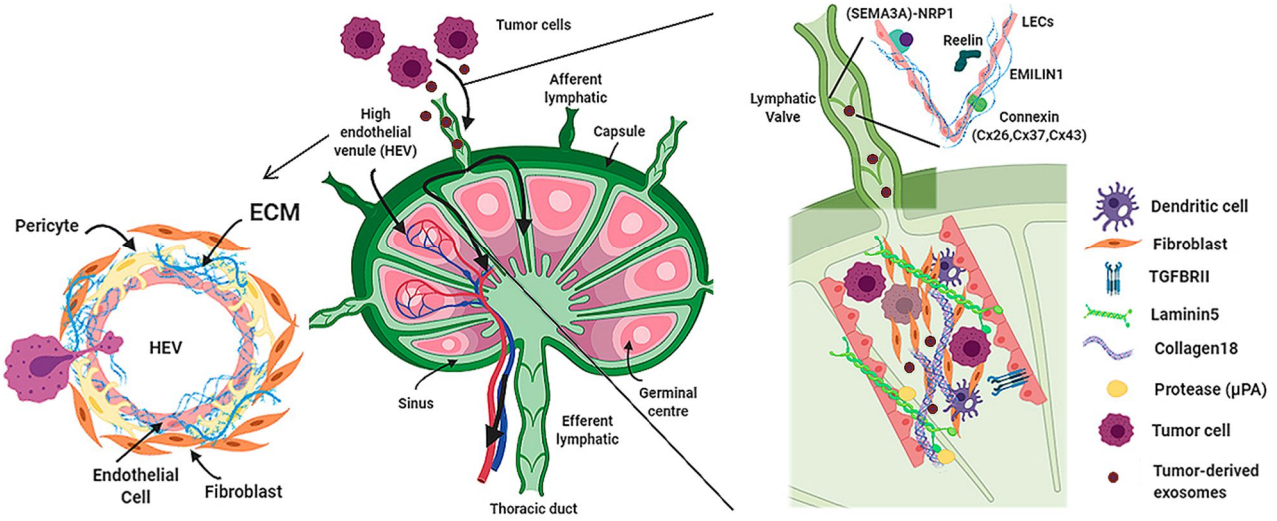

Fig.7 Schematic representation extracellular matrix environment of a lymph node during spread of tumour cells [91]. Melanoma-derived exosomes promote cancer cell recruitment, extracellular matrix deposition. Tumor-secreted exosomes induce the expression of a network of interconnected extracellular matrix factors as urokinase plasminogen activator (uPA) protease, collagen 18, and laminin 5 that may promote trapping of melanoma cells within sentinel LNs [41]. New molecules have been identified in the maturation of lymphatic vessels and lymphatic valve formation, including Cx26, Cx37, and Cx43 [92], Reelin [93], (SEMA3A)-NRP1 [94, 95], or transforming growth factor beta receptor II (TGFBR2) [96]. Emilin1 was described also as an important component of the lymphatic perivascular [97, 98].

1.6. EMILIN/Multimerin Family

Elastin microfibrillar interface proteins (EMILINs) a.k.a Multimerins (EMILIN1, EMILIN2, Multimerin1, and Multimerin2) constitute a four-member family of glycoproteins with a C-terminus gC1q domain typical of the gC1q/TNF superfamily members and also contain N-terminus unique cysteine-rich EMI domain [97] **(Fig.8)**. This family of glycoproteins is part of the superfamily of collagenous and non-collageneous proteins containing the gC1q signature [99]. The C1q domain has been analysed in the human genome and 31 independent gene sequences have identified carrying this domain. Phylogenetic analysis has shown that EMILINs/Multimerins form a small family well distinct from the rest of the superfamily [100]. Coding sequences of EMILIN/Multimerin family components comparison against *Drosophila melanogaster* and other invertebrate genome database gives no matches, indicating that this gene family emerged during vertebrate evolution, first appearing in lower cordate, where orthologs of EMILIN1, EMILIN2, and MMRN2 have been identified [101, 102].

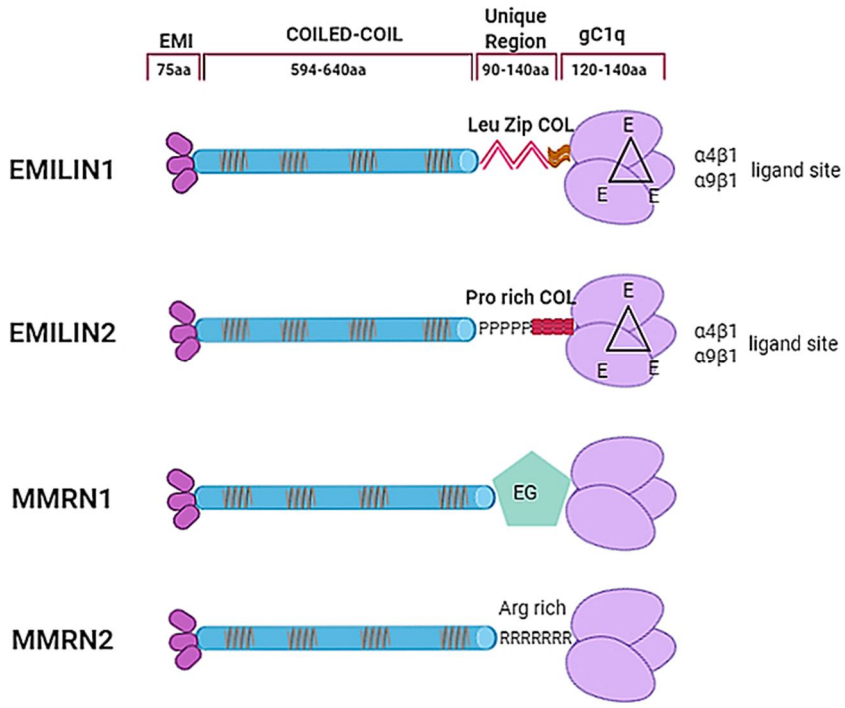

Fig.8 EMILIN/Multimerin family members and structure. EMI domain; there is evidence suggesting that EMI domains might self-interact. Coiled-coil regions; the similarity between the central regions of the family members is only structural; the heptad repeats are placed in different positions along the primary sequence of the different members of the family. "Unique Region" is represented in EMILIN1 by two leucine zippers followed by a functional 17 triplets long collagenic sequence; in EMILIN2 by a proline rich sequence followed by a non-functional 17 triplets long collagenic sequence; in MMRN1 by an arginine rich sequence; in MMRN2 by an EGF-like domain**;** gC1q domain of EMILIN1 and EMILIN2 consist in three unstructured loops (black triangles) each bearing a glutamic acid (E) able to interact with the α4β1 and α9β1 integrin [97].

1.6.1. EMILIN1

EMILIN1 has been characterized in multiple scenarios such as in blood pressure control, TFG-β1-processing, interaction with α4β1 and α9β1 integrins through gC1q domain, cell migration and proliferation, lymphatic vessel function, skin homeostasis and cancer development.

1.6.1.1. Role of EMILIN1 gC1q in physiology

Emilin1 has been defined in multiple physiological processes including:

- *Blood pressure:* The integrity and elasticity of the vessels and the modulation of blood pressure are determined by smooth muscle cells and endothelial cells (ECs) lining the vascular walls and by their relationship with ECM. EMILIN1 is intimately associated with elastic fibres and microfibrils for the maintenance of blood vascular cell morphology [103, 104]. It has been studied how EMILIN1 binds to pro-TGF-β1 prior to the cleavage of the latency-associated peptide (LAP) and upstream of the furin convertases and prevents its processing. Due to this pathway, increased levels of TGF-β in *Emilin1(-/-)* mouse model leads to reduced vascular cell proliferation, narrower blood vessels and increased peripheral resistance developing hypertension [105].

- Cell adhesion: α4β1 integrin binds to the cell surface vascular cell adhesion molecule-1 (VCAM-1) on activated endothelium [106] and to the ECM molecule fibronectin (FN) [107]. Analysis of EMILIN1 gC1q domain demonstrated that it is a binding-partner of integrin α4β1 regulating the static and flow adhesion of T cells and migration of endothelial cells [108]. In this interaction the authors found that the glutamic acid at position 933 (E933) in the gC1q is crucial, since its mutation (E933A) results in no longer functional cell adhesion due to disruption of α4β1-Emilin 1 interaction [108].

- Cell proliferation: It was shown that the lack of EMILIN1 caused dermal and epidermal hyperproliferation and accelerated wound closure [109]. In this work the authors found a direct interaction of extracellular EMILIN1 to α4β1 and α9β1 integrins in keratinocytes as the main mechanism underlying the homeostatic keratinocyte proliferation [109]. EMILIN1-positive fibrils, secreted by skin fibroblast, are normally deposited in the basal keratinocyte layer in the dermal stroma that in turn regulates keratinocyte proliferation. The lack of EMILIN1-α4/α9 integrin interaction in the knock out was accompanied by the activation of PI3K/Akt and Erk1/2 pathways. This study highlights the role of EMILIN1 in the ECM regulating skin proliferation [109].

- Cell migration: EMILIN1 deposition in the ECM has also a role regulating tumour cell migration. EMILIN1, produced by stromal and smooth muscle uterine cells, is deposited in the stroma and in some instances as a gradient of increasing concentrations influencing the migration of trophoblasts involving the interaction with α4β1 integrin [110]. In this setting, function-blocking monoclonal antibodies against α4-integrin and against EMILIN1 as well as the use of EMILIN1-specific short interfering RNA confirmed that trophoblasts interact with EMILIN1 through this integrin [110].

- Regulation of lymphatic endothelial cell function: EMILIN1-integrin α9 interaction has been also defined in the regulation of the lymphatic vasculature, especially in lymphatic valve formation and maintenance acting as a "guiding" molecule in migration of lymphatic endothelial cells [111]. Indeed, the phenotype displayed by *Emilin1(-/-)* mice is the first abnormal lymphatic phenotype resulting in hyperplasia, enlargement, and frequently an irregular pattern of superficial and visceral lymphatic vessels and in a significant reduction of anchoring filaments [112]. The generation of a transgenic mouse model expressing an E933A-mutated EMILIN-1 resulted in abnormal lymphatic vessel architecture. In addition, *ex vivo* thoracic-duct ring assays revealed that E1-E933A-derived lymphatic endothelial cells had a severe reduction in sprouting capacity and were unable to organize into capillary-like structures [113].

1.6.1.2. Role of EMILIN1 in pathological conditions

Having in mind the role of EMILIN1 in regulation of cell proliferation and migration in physiological processes, efforts have been focused in defining the role of EMILIN in tumour progression. Among all the proteolytic enzymes released by the tumour, neutrophil elastase (NE) was found as the main enzyme able to fully impair the regulatory function of EMILIN1 in sarcoma and ovarian cancer [114]. The consequence of this proteolytic process was the impairment of its anti-proliferative role [114, 115]. The local administration of sivelestat, an inhibitor of neutrophil elastase prevents EMILIN1 degradation and reduces lymphoedema, restoring a normal lymphatic functionality in a mouse lymphoedema model [115]. Therefore, modulation of EMILIN1 levels in the ECM may represent pharmacological approach to assessing new lymphoedema treatments. Importantly, analysis by site direct mutagenesis in 914 residue of EMILIN1 demonstrated that mutant R914W was resistant to NE proteolytic cleavage and the protein was able to still interact with the α4β1 integrin [115].

Evidences by Spessotto, Doliana and colleagues using *EMILIN1* knock out mice demonstrated that EMILIN1 has a tumor suppressive role in the microenvironment. Analysis of the two-stage model of skin carcinogenesis and B16-F10 melanoma models in *Emilin1(-/-)* model showed that both tumor growth and lymph node metastasis were increased in KO mice [116]. Recently, the role of EMILIN1

was analyzed in experimental colitis and colon carcinogenesis models [117]. The results have revealed that *Emilin1(-/-)* mice had a higher tumour incidence, lymph node metastasis bigger adenomas and less survival [117]. Similarly, use of the transgenic mouse model overexpressing Emilin1 E933A mutant protein (which disrupts α4β1-Emilin 1 interaction) were more prone to lymph node metastases in melanoma [117], supporting a *tumour-supressor like* role for EMILIN1. In breast cancer patients, results demonstrated that the suppressive role of EMILIN 1 is related to the grade of tumors, and associated with increased hypoxia in the tumor microenvironment followed by elevated unfolding and degradation of proteins [118].

Overall, data support that EMILIN1 deposition in the ECM has an impact in the regulation of the behaviour of surrounding cells due to its interaction with integrins. Importantly, EMILIN 1 has a *tumour suppressor-like* role in the ECM and its ablation in the microenvironment normally leads to increased tumour growth and metastasis. Since our analysis about the signatures correlated with lymph node metastasis showed that EMILIN1 was one of the main candidates, we wondered if EMILIN1 may be involved in melanoma progression, in this thesis we have analysed the role of EMILIN1 in melanoma progression analysing both intrinsic and extrinsic mechanisms involved.

2. OBJETIVES

Data in the literature support that there is an evolution of the tumour phenotype along metastatic progression. In this process, intracellular and environmental extrinsic mechanisms are involved in the selection of specific phenotypes favoured for metastasis. In this thesis we wanted to analyse the existence of these specific phenotypes associated to lymph node metastasis and if so, which are their intrinsic and extrinsic characteristics. For this purpose we defined the following objectives:

1. Characterize the signatures associated to lymph node metastasis in mouse melanoma models

2. Analyse the role of Emilin1 intrinsically and extrinsically in mouse melanoma models

3. Investigate the role of Emilin1 in melanoma tumour growth and metastasis in mouse melanoma models

4. Characterize EMILIN1 expression in human melanoma

3. OBJETIVOS

Estudios previos respaldan que hay una evolución del fenotipo tumoral a lo largo de la progresión metastásica. En este proceso están implicados tanto mecanismos intrínsecos como extrínsecos favoreciendo el proceso metastásico. En esta tesis, hemos analizado la existencia de fenotipos específicos asociados a metástasis en los ganglios linfáticos y sus características, tanto intrínsecas como extrínsecas. Para ello definimos los siguientes objetivos:

1. Caracterizar las firmas asociadas a metástasis de ganglios linfáticos en modelos de melanoma de ratón.

2. Analizar el papel de Emilin1 intrínseca- y extrínsecamente en modelos de melanoma de ratón.

3. Investigar el papel de Emilin1 en la tumorogénesis y metástasis en modelos de melanoma de ratón.

4. Caracterizar la expresión de EMILIN1 en melanoma humano.

4. MATERIALS AND METHODS

4.1. Table of antibodies

Western-blot

As556 IgG Emilin 1	Rabbit Polyclonal	CRO, Aviano, Italy	1/2000
β-Actin	Mouse Monoclonal	#A5441 (Sigma)	1/10000
Alix (3A9)	Mouse Monoclonal	#2171S (Cell Signaling)	1/1000
γ-Tubulin	Mouse Monoclonal	#T6557 (Sigma)	1/10000

Immunohistochemistry

As556 IgG Emilin 1	Rabbit Polyclonal	CRO, Aviano, Italy	1/300
Lyve-1	Rabbit Polyclonal	#14917 (Abcam)	1/250
CD-31	Rabbit Polyclonal	#2836 (Abcam)	1/50

Immunofluorescence

As556 IgG Emilin 1	Rabbit Polyclonal	CRO, Aviano, Italy	1/100
Lyve-1	Rabbit Polyclonal	#ab14917 (Abcam)	1/100
CD31 Clon MEC13.1-APC	Mouse Monoclonal	#102510 BD	1/100

Secondary antibodies

Goat	Rabbit IgG	#NA934 V (GE Healthcare)	***HPR***	1/ 5000
Goat	Mouse IgG	#NA931 V (GE Healthcare)	***HPR***	1/5000
Donkey	Rabbit IgG	#A21206 (Life Technologies)	***Alexa Fluor 488***	1/200
Donkey	Mouse IgG	#A-31570 (Life Technologies)	***Alexa Fluor 555***	1/200
Chicken	Rabbit IgG	#A21443 (Life Technologies)	***Alexa Fluor 647***	1/200

4.2. Cell lines

B16-F1 was purchased from American Type Culture Collection (ATCC). The lymph node metastatic variant B16-F1R2 was kindly provided by Dr. Michael Detmar and Dr. Steven Proulx (ETH Zurich, Switzerland) [119]. Human melanoma cell lines derived from primary tumour (IGR 39) and paired lymph node metastasis from the same patient (IGR 37) [120] were kindly provided Dr. Manel Esteller (Bellvitge Institute Biomedical Research (IDIBELL), Barcelona). Primary human melanocytes (FMC 112) and spontaneously immortalized mouse melanocytes cell line (melan-a) were kindly provided by Dr. M. Soengas (Spanish National Cancer Research Centre, Madrid). All melanoma cell lines were grown in high glucose DMEM (Lonza #D6429) supplemented with 10% fetal bovine serum (Hyclone #SH30071.03IH), 2 mM glutamine and 20 µg/ml gentamicin (Sigma #G1272). Primary melanocytes were cultured in 254CF medium (Gibco #10093) supplemented with human melanocyte growth supplement (Gibco #S0025). melan-a was cultured in RPMI (Gibco #11875-093), supplemented with 5% fetal calf serum (Gibco #16030074) and 200 nM 12-***o***-tetradecanoyl phorbol-13-acetate (Sigma #16561-29-8). All cells were grown at 37ºC in a humidified 5% CO^2 atmosphere and routinely tested for mycoplasma contamination.

4.3. Exosome purification

Cells were cultured in media supplemented with 10% exosome-reduced fetal bovine serum (Hyclone). FBS was reduced from bovine exosomes by ultracentrifugation at 100.000xg for 70 min. For exosome isolation, conditioned media for 72 hours was centrifuged at 500xg for 10 min room temperature to remove cell contaminants. Then, to remove big debris and microvesicles the supernatant fraction was centrifuged at 12.000xg for 20 min 10ºC. Exosomes were then harvested by ultracentrifugation at 100.000xg for 70 min. The exosome pellet was washed in 20 ml of PBS and exosomes were collected by ultracentrifugation at 100.000g for 70 min. All ultracentrifuge spins were performed at 10ºC using a BECKMAN Optima X100 centrifuge with BECKMAN TYPE 70.1Ti rotor. When indicated, exosome pellets were labelled with 3 µg of infrared fluorescent dye NIR815 (eBiosciences) or PKH67 (Sigma #PKH67GL) in 1 mL of PBS. Labelled exosomes were washed twice in 20 mL of PBS, collected by ultracentrifugation and resuspended in PBS collected by ultracentrifugation and resuspended in PBS using standard techniques as described above. Final exosome pellet was resuspended in 100 µL of PBS and the protein content was measured by bicinchoninic acid assay (Pierce™ BCA Protein Assay Kit, Thermo Scientific #23225). The NS500 nanoparticle characterization system (NanoSight) equipped with a blue laser (405 nm) was used for real-time characterization of the vesicles.

4.4. Sample preparation for proteomic analysis

Proteins were solubilized using 8 M urea in 100 mM Tris-HCl pH 8.0. Samples (10 µg) were digested by means of the standard FASP protocol1. Briefly, proteins were reduced (15 mM TCEP, 30 min, RT), alkylated (30 mM CAA, 20 min in the dark, RT) and sequentially digested with Lys-C (Wako) (protein:enzyme ratio 1:50, o/n at RT) and trypsin (Promega) (protein:enzyme ratio 1:50, 6 h at 37 °C). Resulting peptides were desalted using C18 stage-tips.

4.5. Mass spectrometry

LC-MS/MS was done by coupling a nanoLC-Ultra 1D+ system (Eksigent) to a LTQ Orbitrap Velos mass spectrometer (Thermo Fisher Scientific) via a Nanospray Flex source (Thermo Fisher Scientific). Peptides were loaded into a trap column (NS-MP-10 BioSphere C18 5 µm, 20 mm length, NanoSeparations) for 10 min at a flow rate of 2.5 µl/min in 0.1% FA. Then peptides were transferred to an analytical column (ReproSil Pur C18-AQ 2.4 µm, 500 mm length and 0.075 mm ID) and separated using a 120 min linear gradient (buffer A: 4% ACN, 0.1% FA; buffer B: 100% ACN, 0.1% FA) at a flow rate of 250 nL/min. The gradient used was: 0-2 min 6% B, 2-103 min 30% B, 103-113 min 98% B, 113-120 min 2% B. The peptides were electrosprayed (1.8 kV) into the mass spectrometer with a PicoTip emitter (360/20 Tube OD/ID µm, tip ID 10 µm) (New Objective), a heated capillary temperature of 325°C and S-Lens RF level of 60%. The mass spectrometer was operated in a data-dependent mode, with an automatic switch between MS and MS/MS scans using a top 15 method (threshold signal ≥ 800 counts and dynamic exclusion of 45 sec). MS spectra (350-1500 m/z) were acquired in the Orbitrap with a resolution of 60,000 FWHM (400 m/z). Peptides were isolated using a 1.5 Th window and fragmented using collision induced dissociation (CID) with linear ion trap read out at a NCE of 35% (0.25 Q-value and 10 ms activation time). The ion target values were 1E6 for MS (500 ms max injection time) and 5000 for MS/MS (100 ms max injection time). Samples were analyzed twice.

4.6. Proteomic data analysis

Raw files were processed with MaxQuant (v 1.5.3.30) using the standard settings against a human (UniProtKB/Swiss-Prot, August 2014, 20,187 sequences) or mouse (UniProtKB/Swiss-Prot/TrEMBL, August 2014, 43,539 sequences) protein database, supplemented with contaminants. Label-free quantification was performed with match between runs (match window of 0.7 min and alignment window of 20 min). Carbamidomethylation of cysteines was set as a fixed

modification whereas methionine oxidation and N-term acetylation were variable protein modifications. The minimal peptide length was set to 7 amino acids and a maximum of two tryptic missed-cleavages were allowed. The results were filtered at 0.01 FDR (peptide and protein level) and subsequently the "proteinGroup.txt" file was loaded in Perseus (v1.5.1.6) for further statistical analysis. Missing values were imputed from the observed normal distribution of intensities. Then, a two-sample Welch's T-Test with a permutation-based FDR was performed for human exosome samples. Only proteins with a q-value<0.05 and log2 ratio >1 or < -1 were considered as regulated. For mouse exosome samples, a two-sample Student's T-Test with a permutation-based FDR was performed. Only proteins with a q-value<0.1 and log2 ratio >1 or < -1 were considered as regulated [121].

4.7. RNA sequencing (RNA-Seq) and bioinformatics analysis

Total RNA was isolated from cells or xenografts using the RNeasy Mini Kit (Qiagen #74106). The quantity and quality of the extracted RNA was assessed using NanoDrop ND-1000 Spectrophotometer (Thermo Scientific) and Agilent 2100 Bioanalyzer. RNA sequencing (RNA-seq) was performed by the CNIO Genomics Unit. 1 µg of total RNA from each sample was used. PolyA+ fraction was purified and randomly fragmented, converted to double stranded cDNA and processed through subsequent enzymatic treatments of end-repair, dAtailing, and ligation to adapters as in Illumina's "TruSeq Stranded mRNA Sample Preparation Part # 15031047 Rev. D" kit (this kit incorporates dUTP during 2nd strand cDNA synthesis, which implies that only the cDNA strand generated during 1st strand synthesis is eventually sequenced). Adapter-ligated library was completed by PCR with Illumina PE primers (8 cycles). The resulting purified cDNA library was applied to an Illumina flow cell for cluster generation and sequenced using the Illumina HiSeq2500 platform by following manufacturer's protocols.

50bp single-end sequenced reads were analysed with the next*presso* pipeline (DOI:10.2174/1574893612666170810153850), as follows: sequencing quality was checked with FastQC v0.10.1 (http://www.bioinformatics.babraham.ac.uk/projects/fastqc/). Reads were aligned to the mouse genome (NCBI37/mm9) with TopHat-2.0.10 [122] using Bowtie 1.0.0 [123] and Samtools 0.1.1.9 [124], allowing two mismatches and 20 multihits. Differential expression was calculated with DESeq2 [125], using the human NCBI37/mm9 transcript annotations from https://ccb.jhu.edu/software/tophat/igenomes.shtml. GSEAPreranked [126] was used to perform gene set enrichment analysis of the described gene signatures on a pre-ranked gene list, setting 1000 gene set permutations. Only those gene sets with significant enrichment levels (FDR q-value < 0.1) were finally considered.

4.8. Proteomic and RNAseq integration

We integrated the profiles associated to lymph node metastatic mouse model (B16-F1 vs B16-F1R2) data from RNAseq and proteomic analysis. Results were represented as the correlation of the ratios at the protein level and at the RNAseq level (in log2). Analysis of KEEG and Reactome pathways was performed using the ClueGO plug-in v2.5.1 run on Cytoscape v3.6.0. The large cluster of genes obtain after proteomic and RNA sequencing data integration was considered as the reference set list and Enrichment/ Depletion two-side hypergeometric test was selected for enrichment analysis. A Bonferroni stepdown test was applied and pathways with at least $p < 0.05$ were considered for analysis.

4.9. Gene expression analysis / Quantitative real-time PCR analysis

Frozen tissues or cell lines were analyzed for specific gene expression using pre-designed TaqMan® assays from Applied Biosystems listed below:

EMILIN1	Hs_00918337_g1
Emilin1	Mm_00467244_m1
HPRT	Hs_02800695_m1
Hprt	Mm_03024075_m1

Pre-designed primers listed below were used for real-time PCR analysis:

	Forward 5´→ 3´	**Reverse 5´→ 3´**
EMILIN1	CCTTGAGGATGGAGTGGAGA	GTCTTGTAGGCCACACGGTAG
SLC40A	CCATGAGCTTGAACATGAGC	CATCTCGGAAGGTACGGAAG
CD37	GGCCTGTATTTTGGGATGC	GAGGATTCCCAGGGTGATCT
HPRT	TGACCTTGATTTATTTTGCATACC	CGAGCAAGACGTTCAGTCCT
Emilin1	CCTGTCTGGCTCCAGTGC	GCTCTAGCTGCTGCACCTTC
Slc40a1	GCAGCTGACCTCACCTAAAGA	GAAGGGCTCTGCCATCTG
Cd37	TCTCCTGGGCCTGTATTTTG	CAATTCCTGCACCCTTCG
Hprt	TCCTCCTCAGACCGCTTTT	CCTGGTTCATCATCGCTAATC

In brief, total RNA was extracted from tissues or cells as described above and reverse-transcribed using the QuantiTect Reverse Transcription Kit (Qiagen #205313). Quantitative real-time PCR (QRT-PCR) was performed on a 7500 Fast Real Time PCR System (Applied Biosystems), using TaqMan Universal PCR Master Mix (Life Technologies #4304437). Gene expression was analyzed using the delta-deltaCT method for relative quantification and all samples were normalized to a housekeeping gene, HPRT.

4.10. Western blot analysis

Cells were lysed with RIPA buffer containing a complete protease and phosphatase inhibitor tablet (Roche #11836153001, #PHOSS-RO). Lysates were cleared by centrifugation at 14,000 × g for 15 min at 5ºC. Supernatant fractions were used for Western blot. Protein extracts or purified exosomes were quantified for protein content using the bicinchoninic acid assay (Pierce™ BCA Protein Assay Kit, Thermo Scientific #23225). Equal amounts of cell lysate or purified exosomes were resolved by SDS-PAGE and transferred into a polyvinylidene difluoride (PVDF) membrane (Millipore #IPVH00010). After blocking for 1 hour at room temperature (RT), membranes were incubated with the antibodies indicated in the table of antibodies overnight at 4ºC. Antibodies to β-actin or γ-Tubulin for cells, and Alix for exosomes, were used as loading controls. The intensities of the immunoreactive bands were quantified by densitometry using ImageJ software (NIH).

4.11. Plasmids design and cloning strategies

For Emilin1 overexpression experiments human Emilin1 cDNA was cloned in pcDNA3 plasmid. The neutrophil elastase-resistant R914W Emilin1 mutant [115] was cloned in, pCEP4 plasmid. Both plasmids were kindly provided by Dr. Paola Spessotto and Dr. Roberto Doliana (Centro di Referimento Oncologico, CRO, Aviano, Italy). For transfection experiments we used the Lipofectamine 2000 Transfection Reagent (Thermo Fisher #11668019). The transfection were done in suspension, where $5x10^5$ B16-F1R2 GFP-luc cells were seeded in a T6 multi-well with 8 µL of Lipofectamine reagent and 8 µg of DNA (ratio 1:1 according to manufacturer's protocol). 16h later, medium was removed and fresh medium as added. Neomycin (G-418 Sigma #G8168) and hygromycin (Sigma #H3274) selection were added 48h later at 2 mg/ml and 500 µg/ml, respectively for 14 days.

For genetation of HA-Emilin transfectants, B16-F1 GFP-luc cell line was transfected with pCMV3-N-HA (N-terminal HA-tagged) plasmid (Sinobiological #CV017) **(Fig.1)** in which human Emilin1 full sequence cDNA was cloned, control cell line was generated using the empty vector pCMV3-N-HA.

The cloning and primers designed for the generation of the vector and the insert fragments sharing overlapping were done following Gibson Assembly NEB protocol (NEB #E2611S/L) and *SnapGene* Software. The transfection was done as indicated above with lipofectamine. Neomycin (G-418 Sigma #G8168) was added 48h later at 2 mg/ml for 14days. Stable transfectant clones were isolated from the selected cells using "cloning cylinders" (Sigma #CLS31668) and tripsinization.

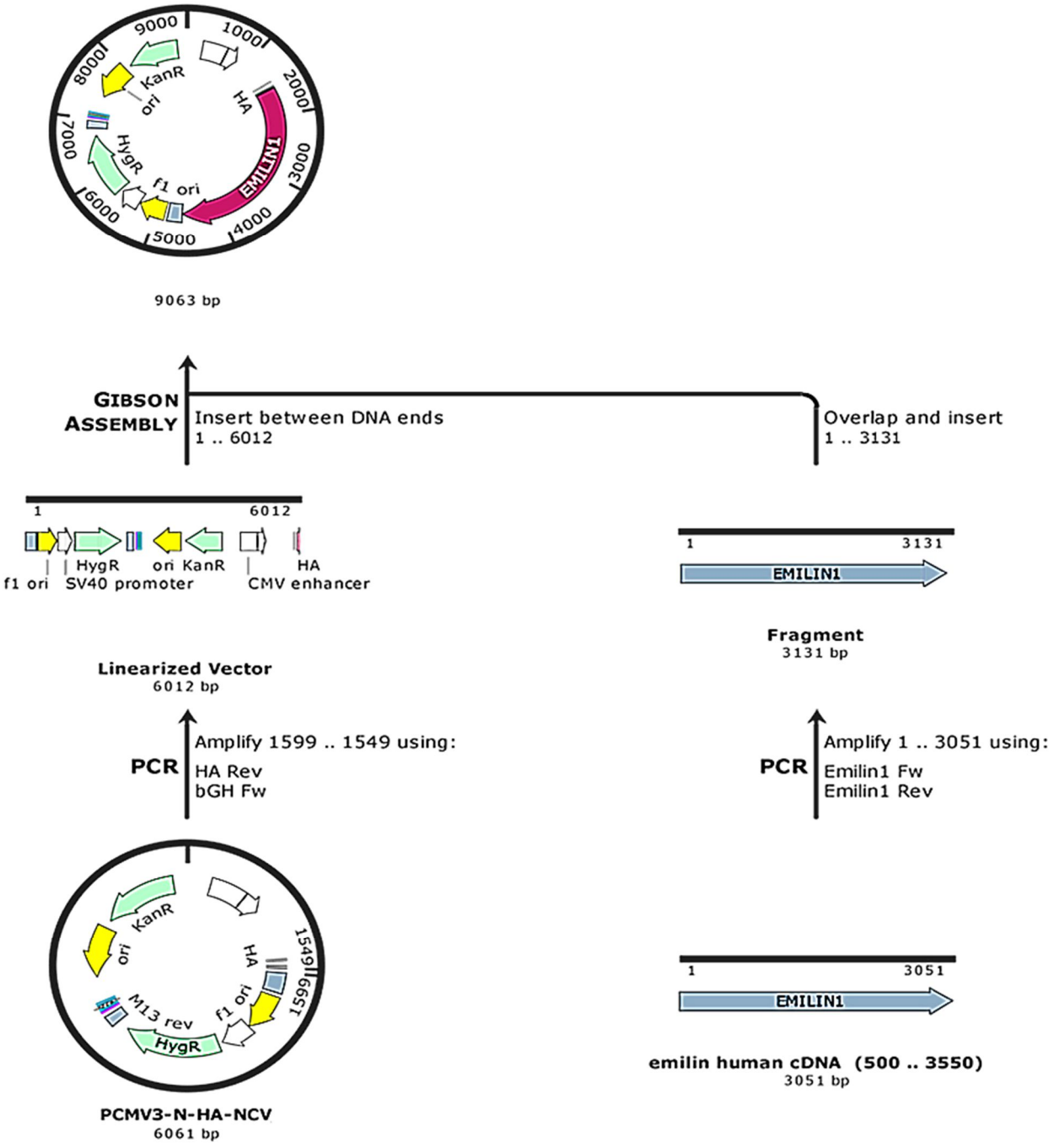

Fig.1 Human Emilin1 full sequence cDNA cloning. Protocol obtained by *Snapgene Software* based on Gibson Assembly NEB protocol.

The primers used for cloning were the following ones:

	Sequence 5´→ 3´
EMILIN1 Fw	TGGAGCTCTGGCTTATCCTTACGACGTGCCTGACT**ACGCC*atggccccccgcaccctctg***
EMILIN1 Rv	GAGGGGCAAACAACAGATGGCTGGCAACTAGAAGG**CACAG*ctacgcgtgttcaagctctggg***
bGH (poly A) Fw	**CTGTG**CCTTCTAGTTGCCAGCC
HAtag Rv	GGCGTAGTCAGGCACGTCGTA

Two different polymerases were used due to the length of the vector. Platinium SuperFi DNA polymerase (Invitrogen #12351010) was used for vector amplification following the 3-steps protocol (<10 kb) and Platinum™ Pfx DNA Polymerase (Life Techlogies #11708021) was used for the insert. The amount of fragments used for assembly was 100 ng of the vector and 150 ng of EMILIN1 insert.

Platinium SuperFi-DNA Polymerase

		3 step protocl (<10 kb)	
		50 ng of vector	
		Temp.	**Time**
Initial denaturation		98ºC	30 sec
35 cycles	**Denature**	98ºC	10sec
	Anneal	63ºC	10 sec
	Extend	72ºC	30 sec/kb--8min
Final extension		72ºC	5min
		4ºC	hold

Platinum™ Pfx DNA Polymerase

		100 ng of EMILIN1	
		Temp.	**Time**
Initial denaturation		94ºC	2min
35 cycles	**Denature**	94ºC	15sec
	Anneal	56ºC	30 sec
	Extend	68ºC	1min/kb--4min
Final extension		68ºC	10min
		4ºC	hold

For generation of R914W mutant [115], we performed a site-directed mutagenesis following QuickChange II Sited-Directed Mutagenesis protocol (Aligent Technologies #200523). The primers used for site-directed mutagenesis were:

	Sequence 5´→ 3´
R914W Fw	AAGTGGAGGCCGTGCTGTCC***T***G***G***TCCAACCAGGGCGTGGCCCGC
R914W Rv	GCGGGCCACGCCCTGGTTGGA***C***C***A***GGACAGCACGGCCTCCACTT

All the constructions were validated at the CNIO Genomic Unit. The primers used for the sequencing procedure were:

	Sequence 5´→ 3´
Primer 1- 403…422	CAGCGCTGGGGCCTGCGTC
Primer 2- 729…750	CTGCAGCTCCTGGACACCCGC
Primer 3- 1050…1074	CAGGAATGCTGCTCTCCAGAGCTGG
Primer 4- 1384…1407	GGCGGTTGGATCTGTTGGAGGAGC
Primer 5- 1749…1771	GCCTGTGGCGGAGTCCAAGAGG
Primer 6- 2104…2128	CAGAGAGTGAAGAGCGCTTCCGAG
Primer 7- 2472…2491	CCTGGGCTGCAGGGACCCC
HAtag	GGCGTAGTCAGGCACGTCGTA
bGH (poly A)	CTGTGCCTTCTAGTTGCCAGCC

Chemically competent cell transfection protocol from Gibson assembly protocol was followed. 50 µl of competent cells (Stbl3™ Chemically Competent E. coli, Invitrogen #C737303) were incubated with 50 ng of DNA on tubes during 30 min on ice. Then, the tubes were incubated during 45 sec at 42 ºC and on ice again for 2 min. After that, 450 µl of SOC medium , which has to be at 42 ºC, was added and the mix was incubated 1h at 37 ºC in an orbital incubator at 200 rpm. One volume of

each tube of transfection was added on LB agar+ Kanamycin plate. The LB agar was incubated O/N at 37 ºC in the incubator.

4.12. Human studies

Analysis of tumour tissue specimens from melanoma patients were performed in collaboration with Dr. Juan Angel Recio and Dr. Eva Muñoz (Vall d'Hebron Barcelona Hospital Campus). TMA designed with primary melanoma, skin metastasis, lymph node and lung metastasis were performed in collaboration with Dr. Jose Luis Peralto (Hospital 12 de Octubre). Emilin1 levels were evaluated in each series. Emilin1-specific staining was not scored according to its intensity of expression due to its presence in all samples at high levels, independently of melanoma grade. The study was carried out with the corresponding informed consent and approved by local institutional guidelines

4.13. Histological studies

Tissue samples were fixed in 10% neutral buffered formalin (4% formaldehyde in solution), paraffin-embedded and cut at 3 µm, mounted in superfrost®plus slides and dried overnight. For different staining methods, slides were deparaffinized in xylene and re-hydrated through a series of graded ethanol until water. Consecutive sections were stained with hematoxylin and eosin (H&E), and several immunohistochemistry reactions were performed in an automated immunostaining platform (Autostainer Link 48, Dako; Ventana Discovery XT, Roche). Antigen retrieval was first performed with the appropriate pH buffer, (Low pH buffer, Dako; CC1m, Ventana, Roche) and endogenous peroxidase was blocked (peroxide hydrogen at 3%). Then, slides were incubated with the appropriate primary antibody as detailed in Table of antiboides. After the primary antibody, slides were incubated with the corresponding secondary antibodies. Immunohistochemical reaction was developed using 3, 30-diaminobenzidine tetrahydrochloride (DAB) or Purple Kit (Chromo Map DAB or Purple Kit, Ventana, Roche; DAB (Dako)) and nuclei were counterstained with Carazzi's hematoxylin. Finally, the slides was dehydrated, cleared and mounted with a permanent mounting medium for microscopic evaluation. Positive control sections known to be primary antibody positive were included for each staining run.

4.14. TCGA data analysis

Clinical expression analysis was based on mRNA levels (Illumina RNA seq V2 data set TCGA-SKCM.htseq_fpkm-uq.tsv) obtained from the GDC TCGA Melanoma (SKCM) cohort downloaded

from www.xenabrowser.net that contained 472 samples. FPKM-UQ normalized values were used for comparing EMILIN1 between indicated patients' groups.

4.15. Immunofluorescence

Cells were fixed with 4% paraformaldehyde (PFA, Electron Microscopy Sciences) for 20 min RT, followed by permeabilization with 0.1% Triton X-100 (Sigma #11332481001) in PBS for 10 min RT. After washing with PBS, to avoid antibody unspecific interactions coverslips were incubated with PBS 5% Donkey Serum (Sigma #D9663), 1% BSA, and 0.05% Triton for 45 min at RT and stained with primary antibodies at indicated dilutions (Table antibodies) 4ºC overnight. Then, samples were rinsed and incubated with an Alexa conjugated secondary antibodies at indicated dilutions (Table antibodies). 40,6-diamidino-2-phenylindole (DAPI) was used for nuclear staining. Digitized images were generated using a Leica TCS SP5 X AOBS or Leica TCS SP5 AOBS confocal microscopes and analysed using Fiji software.

For immunofluorescence of lymph nodes, tissues were fixed in 4% PFA O/N at 4ºC and then in a mix of PBS and 20-30% sucrose solution during 24h at 4ºC, embedded in Tissue-Tek O.C.T. (Electron Microscopy Sciences). The blocks were frozen in dry ice and ethanol bath and stored at -80ºC. 6 µm O.C.T. sections were treated with glycine 100mM for 10 min. After 3 washes with PBS, sections were incubated with PBS-0.3% triton X-100 for 15 min. Non-specific sites were blocked by incubation in PBS containing PBS 1% BSA 5% Donkey Serum – 0.05% triton X-100 for 1 h at RT. Tissues were then washed 3 times in PBS and incubated 1 h or overnight with primary antibodies at indicated dilutions (Table antibodies). After 3 washes with PBS, sections were incubated 1 h with secondary antibodies from the Alexa Fluor series from Molecular Probes at indicated dilutions (Table antibodies) and washed again. DAPI was used for nuclear staining. Finally, samples were mounted with ProLong (Thermo Ficher #P36930) and fluorescent images were obtained using Leica TCS SP5 X AOBS or Leica TCS SP5 AOBS confocal microscopes and analysed using Fiji software. Primary antibodies detailed in the table of antibodies.

4.16. GW4869 treatment *in vitro*

Melanoma cells were treated during 24h with the inhibitor GW4869 (Selleckchem #S7609) at 10µM per $3x10^5$ of cells seeded in well of T6 plate. PBS-DMSO was added as control. After the treatment, cells were stained following the protocol of immunofluorescence previously described. Digitized images were generated using a Leica TCS SP8 FSU AOBS confocal microscope and analysed using Fiji software.

4.17. Cell Cycle

Cell cycle histograms for bulk DNA staining (PI), after addition of EdU, from B16-F1 and B16-F1 E1 model were performed at 24,48,72,96 h and 1 week following manufacture protocol (Invitrogen #C10337). Percentage of B16-F1 and B6-F1 E1 cells in S phase were calculated. The modified thymidine analogue EdU was added 30 min before cell fixation. Cells were fixed by adding 100 µl PFA 4% (in PBS, freshly prepared) and Streptavidin-AF647 was used after EdU detection mix step. Data were acquired on BD FACSCanto II, at least 5.000 single alive events were acquired and all data was analysed using FlowJo software v10 (TreeStar).

4.18. Cell viability assay

Luminescent Cell Viability Assay, CellTiter-Glo, (Promega #G7570) at different time points (24, 48, 72 h) following manufactures protocol. Cells were seeded into T96 plate and luminescent were measured at VICTOR Multilabel Plate Reader.

4.19. Cell tracking and motility assay

Cell tracking and motility analysis were performed overnight in chamber slide with a removable 8 well silicone chamber for cell culture (Ibidi #80841). Videos were acquired in DM16000B Widefield microscope (Leica Microsystems). The number of positions for each cell model was three and four tracks per position were analysed. Distance and velocity of cell tracking analysis were measured by ImageJ software.

4.20. Xenograft studies

All animal experiments were performed according to protocols approved by the Institutional Ethics Committee for Research and Animal Welfare (CElyBA) of the CNIO, the Instituto de Salud Carlos III (CNIO-ISCIII) and the comunidad Autónoma de Madrid (CAM).

4.20.1. Tumor growth and metastasis studies

To 8- to 10-week-old C57BL/6J – C57BL/6J *EMILIN1 (-/-)* [127] mice were injected in the flank with melanoma cells. Tumour volume was monitored 2-3 times per week. Animals were sacrificed when tumour volume get 1.2 cm^3.

To analyse the metastasis spread though lymphatic system, 8- to 10-week-old C57BL/6J and C57BL/6J *EMILIN1 (-/-)* [127] mice were injected intra-footpad with $2x10^4$ with melanoma cells. Animals were sacrificed 21 days after injection. Luciferase imaging was done *ex vivo* using the IVIS Spectrum system in both approaches. Popliteal lymph nodes were paraffin embedded and stained with HMB45, percentage of melanoma positive cells quantification was also performed.

4.20.2. GW4869 treatment *in vivo*.

8- to 10-week-old C57BL/6J.OlaHsd male mice were injected in the flank with $1×10^6$ melanoma cells. Five days later, mice were treated (intraperitoneal injection (i.p)) three times per week with the inhibitor GW4869 (3 microg/g of mice, Selleckchem #S7609) and PBS-DMSO as control. Tumour volume was monitored 2-3 times per week. Animals were sacrificed when tumour volume got 1.2 cm^3. Luciferase imaging was performed using the IVIS Spectrum system. Tumour tissues (n=3 per group) were snap frozen in liquid nitrogen for RNA extraction and RNAseq analysis.

4.20.3. *In vivo* Imaging System

Luciferase imaging was performed using the IVIS Spectrum system (Caliper, Xenogen). Tumour-bearing mice were anesthetized (using isoflurane 3-4% and 0,5% O^2), and D-luciferin (50 mg kg−1 in 100 µl PBS) was administered. Eight minutes later, mice were euthanized and their organs were analysed for luciferase expression. Data were quantified with Living Imaging software 4.7.2.

4.20.4. Distribution analysis of exosomes through the lymphatic system

C57BL/6J.OlaHsd female mice were injected intra-footpad to deliver exosomes directly into the lymphatic circulation as described. A total of 0.5 µg of NIR815-labeled exosomes were injected intra-footpad in a total volume of 20 µl PBS twice a week for 3 weeks. To determine the systemic exosome distribution and LN uptake (popliteal, inguinal and axillary LNs), mice were monitored *in vivo* using the IVIS Spectrum real time imaging system. Fluorescence signal was assessed to quantify exosome uptake.

4.20.5. Exosome homing in sentinel lymph nodes

10 µg of PKH-67-labelled exosomes (as described in exosomes isolation) were injected in the footpad of 8- to 10-week-old C57BL/6J.OlaHsd mice previously anesthetized using isofluorane and

0.5 %O^2. Animals were sacrificed after 16h. Tissues were fixed in 4% PFA overnight at 4ºC, then were transferred into a 20-30% sucrose-PBS solution during 24h at 4ºC and embedded in Tissue-Tek O.C.T. (Electron Microscopy Sciences). The blocks were frozen in a dry ice and ethanol bath and stored -80 ºC. Immunofluorescence analysis of PKH-67 was performed by confocal microscopy.

4.20.6. Exosome treatment in the footpad: analysis of exosome uptake and lymphangiogenesis

8- to 10-week-old C57BL/6J.OlaHsd mice were injected intra-footpad three times during the first week, and two times during the second week with 5 µg of exosomes (mice were injected into both footpads). The next day after the last injection animals were sacrificed. Popliteal lymph nodes paraffin embedded and stained with anti-HA, Emilin1 (As556IgG) and Lyve-1. Exosome uptake and lymphangiogenesis were evaluated by microscopy and quantified with ImageJ software. Immunofluorescence analysis of Emilin1 (As556IgG), Lyve-1 and CD31 were performed by confocal microscopy.

4.20.7. TNF-α treatment

8- to 10-week-old C57BL/6J.OlaHsd females mice were injected intra-footpad three times during the first week, and two times during the second week with 20 ng of TNF-α (#315-01A-B BioNova) in a final volume of 30 µl per mice. The next day after the last injection animals were sacrificed. Popliteal lymph nodes paraffin embedded and stained with Emilin1 (As556IgG), Lyve-1 and CD31 antibodies. Immunofluorescence analysis of Emilin1 (As556IgG), Lyve-1 and CD31 were performed by confocal microscopy.

4.20.8. Exosome education treatment: homing and metastasis analysis

8- to 10-week-old C57BL/6J.OlaHsd mice were injected intra-footpad three times during the first week, and two times during the second week with 5 µg of exosomes (mice were injected into both footpads). The next day after the last injection, $2x10^4$ B16-F1 HA cells were injected in both footpads of the mice. For the analysis of homing, mice were sacrificed at 24h later, however, for metastasis analysis, at 21 days. Luciferase imaging was done *ex vivo* using the IVIS Spectrum system in both approaches. Popliteal lymph nodes were paraffin embedded and stained with HMB45, percentage of melanoma positive cells quantification was performed.

4.21. Statistical analyses

Error bars in the graphical data represent means ± s.e.m. Mouse experiments were performed using at least three mice per treatment group. P values of $P < 0.05$ were considered statistically significant by Student's *t* test or ANOVA. For the tumour growth analyses, we performed two-way ANOVA statistical analyses using GraphPad Prism software.

5. RESULTS

We have characterized secreted exosomes from a panel of mouse melanoma models representative of low metastatic potential (B16-F1), high metastatic potential (B16-F10) and lymph node metastasis (B16-F1R2) [119]. These studies were complemented using two models of human melanoma cell lines derived from primary tumor (IGR39) and matched lymph node metastasis from the same patient (IGR 37) [120] **(Fig.1)**.

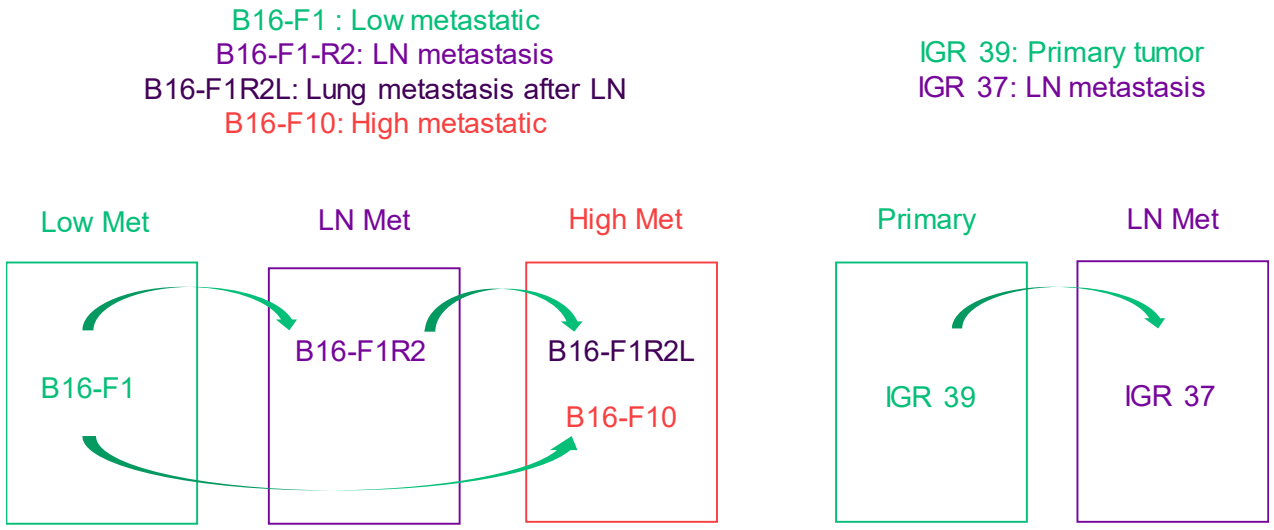

Fig.1 Models used in the analysis. Schematic representation of the models used in the thesis. Left panel, melanoma mouse models used included B16-F1 (low metastatic model), B16-F1R2 (lymph node metastatic model), B16-F1R2L lung metastatic model derived from B16-F1R2 and B16-F10 model (high metastatic model). Right panel, human metastatic models include IGR39 (primary tumor) and matched lymph node metastatic model IGR37.

5.1. Characterization of lymph node metastatic signatures in melanoma models

5.1.1. Characterization of secreted exosomes in melanoma models

5.1.1.1. Analysis of exosome number and total protein secreted in exosomes

We first isolated by ultracentrifugation and characterized secreted exosomes from melanoma models described above. Analysis of exosome number and protein associated demonstrated that the lymph node metastatic cell line (B16-R2) and the high metastatic model (B16-F10) secrete a

significant higher number of exosomes **(Fig.2a)** with increased protein cargo **(Fig.2b)** in the exosomal fraction than the poorly metastatic cell line B16-F1. We obtained the same results with human models and found that the lymph node metastatic model IGR37 secretes a significantly higher amount of exosomes **(Fig.2c)** with increased protein cargo **(Fig.2d)** than the parental model IGR39. These data support previous observations in which exosome protein concentrations were higher in highly metastatic cell lines compared to low metastatic models of melanoma [30].

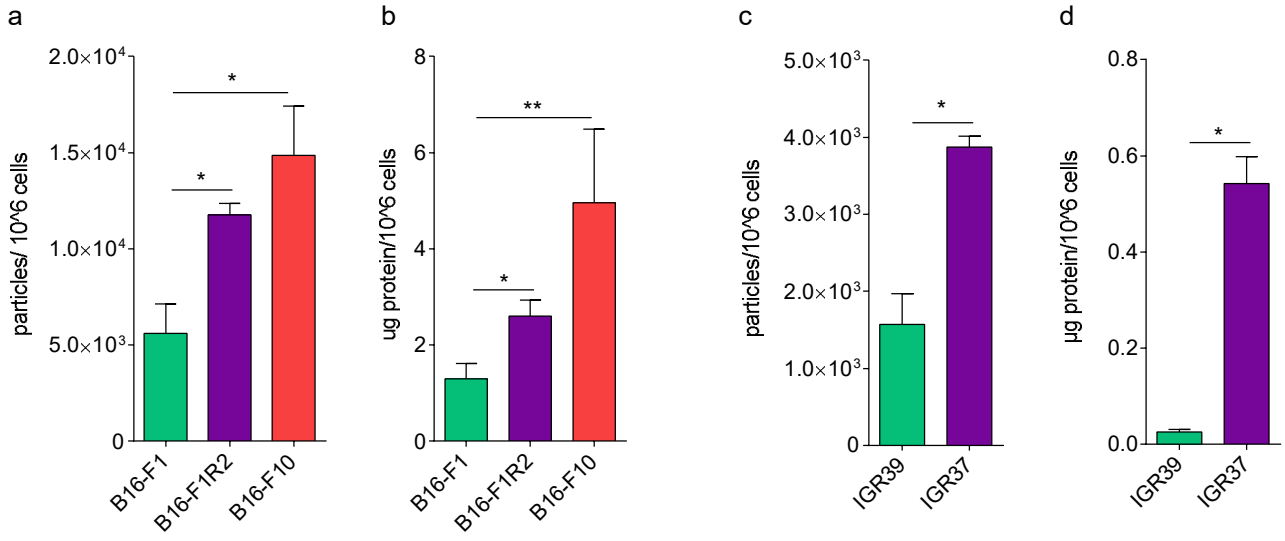

Fig.2 Analysis of exosome number secretion (a, c) and total protein secreted in exosomes (b, d) in mouse **(a, b)** and human **(c, d)** melanoma cells lines derived from primary tumour (green), lymph node metastasis (purple) and distal metastasis (dark purple and red), n= 5 (mouse), n=4 (human), p <0.05 using Mann Whitney test.

5.1.1.2. Biodistribution of melanoma-derived exosomes in sentinel lymph nodes

We wanted to study the biodistribution of melanoma-derived exosomes through the lymphatic system. To understand this process, we treated for 3 weeks (intra-footpad) with NIR815-labeled exosomes derived from melanocytes (melan-a), low and high metastatic melanoma models (B16-F1 and B16-F10 cell lines, respectively) and the LN-metastatic model B16-F1R2. We observed that B16-F1 or melan-a-derived exosomes presence is mainly detected in the sentinel lymph node (sLN). However the signal of exosomes from B16-F1R2 and B16-F10 is much higher in sLN and is also present in additional LNs **(Fig.3a).** Analysis by Odyssey scanner of lymph nodes demonstrated that exosomes derived from B16-F1R2 showed that besides reaching sentinel lymph nodes, they are significantly increased in inguinal lymph nodes **(Fig.3b, c),** suggesting that their mobility through the lymphatic system is faster and wider than B16-F1-derived exosomes**.**

We next analysed the homing of tumour-derived exosomes in shorter time periods. We isolated exosomes from B16-F1 and B16-F1-R2 models, labelled them fluorescently with PKH67 and injected them in the footpad. The analysis of exosome distribution in the popliteal lymph nodes 16 hours after injection showed that B16-F1-R2-derived exosomes spread out more inner in the lymph node structure while B16-F1-derived exosomes remained mainly in the cortical area **(Fig.3d, e)**. All these results suggest that exosome derived from lymph node metastatic models have a faster and wider distribution in sentinel lymph nodes.

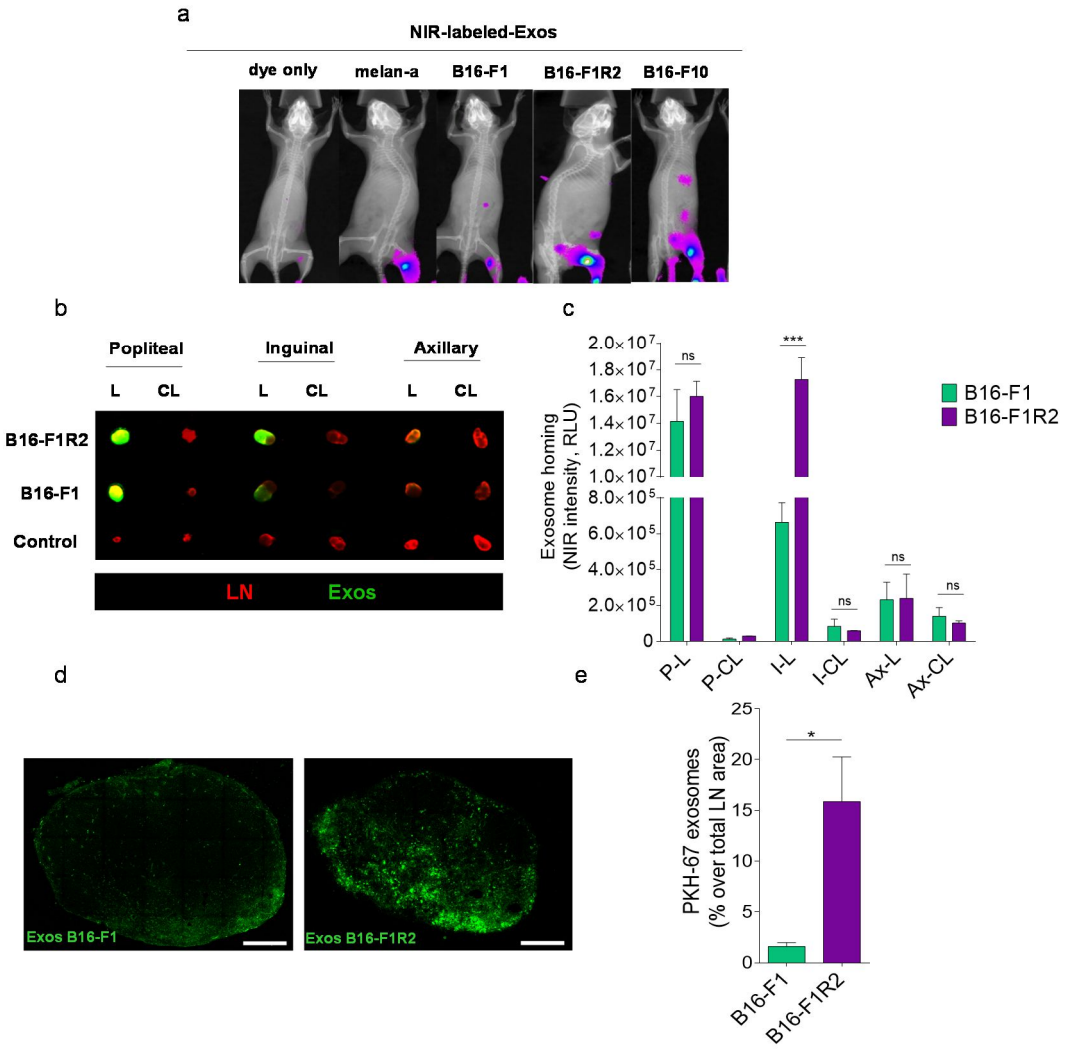

Fig.3 Melanoma-secreted exosomes are retained through the lymphatic system according the metastatic potential of melanoma cells. (a) Representative images, from Quantum FX μCT scan, showing fluorescence signal in mice treated for 3 weeks with exosomes from the indicated cell lines (n=4 mice per group). Exosomes were previously labeled with NIR815 and injected intra-footpad twice a week. **(b)** Representative Odyssey-scanned images of LNs from mice injected with NIR815-labeled exosomes derived from the indicated melanoma cell lines. Exosomes were injected intra-footpad twice a week during 3 weeks. **(c)** Quantification of NIR815-associated fluorescence related to experiment shown in **(b)** n=2 ***p<0,001 2way ANOVA. **d)** Immunofluorescence analysis by confocal microscopy of B16-F1-derived exosomes (left panel) and B16-F1R2 (right panel). Scale 100 μm. **(e)** Quantification of exosomes area over total lymph node n=3 *p <0.05 using Unpaired t-test.

5.1.1.3. Analysis of exosomal signatures associated to lymph node metastasis in mouse and human melanoma models.

To investigate the proteomic signatures in the exosomes associated to the lymph node metastatic melanoma model B16-F1R2 we collected exosomes from this model and the parental model B16-F1 and performed mass spectrometry analysis **(Fig.4)**. We analysed the hierarchical cluster obtained from B16-F1 and B16-F1R2. We observed the existence of a proteomic signature associated to the lymph node metastatic model**.** Analysis by Reactome database showed that proteins related with extracellular matrix organization (Emilin1, Icam2, Nid1, Nid2, Col5a1, Hspg2 and Agrn) were the most represented in the exosomal signature from B16-F1R2 **(Table 1).**

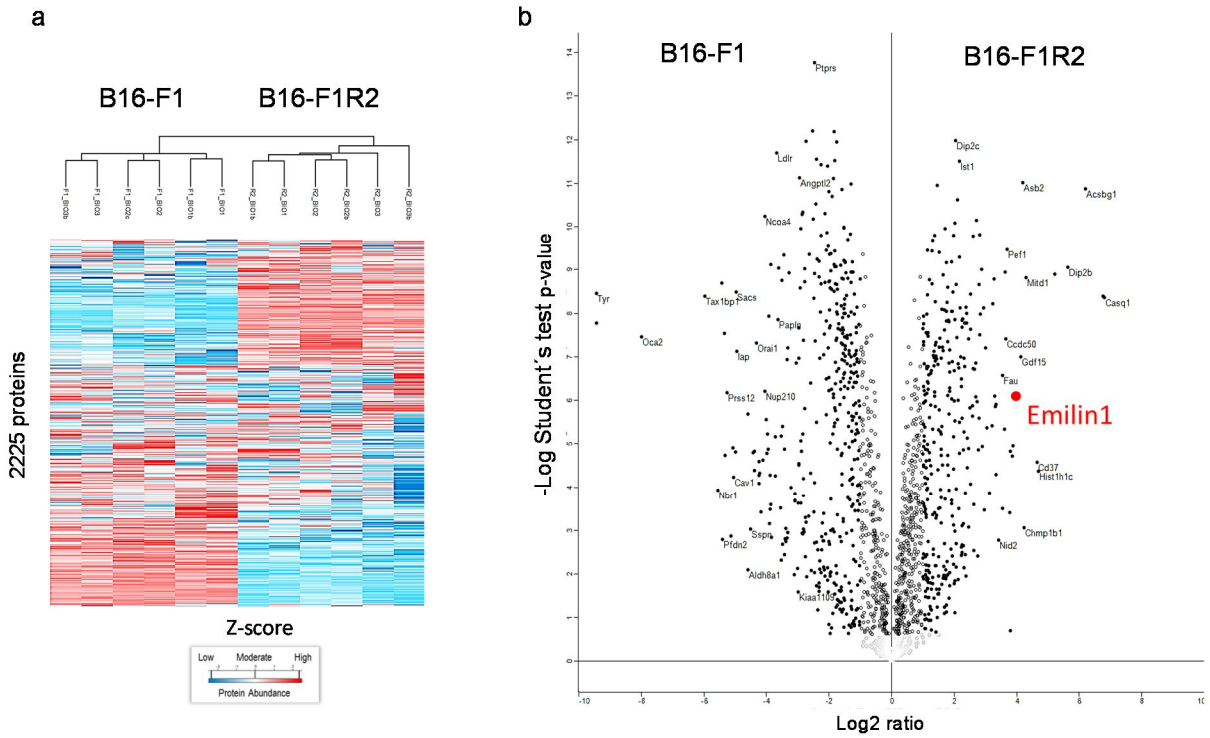

Fig.4 Analysis by mass spectrometry of exosomes secreted by mouse melanoma cell lines to define exosomal signatures associated to lymph node metastasis. **(a)** Hierarchical clustering and **(b)** Significant proteins (Student´s t-test) identified in exosomes derived from B16-F1 and B16-F1R2 cell lines.

5.1.2. Analysis of gene expression patterns by RNAseq in mouse melanoma models

5.1.2.1. Gene expression signatures associated to metastatic progression in mouse melanoma models

We next decided to correlate the cargo of secreted exosomes with gene expression pattern in B16-F1 and B16-F1R2. We first performed RNA sequencing analysis from B16-F1, B16-F1R2 and B16-F1-R2L models. We observed that there were several differential gene expression profiles overexpressed in B16-F1R2 and B16-F1R2L cell lines **(Fig.5).** We selected a cluster of genes that showed an increased correlation with metastatic profile.

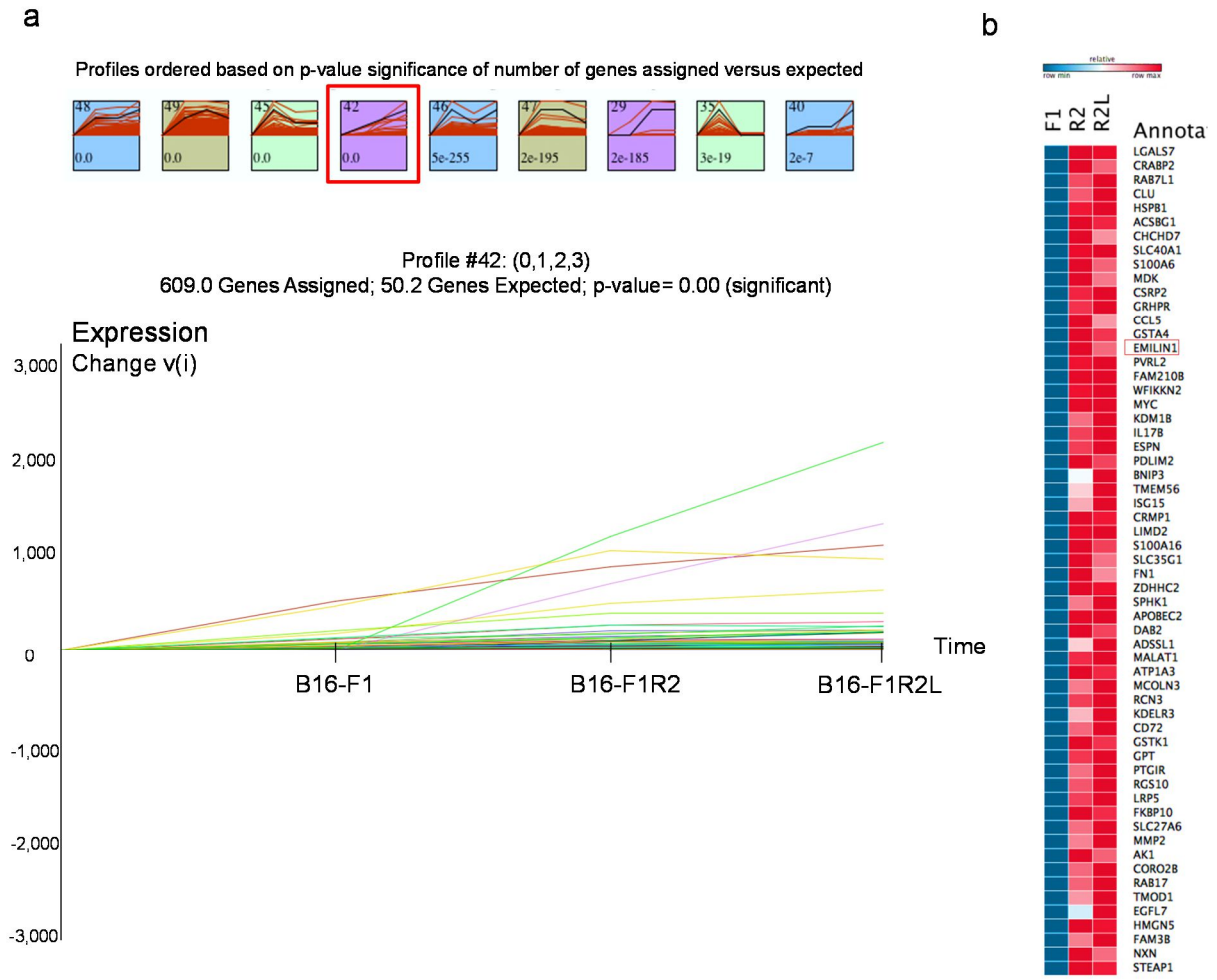

Fig.5 Analysis of gene expression profiles by RNAseq in B16-F1, B16-F1R2 and B16-F1R2L cell lines. **(a)** Gene cluster based on the differential gene expression referred to control cells B16-F1. **(b)** Heatmap of genes overexpressed in B16-F1-R2 and -R2L in profile 42.

We explored more in detail the differential expression profile between B16-F1 and B16-F1R2. We identified >3000 genes significantly up-regulated and >1000 significantly down-regulated in B16-F1R2 model compared to B16-F1, using a false discovery rate (FDR) of 0.05. Gene set enrichment analysis (GSEA) was done and we obtained a heatmap showing the principal down- and up-regulated pathways based on KEEG and REACTOME database **(Fig.6)**. As proteins related with extracellular matrix has appeared hyper-secreted after the mass spectrometry analysis, we

focused our attention on up-regulated pathways in B16-F1R2 cells. We observed that several pathways related with the extracellular matrix remodeling, integrin signaling were significantly increased in the analysis **(Fig.6)**.

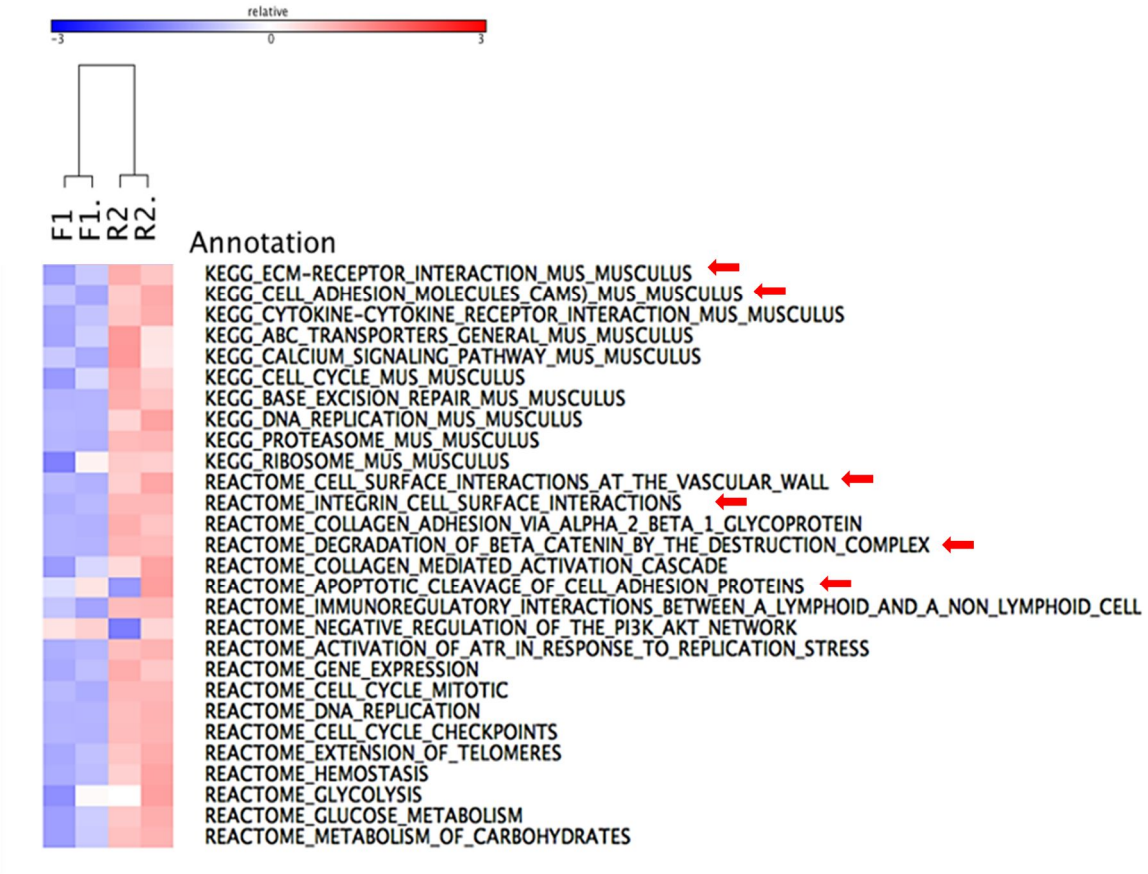

Fig.6 Heatmap showing the principal up-regulated pathways of mouse melanoma cell lines B16-F1 and B16-F1R2 based on KEEG and REACTOME database. Up-regulated pathways in B16-F1R2 model related with extracellular matrix and linked processes are indicated by the arrows.

5.1.3. Integration of exosome proteomic and RNA sequencing data

5.1.3.1. Correlation of proteomic and transcriptomic data

We observed that some overexpressed genes were codifying proteins hypersecreted in exosomes from B16-F1R2; therefore we performed an integration of the data obtained by mass spectrometry (proteins secreted in exosomes) with the data from the RNA sequencing **(Fig.7).**

Interestingly, out of several candidates we found that EMILIN1, a protein related to extracellular matrix remodelling, was hyper-secreted in the exosomes and also overexpressed at mRNA level. Other candidates found were Cd37 and Slc40a1 **(Table 2)**.

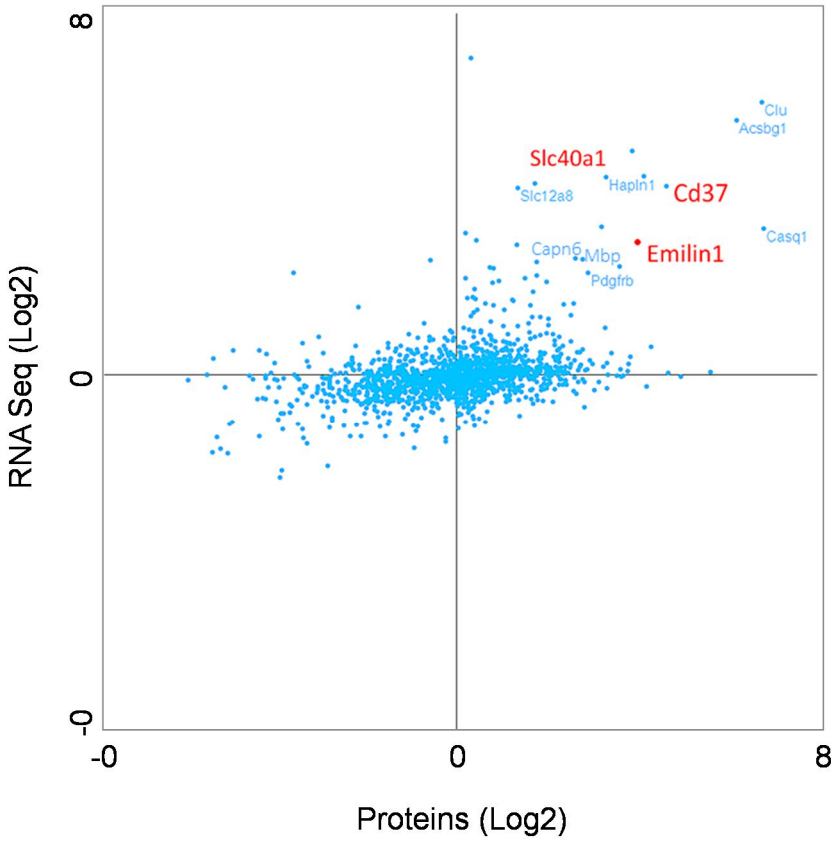

Fig.7 Correlation of proteomic and transcriptomic data to define the main genes overexpressed and proteins hyper-secreted in exosomes from B16-F1R2 compared to B16-F1 cell line. Main candidates are highlighted in red.

5.1.3.2. Biological interpretation of up-regulated and down-regulated genes set by ClueGo and Panther tools

Analysis of the proteins hyper-secreted and overexpressed in our lymphatic model B16-F1R2 by CluegGo [128] (Cytoscape plug-in) showed proteins and genes related with extracellular matrix and processes linked to tumour-microenvironment interaction such as ECM-receptor interaction, focal adhesion, laminin interaction and extracellular matrix organization **(Fig.8)**.

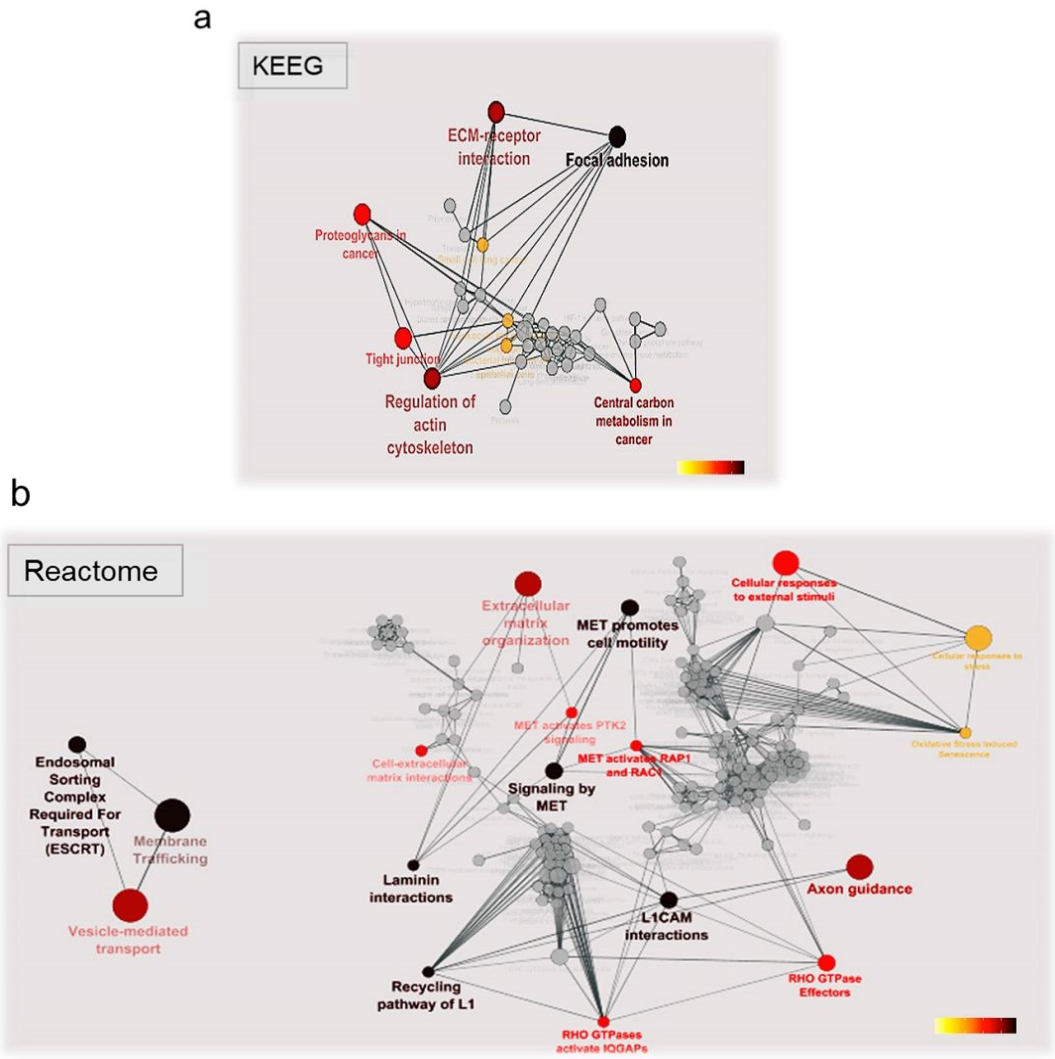

Fig.8 Principal complex networks visualized with ClueGO (Cytoscape plug-in) from the large cluster of genes obtain after proteomic and RNA sequencing data integration (a) KEEG and **(b)** REACTOME Pathways Gene Set up-regulated. Enrichment/ Depletion (two-side hypergeometric test) Bonferroni step down.

5.2. Analyze the role of Emilin1 in tumour cells and its secretion in exosomes

5.2.1. Validation of main the candidates found hyperexpressed and hypersecreted in exosomes from B16-F1R2 cell line

5.2.1.1. Analysis of mRNA expression in mouse melanocyte and melanoma cell lines

We next validated by qPCR, the expression of genes that were significantly hyper-secreted in exosomes and also overexpressed at mRNA level in B16-F1R2. We analyzed the expression in a panel of mouse melanocytes (melan-a), and mouse melanoma cell lines (B16-F1, B16-F1R2 and B16-F1R2L). Analysis of *Emilin1* expression showed that while it is highly expressed in melan-a cells, levels were downregulated in B16-F1 and then overexpressed again in B16-F1R2, R2L and F10 **(Fig.9a)**. The other candidates (*Cd37* and *Slc40a1*) showed higher levels of expression in B16-F1R2 and B16-F1R2L **(Fig.9b,c)**.

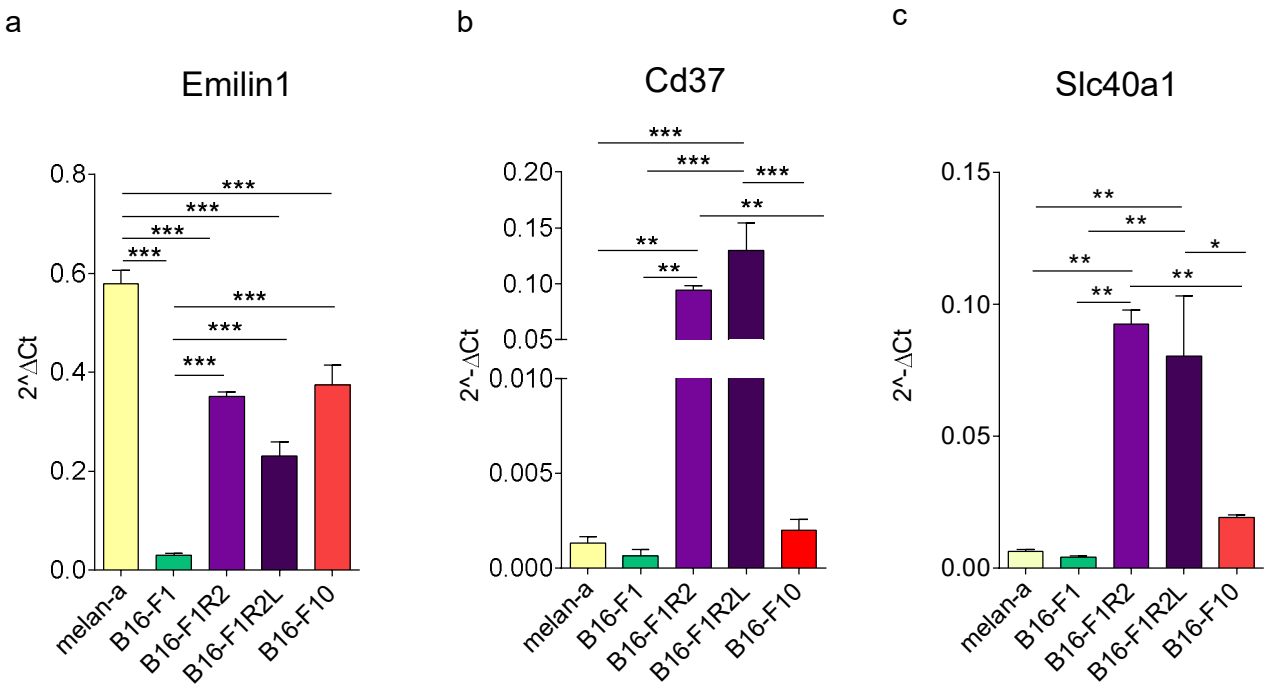

Fig.9 Analysis by qRT-PCR of the main genes found in the integration of proteomic-RNA seq data. **(a)** Analysis of Emilin1 (n=2), **(b)** Cd37 (n=1) and **(c)** Slc40a1 (n=1) expression in mouse melanoma models. *p<0,05 by One-way ANNOVA, Bonferroni´s Multiple Comparison.

We decided to investigate the role of EMILIN1 in melanoma progression and the relevance of its secretion in exosomes based on the functional role secreted exosomes from lymph node metastatic models. Moreover, EMILIN1 it has been previously linked to lymphangionesis, regulating cell adhesion and migration, skin homeostasis and with a potential role as tumour suppressor like protein [97, 115, 129, 130].

5.2.1.2. Analysis of Emilin1 expression at protein level in melanoma cell lines

Analysis of Emilin-1 expression by Western-blot in mouse melanoma models demonstrated that is not detected intracellularly while it is secreted in exosomes derived from lymph node metastatic models B16-F1R2 and B16-F1R2 **(Fig.10a)**. Analysis in human melanoma models showed that contrary to mouse models, Emilin1 was expressed both intracellularly and in exosomes, however secretion in exosomes was only observed in the lymph node metastatic model IGR37 **(Fig.10b)**. Of note, Emilin1 was detected in several bands with a lower molecular weight than expected in secreted exosomes and in human models, suggesting its degradation. Previous evidences suggested that proteolytic activities such as neutrophil elastase fully impair the function of Emilin1 by degradation [115, 129]. Therefore, we hypothesised that exosome secretion and degradation may be a novel mechanism of Emilin1 degradation and expulsion in melanoma.

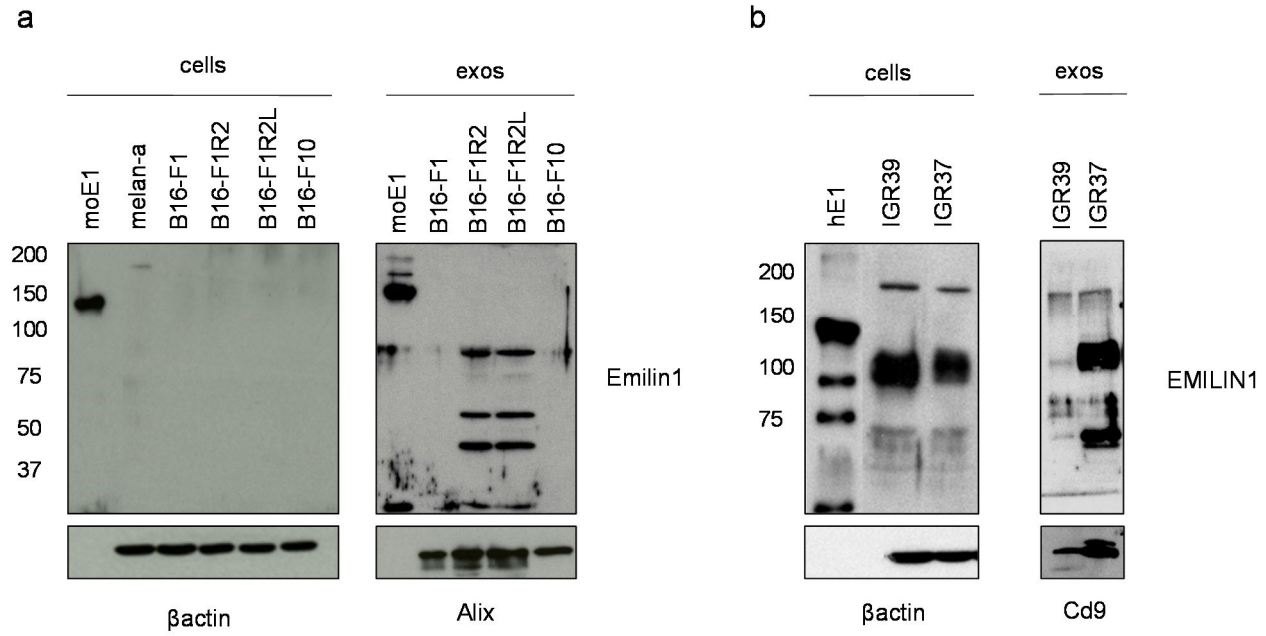

Fig.10 Analysis by Western-blot of Emilin1 in **(a)** mouse cell line models and derived exosomes (B16-F1, B16-F1R2, B16-F1R2L and B16-F10) and **(b)** human cell line models and derived exosomes (IGR39 and IGR37). *moE1* and *hE1* are Emilin1 recombinant mouse and human proteins used as positive control.

5.2.1.3. Analysis of Emilin1 by immunofluorescence in mouse melanocyte and melanoma cell lines

We next analysed the expression of Emilin1 by immunofluorescence. We found that Emilin1 is secreted and deposited as extracellular matrix in melan-a melanocytes **(Fig.11a)**. Analysis in melanoma models showed that Emilin1 levels were almost undetectable B16-F1 **(Fig.11b)** while in

B16-F1R2 were increased compared to F1 cells but not deposited extracellularly as observed by immunofluorescence **(Fig 11c)**. Overall, our results support that Emilin1 is expressed and deposited extracellularly in melan-a melanocytes while its levels drops dramatically in B16-F1 cell line. Analysis in the lymph node metastatic model B16-F1R2 demonstrated that Emilin1 is upregulated at mRNA level but almost not detected intracellularly, secreted and degraded in exosomes and as a consequence, not deposited extracellularly. These data suggest that Emilin1 levels are reduced intracellularly along melanoma progression, its secretion and degradation in exosomes may be a novel mechanism favouring melanoma progression and lymph node metastasis. Nevertheless, analysis in human models showed that the mechanism may differ since Emilin1 is detected also intracellularly.

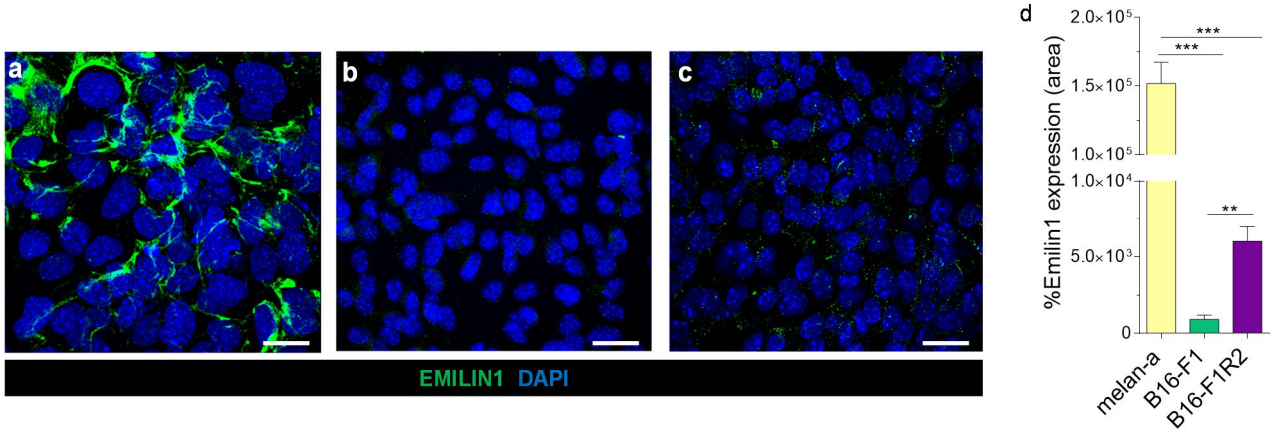

Fig.11 Analysis of Emilin1 expression by confocal immunofluorescence in **(a)** melanocytes, **(b)** B16-F1 and **(c)** B16-F1R2 cell lines. Analysis denote that while Emilin1 is secreted and deposited as an extracellular matrix protein by melanocytes, in melanoma cells Emilin1 levels drop and there is no deposition extracellularly. Scale 18 μm **(d)** Quantification of Emilin1 expression by area. *p<0,05 by Non-parametric t-test.

Since EMILIN1 appeared secreted and degraded in exosomes, we decided to analyse the mechanism involved in EMILIN1 degradation focusing on two pathways:

i) Proteasome
ii) Extracellular vesicle secretion

5.2.1.4. Inhibition of proteasome in mouse melanocyte and melanoma cell lines

To investigate if the proteasome is involved in Emilin1 cleavage, we treated melan-a, B16-F1 and B16-F1R2 cells with the proteasome inhibitor MG-132 **(Fig.12)**. MG-132 is a potent, reversible, and

cell-permeable proteasome inhibitor and reduces the degradation of ubiquitin-conjugated proteins in mammalian cells [131, 132]. We observed that Emilin1 levels remained similar after MG-132 treatment in all cell types **(Fig.12 a-d, b-e, c-f)**, suggesting that proteasome inhibition does not affect Emilin1 levels.

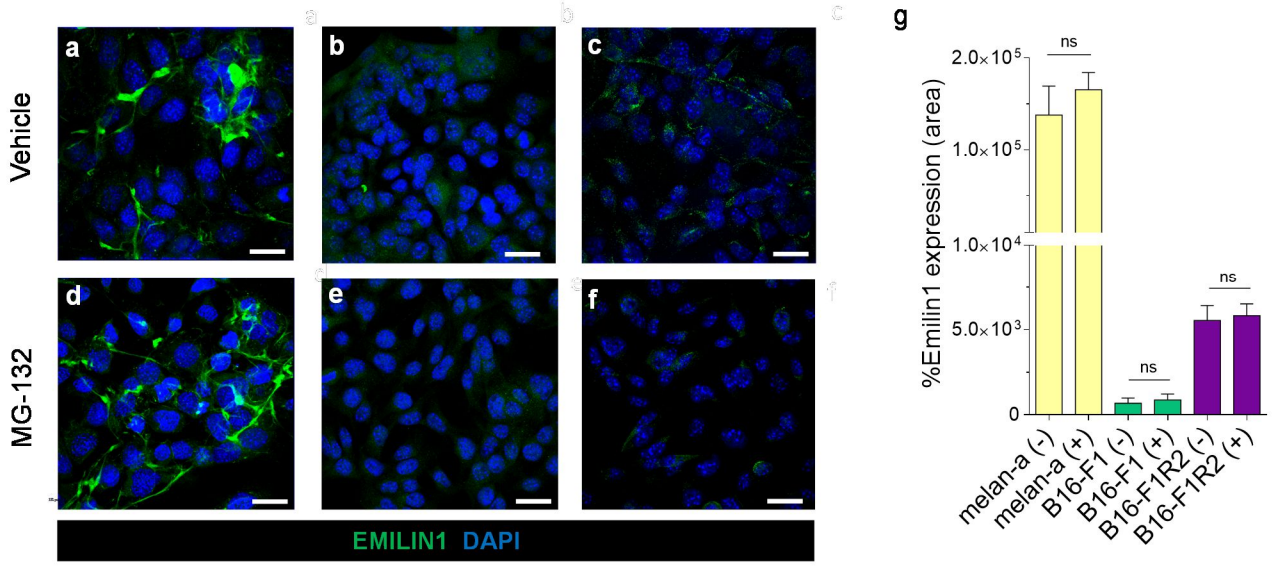

Fig.12 Analysis of Emilin1 expression by confocal immunofluorescence in **(a)** melanocytes, **(b)** B16-F1 and **(c)** B16-F1R2 cell lines before and after the treatment **(d, e, f)** with 8 micromolar **MG-132** during 16 hours. **(g)** Analyses denote that treatment does not affect Emilin1 levels. Scale 18 µm *p<0,05 by Non-paremetric t-test.

5.2.1.5. Inhibition of extracellular vesicle secretion in mouse melanocyte and melanoma cell lines

Next we tested the influence of the extracellular vesicle secretion inhibitor GW4869, a non-competitive inhibitor of sphingomyelinase [133, 134]. We observed that while treatment with GW4869 does not affect Emilin1 in melan-a **(Fig.13a-d)** and B16-F1 cells **(Fig.13b-e)**, the treatment led to a significant accumulation in B16F1-R2 **(Fig.13c-f)**. These data suggest that the main pathway of Emilin1 secretion and degradation in B16-F1R2 is the extracellular vesicle secretion.

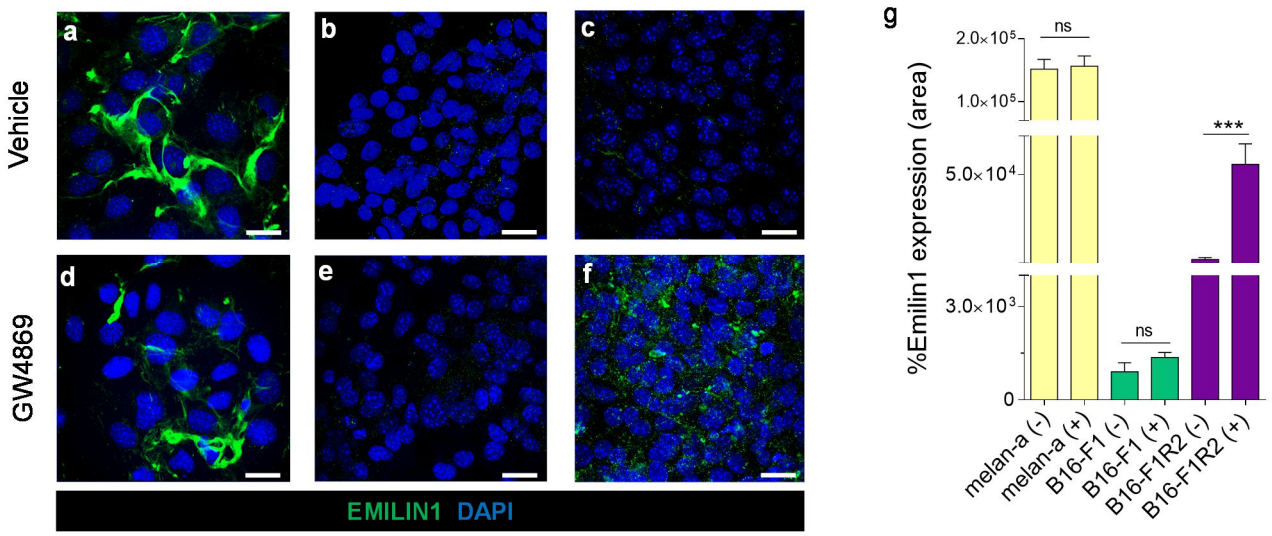

Fig.13 Analysis of Emilin1 expression by confocal immunofluorescence in **(a)** melanocytes, **(b)** B16-F1 and **(c)** B16-F1R2 cell lines before and after after the treatment **(d, e, f)** with 10 micromolar **GW4869** during 24 hours. **(g)** Analyses denote that while Emilin1 increase after the treatment in B16-F1R2 cells. Scale 18 µm *p<0,05 by Nonparemetric t-test.

5.2.2. Effect of extracellular vesicle inhibition in primary tumor growth and metastasis

5.2.2.1. Analysis of B16-F1R2 primary tumor growth and metastasis after GW4869 inhibition

Since we observed Emilin1 accumulation after GW4869 inhibition we analysed its effect in primary tumour growth and metastasis. Mice were injected in the flank with 1×10^6 B16-F1R2 cells. Five days later, mice were treated three times per week with the inhibitor GW4869 and PBS-DMSO as control **(Fig.14a, scheme of the experiment)**. Interestingly, we observed that treatment with GW4869 reduced significantly tumour growth after 16 days **(Fig.14)**. Analysis of metastasis by *ex vivo* IVIS imaging showed a reduction of metastasis to the lungs and liver but not to the lymph nodes **(Fig.14c, d)**. These data support that inhibition of extracellular vesicle secretion reduces primary tumour growth and distal metastasis suggesting that prevention of Emilin1 secretion and degradation may act as *tumour suppressor-like* activity, however we can not rule out the side effect of this inhibitor in other pathways that may be responsible for this effect.

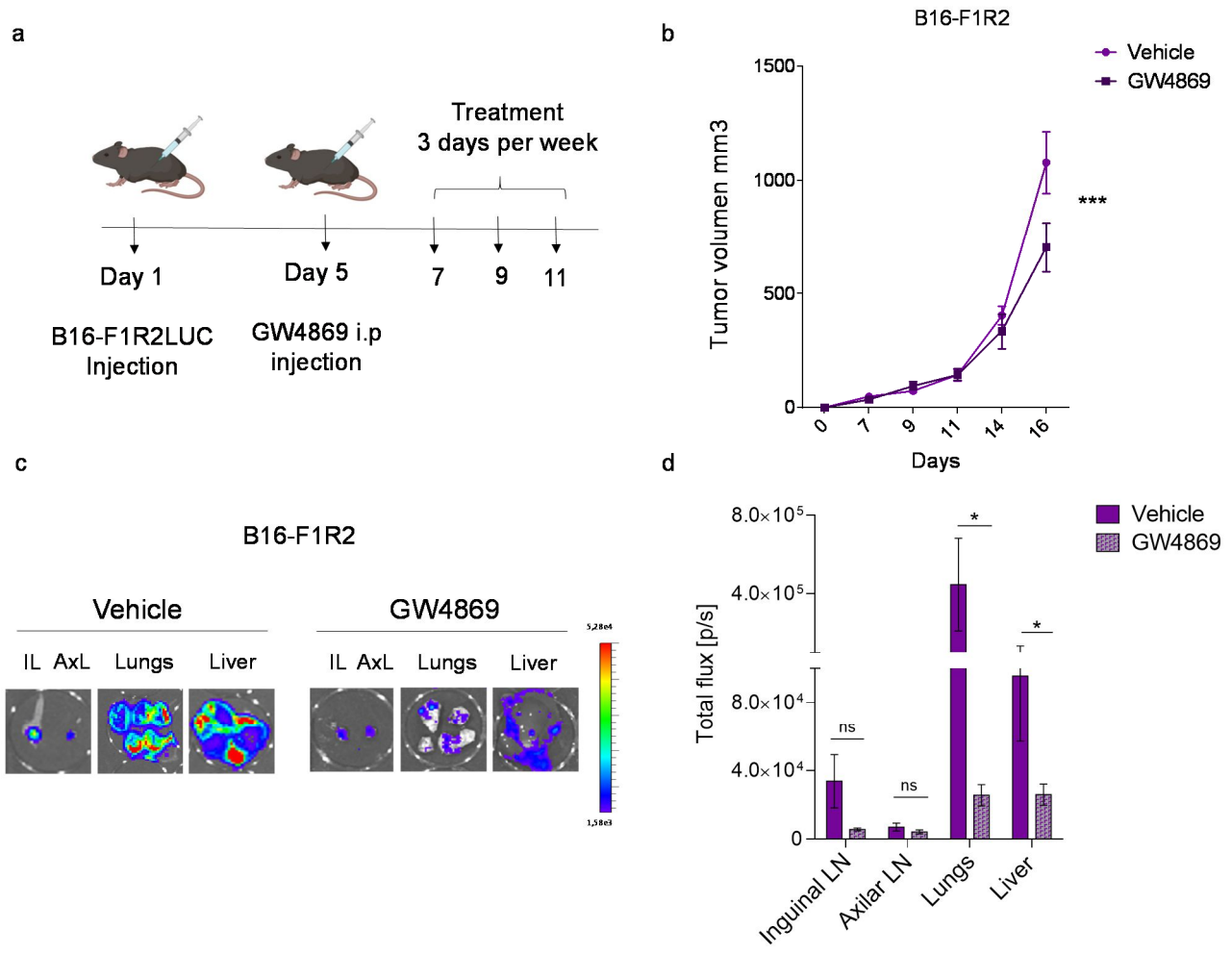

Fig.14 Analysis of the effect of GW4869 in B16-F1R2 primary tumor growth and metastasis. **(a)** Experimental set-up B16-F1R2-LUC xenografts were injected in C57BL/6 mice subcutaneously with $1x10^6$ cells. Five days later, mice were treated (i.p injection) three times per week with the inhibitor GW4869 (60 µg per mice) and PBS-DMSO as control **(b)** Tumor volume was monitored twice a week for 16 days, n=6 tumors per group;***p<0,001 by 2-way ANOVA. **(c)** Representative images of the analysis by IVIS of spontaneous metastasis in inguinal (IL) and axillar (AxL) lymph nodes, lungs and liver. **(d)** Total flux quantification of metastatic organs.*p<0,05 by Nonparametric t-test.

5.2.2.2. Characterization of B16-F1R2 primary tumours after GW4869 inhibition by RNA sequencing

Since treatment with GW4869 reduced primary tumour growth, we wanted to define the gene expression profile by RNA sequencing. Unfortunately, analysis by principal component analysis (PCA) showed a high variability among groups **(Fig.15a)**. Nevertheless, we performed Gene Set Enrichment Analysis (GSEA) in three tumours defining several set of genes significantly affected **(Fig.15b)**. The pathways significantly enriched (FDR<0.1) in B16-F1R2 tumours compare to GW4869 treatment are related with vesicle transport, cell-cell communication and extracellular

matrix, supporting that the inhibition of exosomes in the lymphatic model impairs those biological process.

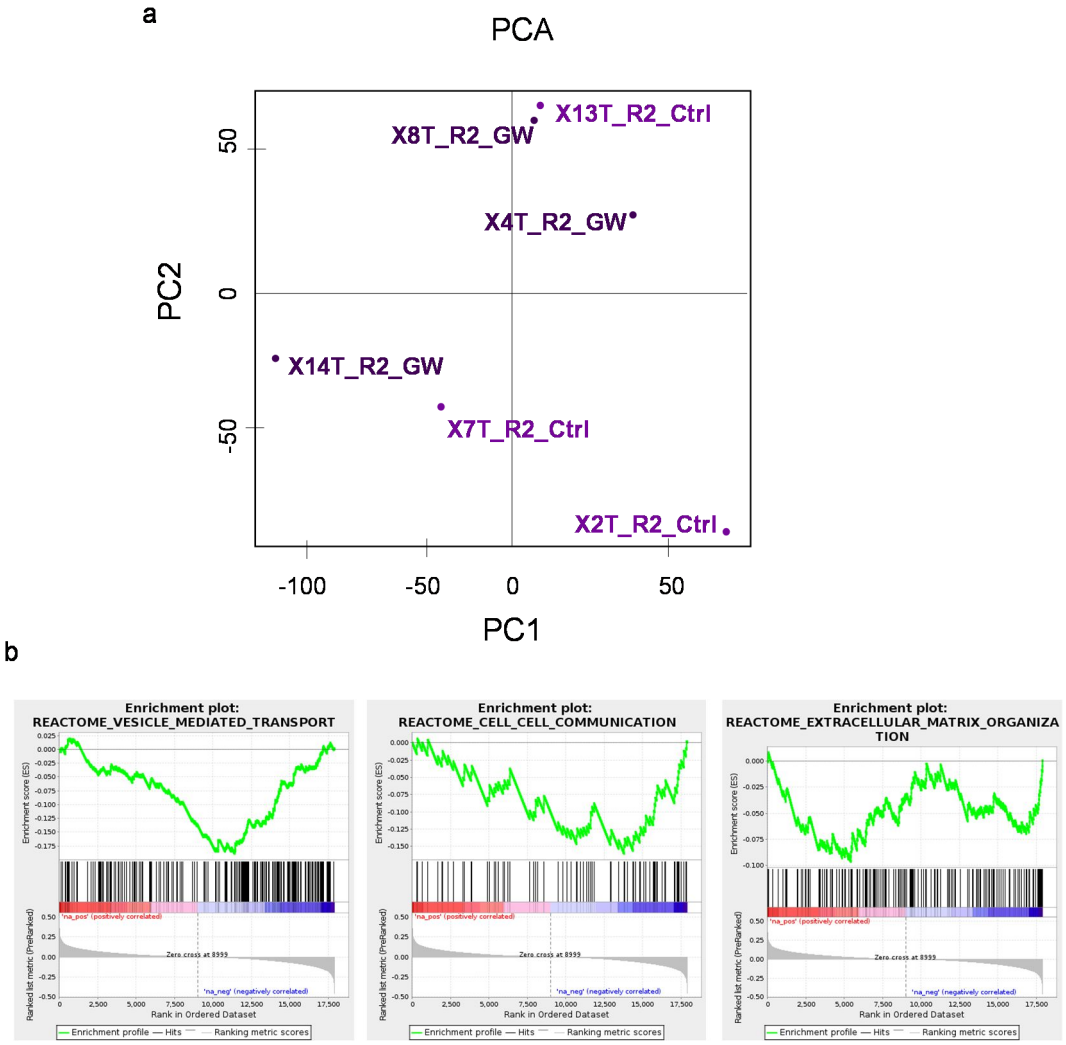

Fig.15 RNA seq analysis of B16-F1R2 primary tumors vehicle and treated with GW4869. (a) Principal component analysis (PCA 2D) of the samples (n=3). The analysis shows an intragroup variability. **(b)** GSEA pathways enriched in B16-F1R2 tumors compare to tumors from exosome inhibitor treatment FDR < 0,1 from REACTOME database.

5.2.3. Defining the role of Emilin1 in melanoma cell lines

5.2.3.1. Generation of HA-EMILIN1 B16-F1 model

Since Emilin1 has been already reported as a *tumor suppressor-like* protein [135] and we observed that in lymph node metastatic cells is hypersecreted and degraded, we postulated that Emilin1 may has a negative effect on melanoma progression. To test the effect of Emilin1 in melanoma, we cloned the full length cDNA fused to the epitope HA and generated stable transfectants.

We first verified HA-Emilin1 overexpression by immunofluorescence **(Fig.16a, b)** and mRNA levels **(Fig.16c)** in B16-F1 cells.

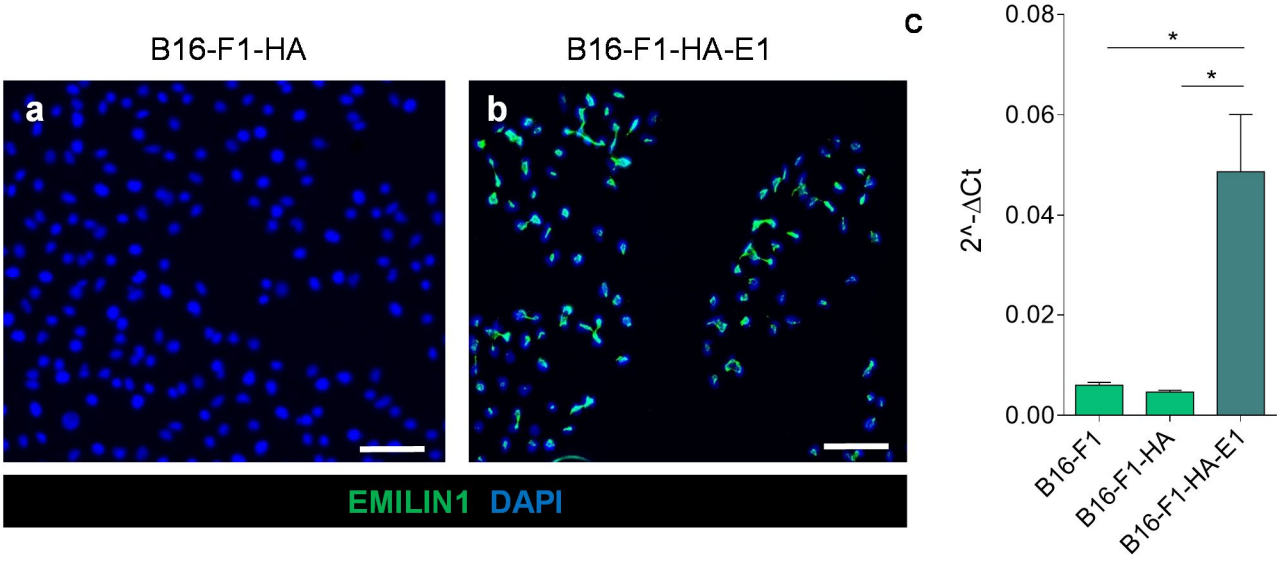

Fig.16 Characterization of HA-Emilin1 overexpression in cell lines. Analysis of HA-Emilin1 expression by immunofluorescence in **(a)** B16-F1HA control cells expressing the empty vector and **(b)** B16-F1-HA-E1 expressing HA-Emilin1. Scale 50 µm. **(c)** Analysis of Emilin1 mRNA levels in indicated models by qRT-PCR. n=1, *p<0,05 by Unpaired t-test

5.2.3.2. Characterization of cell viability and cell cycle after EMILIN1 overexpression in B16-F1

To define the intrinsic role of Emilin1 in melanoma cells we analysed its influence in cell viability and cell cycle assays. To define the effects on cell proliferation we analysed number of viable cells based on quantitation of the ATP present at different time points (24, 48 and 72h). We observed that overexpression of Emilin1 reduced significantly B16-F1 cell viability in three different clones analysed **(Fig.17a).** To determine if this reduction was due to changes in cell cycle, we analysed cell cycle histograms for bulk DNA staining (PI), after addition of EdU, from B16-F1 and B16-F1 E1 model were performed at 24, 48, 72, 96 h and 1 week **(Fig.17c)**. Analysis of the percentage of cells in S phase was also calculated **(Fig.17d)**.

We found that Emilin1 overexpression does not affect significantly cell cycle in B16-F1 cells. These results suggest that Emilin1 affect mainly the metabolic balance and cell viability in cells but not the cell cycle of the cells.

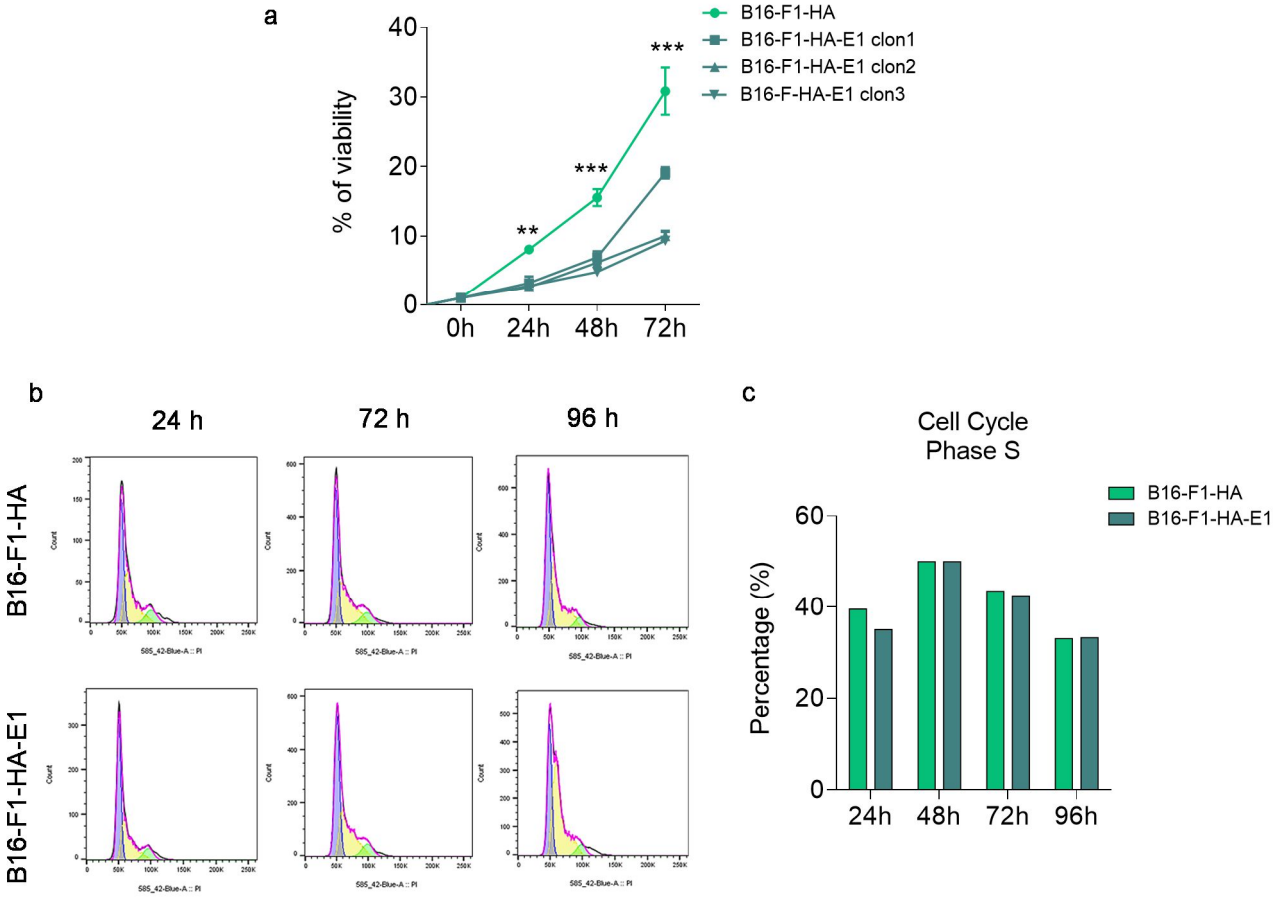

Fig.17 Analysis of cell viability and cell cycle after EMILIN1 expression. (a) Luminescent Cell Viability Assay (*CellTiter-Glo)* of B16-F1-HA and different clones of B16-F1 cells overexpressing EMILIN1 at indicated time point (n=2) **p<0,01 and ***p<0,001 by 2-way ANOVA. **(b)** Cell cycle histograms for bulk DNA staining (PI) by flow cytometry, from B16-F1 and B16-F1 E1 model at 24,72 and 96 hours. **(c)** Percentage of B16-F1 and B6-F1 E1 cells in S phase after addition of Edu.

5.2.3.3. Cell tracking analysis in Emilin1 overexpressing melanoma cells

Then, we performed melanoma cell tracking assays in B16-F1 cells overexpressing Emilin1. These experiments showed that cells overexpressing Emilin1 have no directed migration **(Fig.18).** Data suggest that Emilin1 expression leads to loss migration directionality and reduction of cell viability. Therefore, it is plausible that reduction of intracellular Emilin1 levels observed along melanoma progression could be required for an efficient and independent migration, a well-known property of melanoma cells.

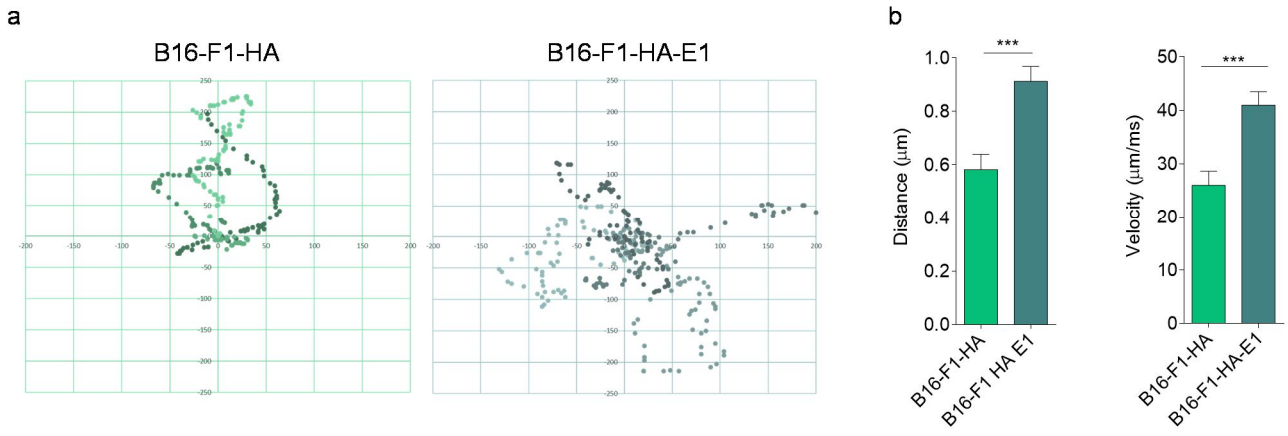

Fig.18 **(a)** Cell tracking and motility analysis of B16-F1-HA and B16-F1-HA E1 models. **(b)** Distance and velocity of cell tracking analysis by ImageJ software ***p<0,001 by Unpaired t-test

5.2.4. Defining the role of Emilin1 secretion in exosomes

5.2.4.1. Influence of exosome-secreted Emilin1 in lymphangiogenesis

Based on our results, Emilin1 is secreted and degraded in exosomes as novel mechanism to discard a *tumor suppressor like*-protein in melanoma. Nevertheless, the role of Emilin1 extrinsically secreted in exosomes have never been studied. Since, Emilin1 deposition in the ECM has been previously related to lymphatic system development [111,112], we wanted to study the influence of exosome-secreted Emilin1 in lymph nodes. For that we isolated exosomes from B16-F1-HA and B16-F1 cells overepressing HA-Emilin1 and and injected intra-footpad three times during the first week, and two times during the second week with 5 µg of exosomes **(Fig.19a, scheme of the experiment)**. Popliteal lymph nodes were stained with HA-Emilin1 and Lyve-1 antibodies. Both proteins were co-localized in the same region of the lymph nodes **(Fig.19b)** and the expression of both proteins showed us a correlation between them **(Fig.19c).**

This result suggests that Emilin-1 positive exosomes reinforce Lyve-1 and correlate with areas where exosomes were taken up. However, we could not find significant differences in Lyve-1 expression when comparing Emilin1 positive exosomes with controls (B16-F1-derived exosomes), suggesting that B16-F1-derived exosomes carry already determinants promoting lymphangiogenesis **(Fig.19d)**.

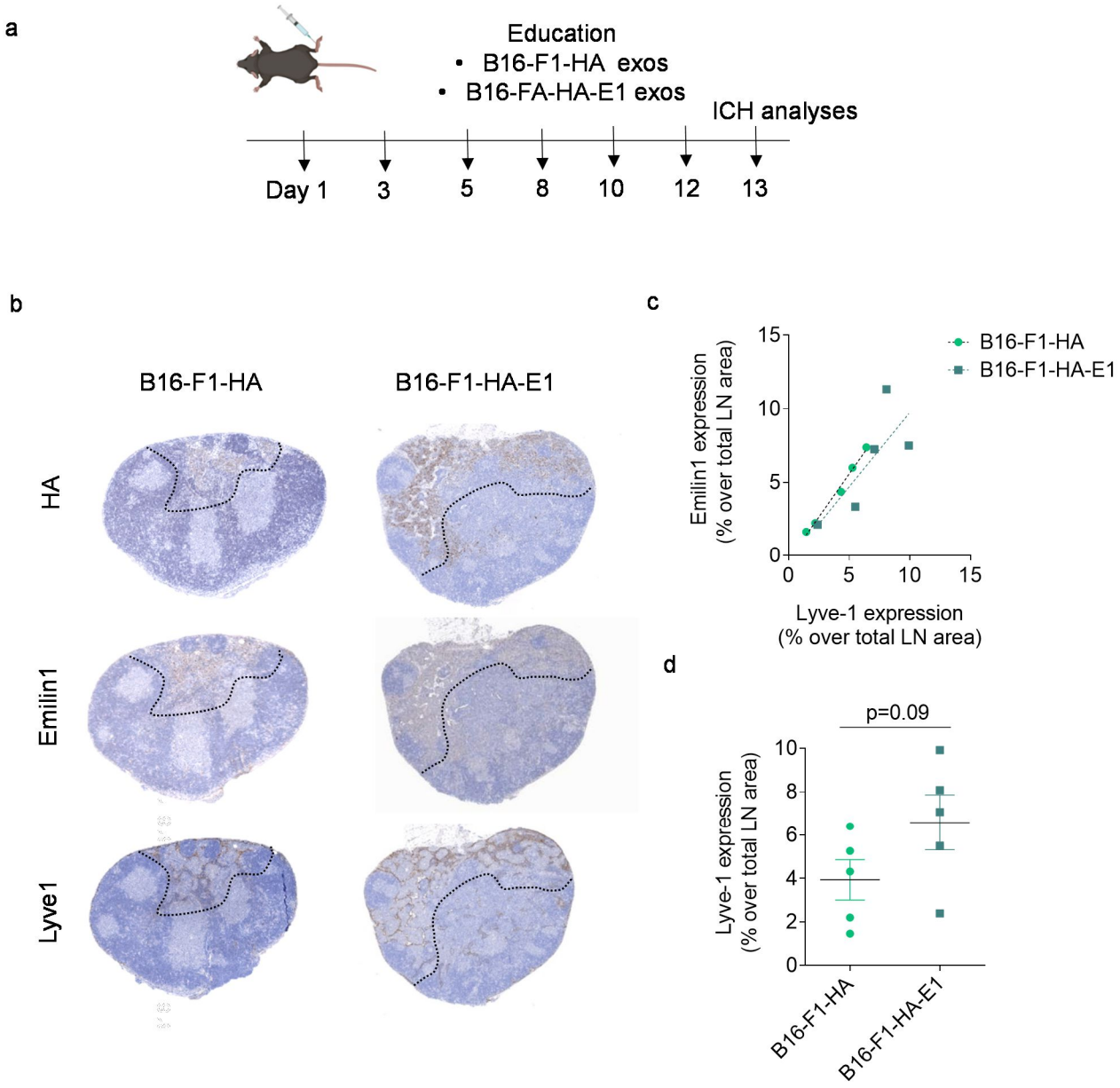

Fig.19 Analysis of exosome uptake and lymphagiogenesis by immunohistochemistry popliteal lymph nodes after 2 weeks of exosome education derived from B16-F1-HA and B16-F1-HA-E1 models. **(a)** Experimental set-up C57BL/6 mice were injected intra-footpad three times during the first week, and two times during the second week with 5 µg of exosomes from B16-F1-HA or B16-F1-HA-E1 **(b)** Representative images of HA, Emilin1 and Lyve-1 staining and localization in the popliteal lymph nodes. **(c)** Correlation of Emilin1/Lyve-1 expression, n=5, R=0,99 (B16-F1-HA) and R=0,61 by Linear regression statistic. **(d)** Quantification of Lyve-1 expression over total LN area (percentage) in both models (B16-F1-HA and B16-F1-HA-E1), p value by Nonparametric t-test

Immunofluorescence analysis of Emilin1, Lyve-1 and CD31 was also performed by confocal microscopy **(Fig.20a).** Treatment with exosomes derived from B16-F1-HA-E1 increased Lyve-1 expression, suggesting an influence of Emilin1 in lymphangiogenesis again, however we could not detect significant differences compared to B16-F1 control exosomes (**Fig.20b).**

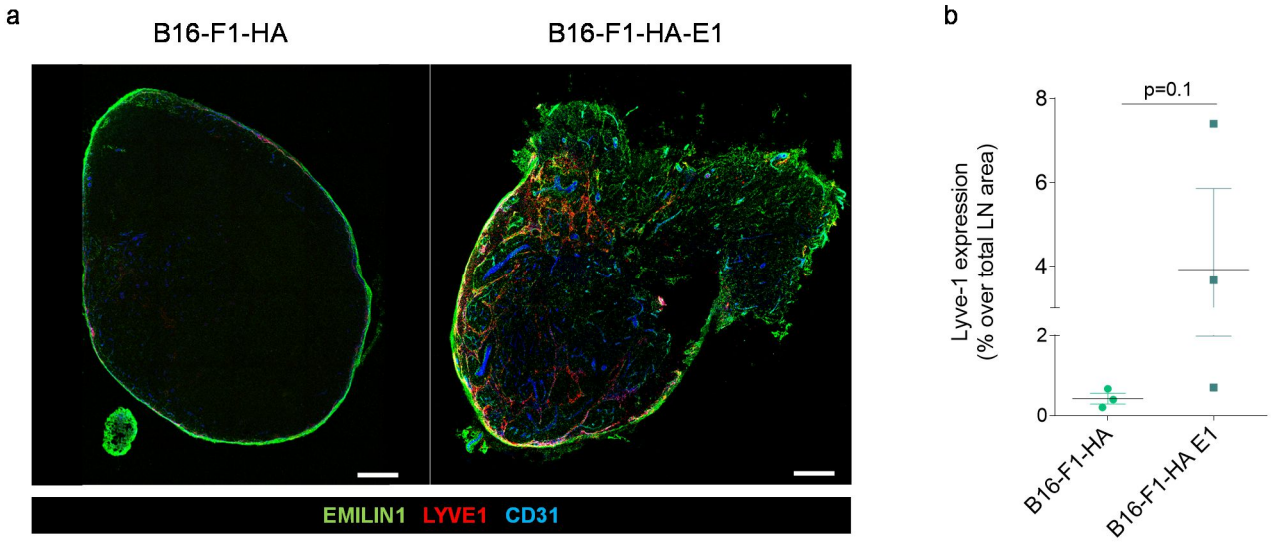

Fig.20 Analysis of exosome uptake and lymphagionesis by immunoflurescence (a) Representative images of Emilin1, Lyve-1 and CD31 staining and localization in the popliteal lymph nodes, Scale 100 µm **(b)** Quantification of Lyve-1 expression over total LN area (percentage) in both models (B16-F1-HA and B16-F1-HA-E1) n=3 p value by Nonparametric t-test.

5.2.4.2. Influence of exosome-secreted Emilin1 in lymph node metastasis (homing)

We wanted to analyse the relevance of Emilin1 secreted in exosomes in lymph node metastasis. To that end mice were injected intra-footpad three times during the first week, and two times during the second week with 5 µg of B16-F1-HA and B16-F1-HA-E1 exosomes **(Fig.21a)**. The next day after the last injection, $2x10^4$ B16-F1-HA cells were injected in both pads of the mice. We analysed melanoma cell homing after 24h. Luciferase imaging was done *ex vivo* to popliteal and inguinal lymph nodes **(Fig.21b)**.

Data showed that both B161-HA and B16-F1-HA-E1 exosomes, increased significantly the homing and metastasis in comparison with PBS- treatment, supporting that melanoma-derived exosomes reinforce metastasis [30]. However, we could not find significant differences comparing exosomes overexpressing Emilin1 with B16-F1-derived exosomes **(Fig.21c)**. Overall, our data suggest that melanoma-derived exosomes from low metastatic models already influence lymphangiogenesis and metastasis, however overexpression of Emilin1 in exosomes does not increase significantly lymphangiogenesis nor metastasis, supporting that discarding and degradation of Emilin1 in exosomes may favour melanoma progression since the relevance of its secretion in exosomes may not confer a selective advantage.

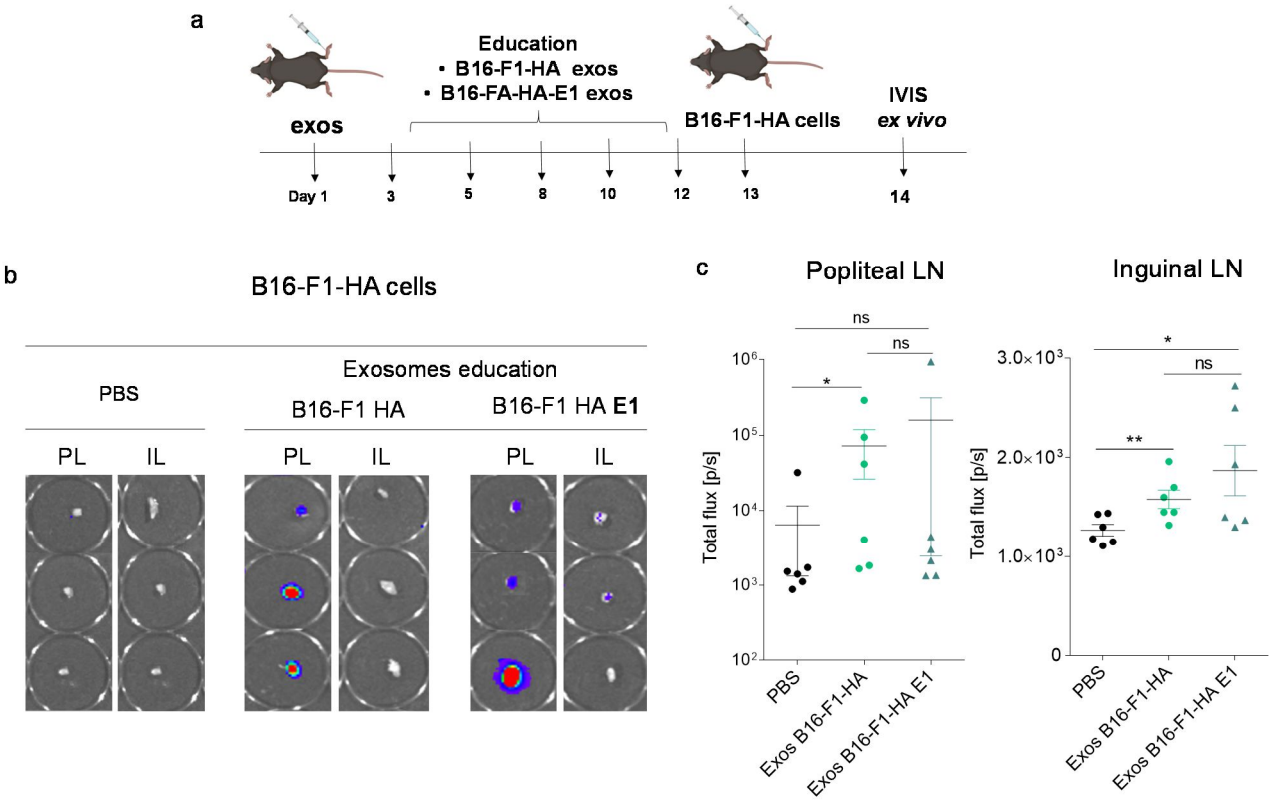

Fig.21 **(a)** Analysis by In Vivo Imaging System (IVIS) of popliteal and inguinal lateral lymph nodes from intra-footpad injected mice with 200.000 B16-F1 HA after 2 weeks of exosome education derived from B16-F1-HA and B16-F1-HA E1 models **(b)** Total flux quantification of popliteal and inguinal lymph node. *p<0.05 by Nonparemetric t-test.

5.2.4.3. Emilin1 expression during lymphangiogenesis

Since the correlation of Emilin1 secretion in exosomes and increased lymphangiogenesis was limited, we wanted to analyse the correlation of endogenous Emilin1 in that process using a well-known lymphangiogenesis inducer such as TNF-α [136] **(Fig.22).** We injected two times per week during 10 days and analysed by immunofluorescence the lymph nodes. We observed an increase in Emilin1 expression after the treatment **(Fig.22b)** and also small vessels in the lymph node stained with Emilin1. Higher magnification images represent better the localization of our proteins that show how Emilin1 is bordering positive Cd31 vessels **(Fig.22a,b)**. These data support that endogenous Emilin1 expression is induced during inflammatory processes that produce and increase in the lymphangiogenesis and deposition in the ECM, supporting the relevance of Emilin1 in the microenvironment during lymph vessel development.

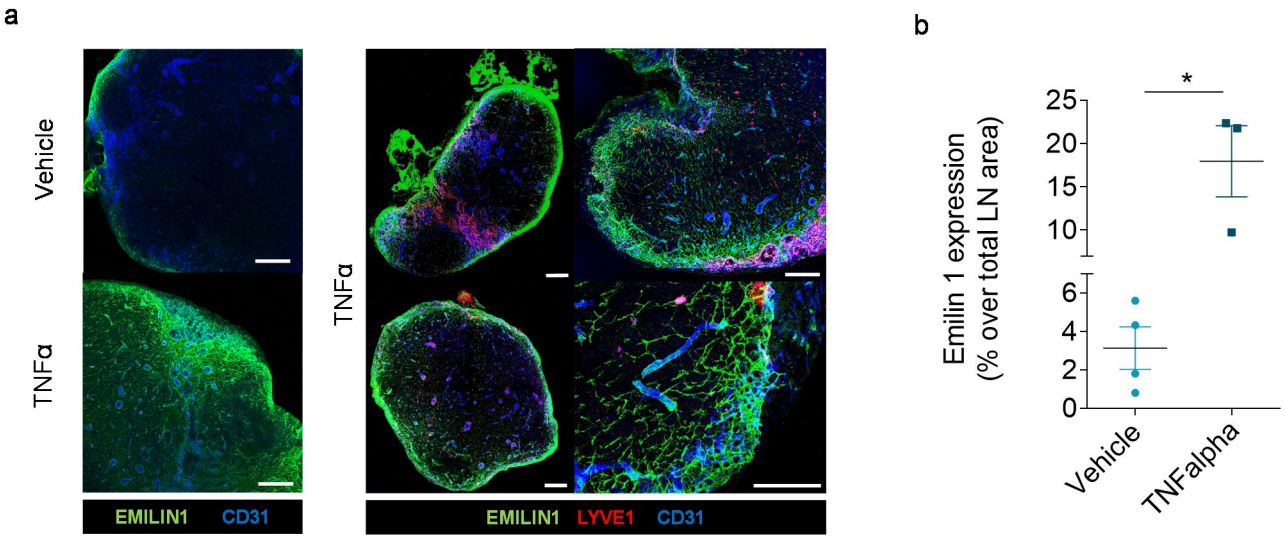

Fig.22 Analysis of Emilin1, CD31 and Lyve1 expression in lymph nodes by immunofluorescence after TNF-α treatment during two times per week by intraperitoneal injection. **(a)** Representative images of vehicle and treated lymph nodes. Scale 100 μm **(b)** Quantification of Emilin1 expression percentages over total lymph node area, p-value by Unpaired t-test

5.3. Investigate the role of Emilin1 in melanoma tumour growth and metastasis

5.3.1. Define the role of Emilin1 in the microenvironment during melanoma progression

5.3.1.1. Analysis of B16-F1R2 cells in tumour growth and metastasis in EMI-/- mice by subcutaneous and intrafootpad injection

Previous data from Dra. Spessotto and colleagues has described that Emilin1 expression in the microenvironment has a *tumour suppressor-like* role [116]. Based on these results, we analysed tumour growth and metastatic behaviour of B16-F1R2 in Emilin1 knock out mice *(EMI-/-)* mice. For the analysis of tumour growth and melanoma spontaneous metastasis, mice were injected in the flank with 1×10^6 B16-F1R2 cells. Tumour volume was monitored 2-3 times per week and the animals were sacrificed when tumour volume got 1.2 cm^3. We observed that tumour growth in *Emilin1(-/-)* mice led to a significantly decrease tumour growth in time **(Fig.23a).** Analysis of proliferative markers of the tumours showed us similar and/or proliferative necrotic areas, suggesting that others processes are involved **(Fig.23b).**

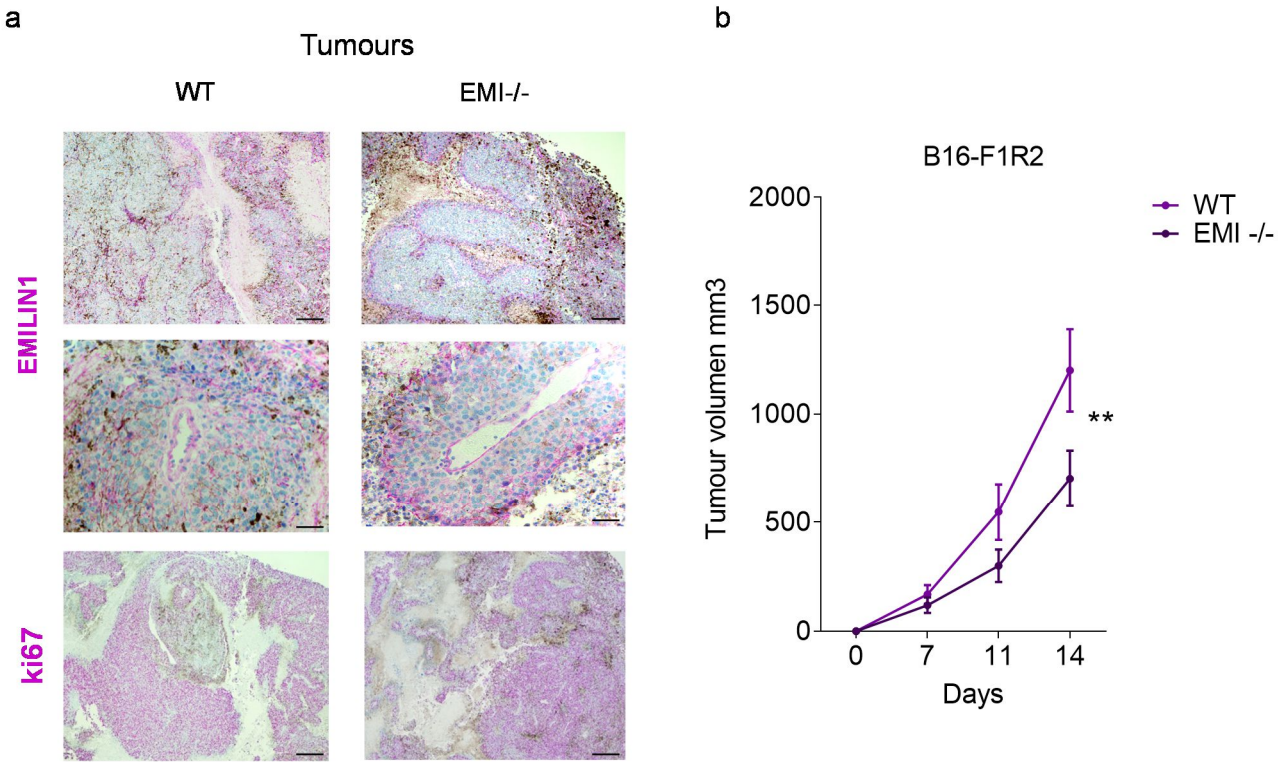

Fig.23 Analysis of the role of EMILIN1 in the microenvironment during melanoma progression *in vivo*. (a) Representative tumour images Emilin1 stained from C57BL/6 mice WT and EMI-/- mice. Scales 500, 200 and 100 µm. **(b)** Tumor growth of B16F1-R2 xenografts. C57BL/6 WT (n=8) and EMI-/- (n=13) mice were injected subcutaneously with $1x10^6$ B16-F1R2 cells. Tumour volume was monitored twice a week during 14 days. n=12 **p<0,01 by 2-way ANOVA

Analysis of lymph node metastasis was performed in spontaneous metastasis from mice injected in the flank as above and in mice injected intra-footpad with $2x10^4$ B16-F1R2 cells for experimental metastasis assays. In the later, animals were sacrificed 21 days after injection. Popliteal and inguinal lymph nodes were stained with HMB45 and the percentage of melanoma positive cells quantification was performed in both approaches **(Fig 24)**. Analysis showed no differences in metastasis, neither in melanoma spontaneous metastasis (subcutaneous injection, **Fig 24 a, b**) nor in experimental metastasis assay (intra-footpad injection, **Fig 24 c,d**) in *WT* and *EMI-/-* mice.

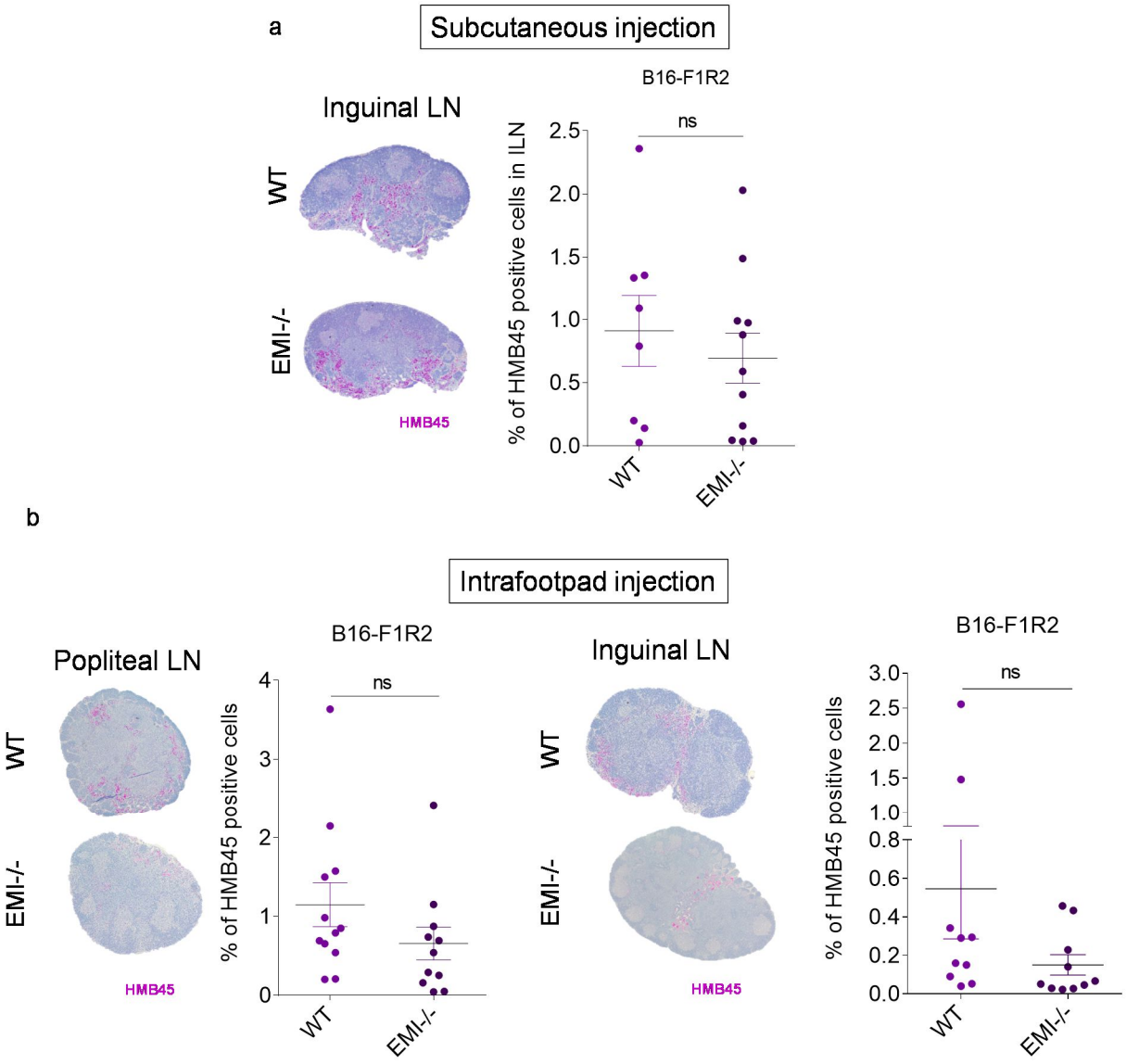

Fig.24 (a) Analysis of lymph nodes from C57BL/6 WT and EMI-/- mice injected subcutaneously with 10^6 B16-F1R2 cells. Representative images of inguinal lymph nodes (HMB45 staining) from C57BL/6 mice WT and EMI-/- mice and percentage of melanoma HMB45 positive cells quantification of inguinal lymph nodes n=8 (WT), n=11 (EMI-/-) p value by Nonparemetric t-test **. (b)** Analysis of lymph nodes from C57BL/6 WT and EMI-/- mice injected intra-footpad with $2x10^4$ B16-F1R2 cells. Representative images of popliteal and inguinal lymph nodes (HMB45 staining) from C57BL/6 mice WT and EMI-/- mice and Percentage of melanoma HMB45 positive cells quantification from popliteal (n=11) and inguinal (n=11), p value by Nonparemetric t-test

Previous analysis supported that Emilin1 microenvironment support both tumour and metastasis in B16-F10 cells [116]. Our experiments showed that there is a reduction of primary tumour growth in *Emilin1 (-/-)* mice while we did not observed changes in metastatic behaviour. This could be explained since B16-F1R2 cells are already tropic to the LNs may not be influenced by an Emilin1

negative microenvironment in the lymph nodes. Analysis of additional factors involved in the control of lymph node metastasis is needed to define a clear model.

5.3.2. Analysis of Emilin1 and mutants in primary tumour and metastasis

5.3.2.1. Analysis of tumour growth and metastasis in B16-F1-HA and B16-F1-HA-E1 models: subcutaneous and intrafootpad injection

Although overexpression of Emilin1 already suggested an intrinsic role reducing cell viability and impairing efficient migration, we wanted to analyse its role *in vivo* defining its effect in tumour growth and metastasis by overexpressing Emilin1 in B16-F1 cells. Importantly, we found significant decrease of tumour growth when Emilin1 is overexpressed **(Fig.25).**

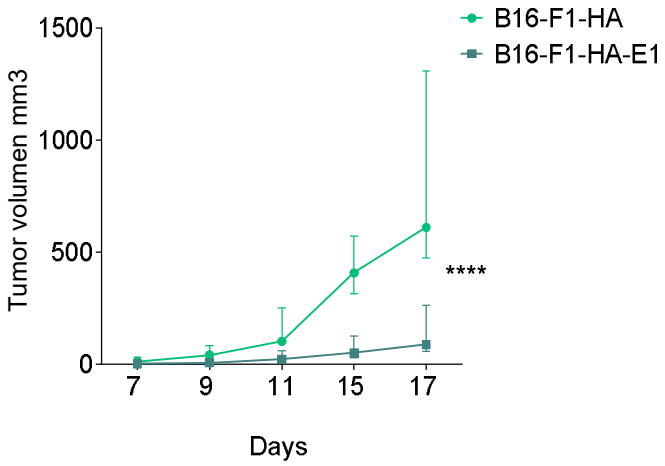

Fig.25 Analysis of Emilin1 role during melanoma progression *in vivo*. Tumour growth of B16F1-HA and B16-F1-HA E1 xenografts. C57BL/6 mice were injected subcutaneously with $1x10^6$ cells. Tumor volume was monitored twice a week during 2-3 weeks, n=5 tumors per group ; ****p<0,001 by 2-way ANOVA.

Moreover, analysis of lymph node metastasis after intra-footpad injection demonstrated a significant reduction of sentinel (popliteal) lymph node metastasis after Emilin1 overexpression **(Fig.26a, b)** and reduction, although not significant, of metastasis in inguinal lymph nodes. These data support the role for Emilin1 not only as *tumour suppressor-like* but also as lymph node *metastasis suppressor-like* in mouse melanoma when overexpressed in cells.

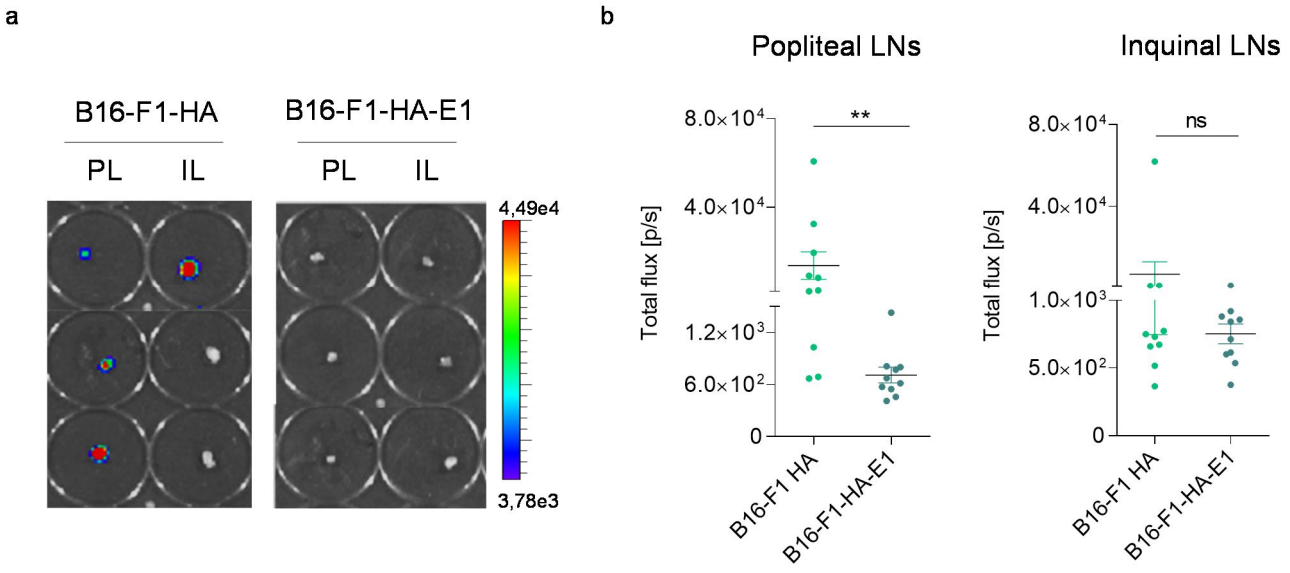

Fig.26 (a) Analysis by *in vivo* Imaging System (IVIS) of popliteal and inguinal lateral lymph nodes from intrafootpad injected mice with 200.000 B16-F1-HA and B16-F1-HA-E1 cells. **(b)** Total flux quantification of popliteal and inguinal lymph node, n=10 **p<0,05 by Nonparametric t-test

5.3.2.2. Analysis of tumour growth and metastasis in B16-F1R2 and B16-F1R2-E1-R914W models: subcutaneous and intrafootpad injection

Finally, we also analysed the effect of the overexpression of an Emilin1 stabilization mutant (E1-R914W) [115, 129] in B16-F1R2 cells and analysed its effect in B16-F1R2 primary tumour growth and metastasis. We verified the overexpression R914W mutant in tumours **(Fig.27a)**.

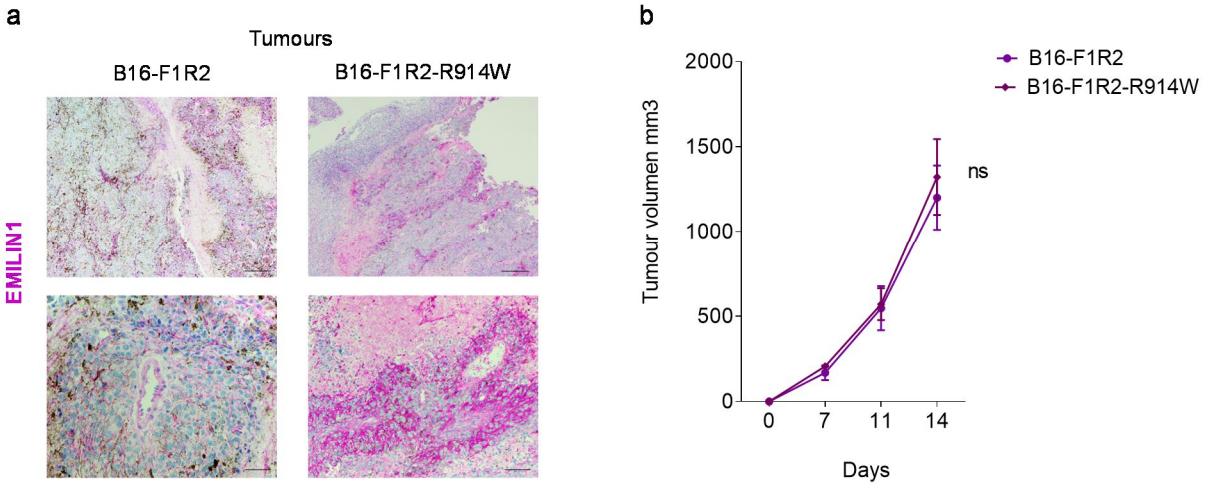

Fig.27 Analysis of the role of EMILIN1 during melanoma progression *in vivo*. Tumour growth of B16-F1R2 and B16-F1R2-R914W xenografts. C57BL/6 mice were injected subcutaneously with 1x106 B16F1-R2 (n=8) and B16F1-R2 R914W (n=10) cells **(a)** Representative B16-F1R2 and B16-F1R2-R914W tumor images, EMILIN1 stained. Scales 500 and 200 µm. **(b)** Tumour volume was monitored twice a week during 2-3 weeks, statistic by 2-way ANOVA.

We observed that Emilin1 mutant (R914W) expression in the cells does not affect tumour growth **(Fig.27b)**. We also analysed the effect in lymph node metastasis by spontaneous lymph node metastasis from flank injected tumours as above and by intra-footpad injection **(Fig.28).** We observed that overexpression of R914W mutant led to a significant reduction of sentinel lymph node metastasis in spontaneous models and, in other lymph nodes (e.g. inguinal) in experimental metastasis assays. These results support that stabilization of Emilin1 reduces lymph node metastasis.

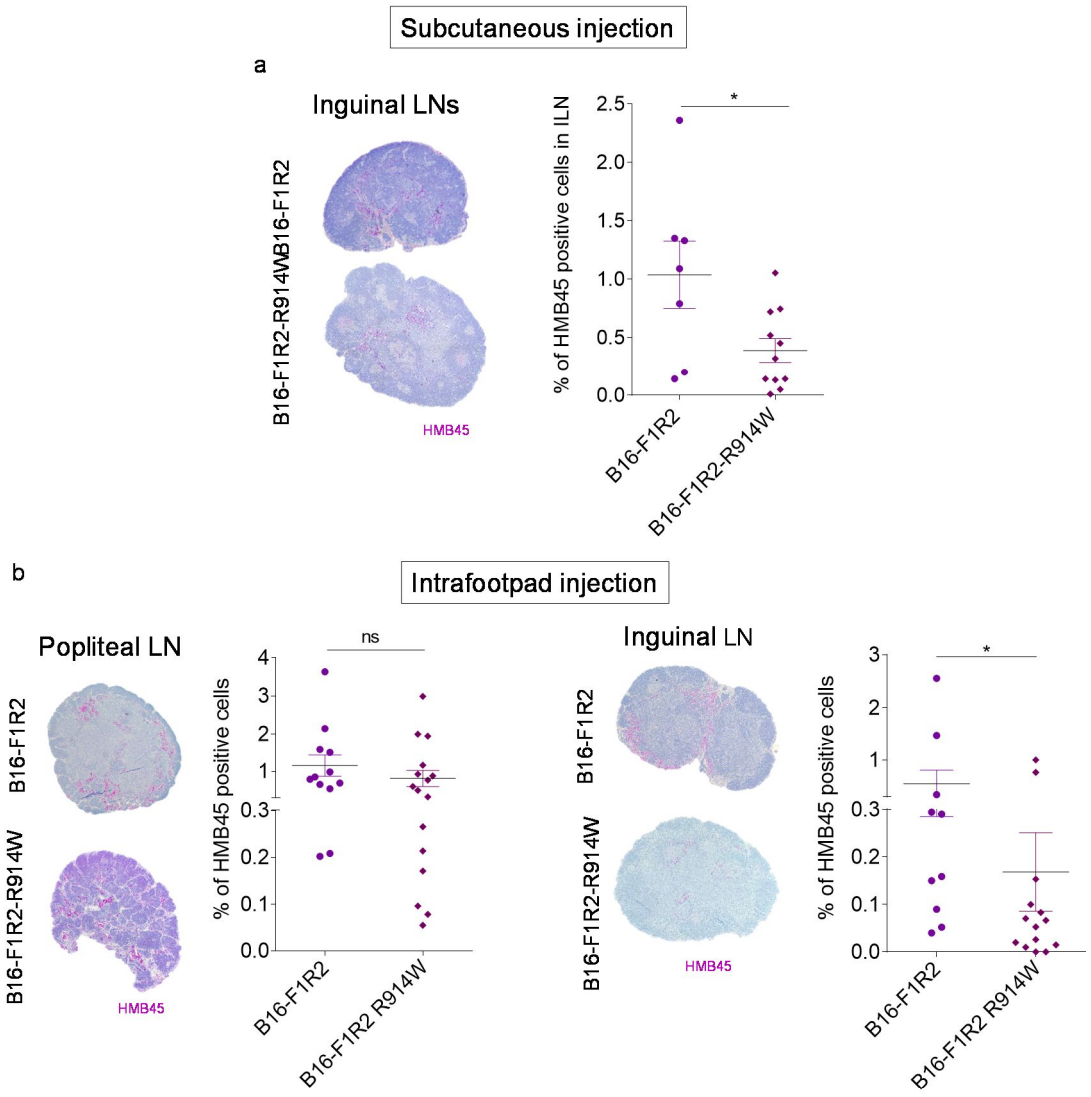

Fig.28 Lymph node metastasis of B16-F1R2and B16-F1R2-R914W xenografts. C57BL/6 mice were injected subcutaneously with 1x106 B16-F1R2 (n=8) and B16-F1R2-R914W (n=10) cells. (a) Representative B16-F1R2 and B16-F1R2-R914W tumor images Emilin1 stained **(b)** Percentage of melanoma HMB45 positive cells quantification from inguinal lymph nodes were used for analyzed lymph node metastasis (B16-F1R2 ,n=7 and B16-F1R2-R914W, n=11) *p<0,05 by Nonparemetric t-test **(c)** Analysis of lymph nodes from C57BL/6 mice injected intrafootpad with 200.000 B16-F1R2 and B16-F1R2-R914W cells. Representative images of popliteal and inguinal lymph nodes (HMB45 staining) from C57BL/6 mice**. (d)** Percentage of Melanoma HMB45 positive cells quantification from popliteal (B16-F1R2 group n=12 and B16-F1R2-R914W group n=16) and inguinal lymph nodes (B16-F1R2 group n=10 and B16-F1R2-R914W group n=14), *p<0,05 by Nonparemetric t-test.

5.3.2.3. Analysis of B16-F1R2-R914W primary tumor growth and metastasis after GW4869 inhibition

Since we observed that treatment with GW4869 reduced significantly tumour growth and metastasis with GW4869 inhibition in mice injected with B16-F1R2 cells **(Fig.14)**, we wanted to see the effect of the treatment in using melanoma cells overexpressing the Emilin1 mutant stable for its degradation (R914W) **(Fig.29a, scheme of the experiment)**. We observed that treatment with GW4869 reduced significantly tumour growth after 16 days in this model **(Fig.29b)**, and reduction of metastasis in the lungs **(Fig.29c,d)**. The levels of metastasis, just due to the presence of EMILIN1 stable protein (R914W), were lower in comparison to the metastasis levels developed by the B16-F1R2 model **(Fig.14).**

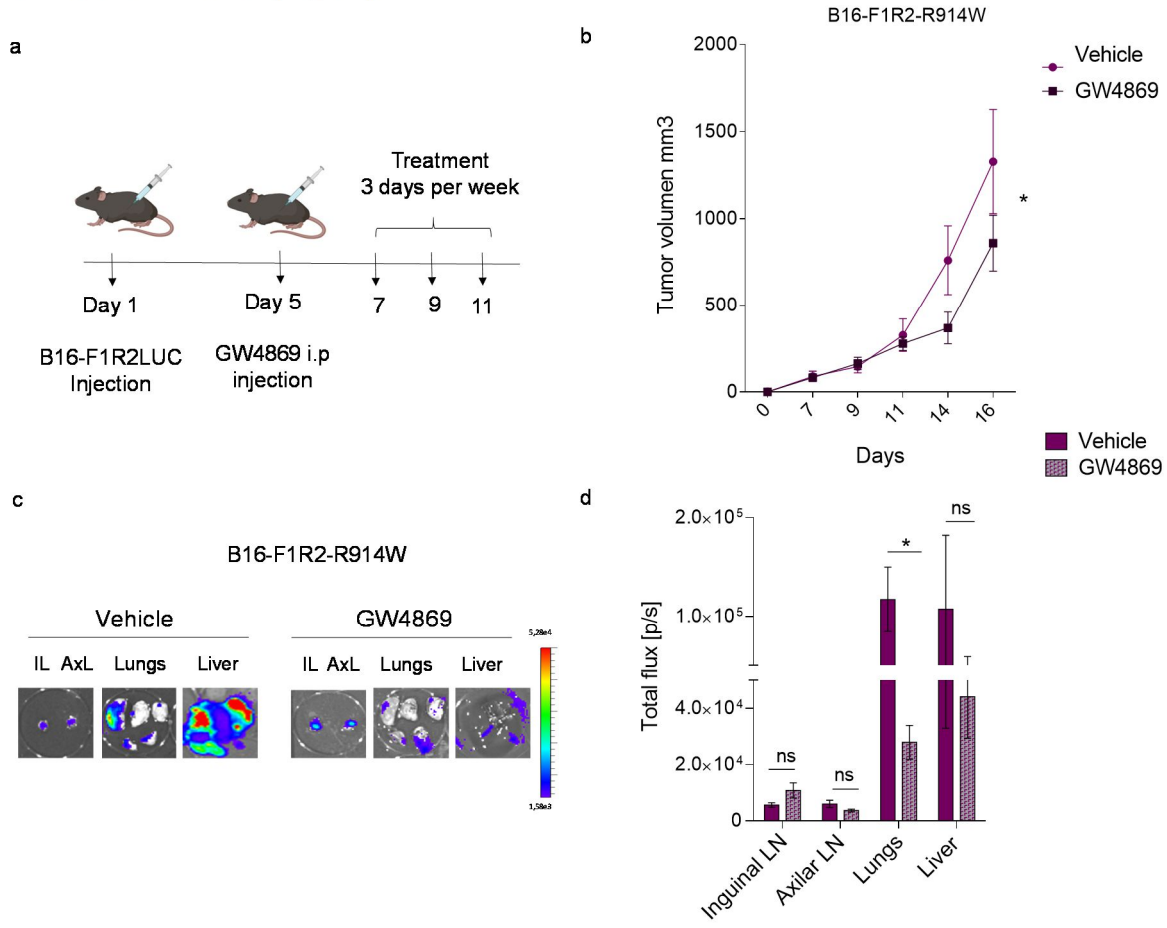

Fig.29 Analysis of the effect of GW4869 B16-F1R2-R914W primary tumour growth and metastasis. (a) Experimental set-up B16-F1R2-R914W-LUC xenografts were injected in C57BL/6 mice subcutaneously with $1x10^6$ cells. Five days later, mice were treated (i.p injection) three times per week with the inhibitor GW4869 (60 µg per mice) and PBS-DMSO as control **(b)** Tumour growth of B16-F1R2-R914W-LUC xenografts in C57BL/6 mice injected subcutaneously with $1x10^6$ cells. Tumor volume was monitored twice a week for 16 days, n=5 tumors per group of control, n=6 tumors per group of treatment;*p<0,001 by 2-way ANNOVA. **(c)** Representative images of the analysis by IVIS of spontaneous metastasis in inguinal (IL) and axillar (AxL) lymph nodes, lungs and liver. **(d)** Total flux quantification of metastatic organs. p-value by Nonparametric t-test.

5.4. Characterization of EMILIN1 in human melanoma

5.4.1. Analysis of EMILIN1 expression in primary tumors and metastatic lessions at mRNA level

To characterize EMILIN1 expression in human melanoma samples, we analysed its expression using the TCGA database that includes data from EMILIN1 expression in 103 primary tumours, 29 lymph node metastasis and 333 distal metastasis. We found that EMILIN1 expression was significantly higher in metastatic tumours and lymph node metastasis at mRNA level **(Fig.30a)** However, we could not find differences in the analysis of primary tumours with different lymph node involvement **(Fig.30b)**

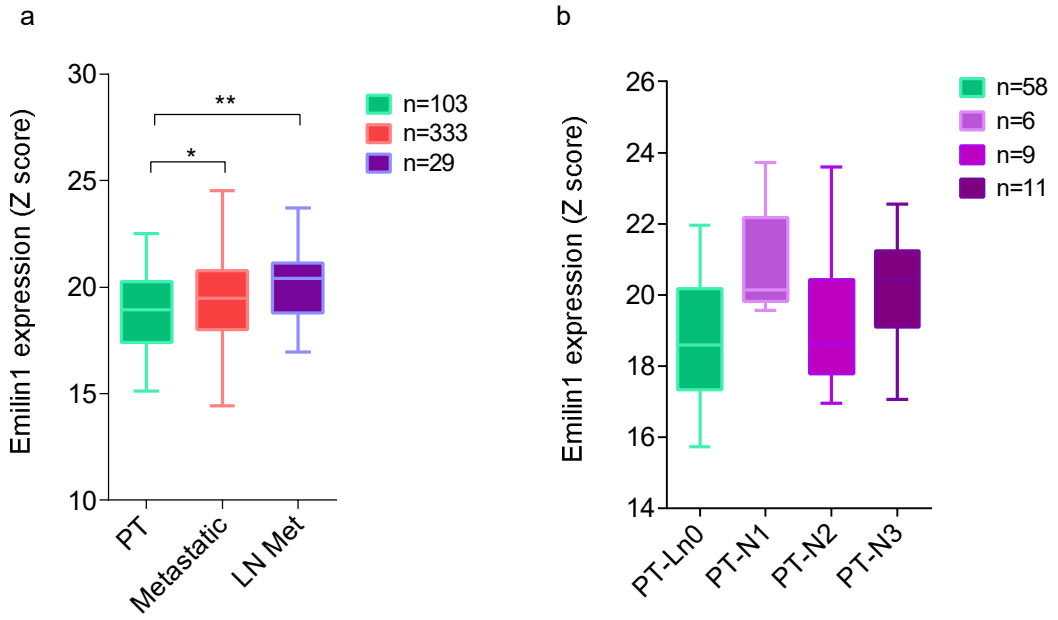

Fig.30 (a) Normalized values of *Emilin1* mRNA levels in primary tumors (PT) and metastatic tumors (Met) and lymph node metastatis (LN met) and **(b)** in primary tumors (PT) and metastatic tumors (Met) with LN involvement according to TCGA melanoma data set= 465 total patients, * $p < 0.05$ according to ANOVA (Kruskal-Wallis test)

5.4.2. Analysis of Emilin1 expression by immunohistochemistry in human samples

Although analysis of the TCGA database gives us relevant information about the expression of EMILIN1 along melanoma progression, it does not allow distinguishing between its expression in tumor and stromal cells. Since Emilin1 has a relevant role both in stromal and tumor cells [97] , we

wanted to analyse more specifically its expression by immunohistochemistry in skin, nevus, primary melanoma and metastatic melanoma human samples. Analysis of EMILIN1 expression showed two different intensities that we defined as high and low **(Fig.31a-d)**.

We next measured the relative percentages of expression of cells expressing low and high levels of EMILIN1. Analysis of expression in a cohort of 9 nevus, 3 primary tumours and 10 metastatic lesions showed that the percentage EMILIN1^{Hi} cells was significantly reduced in distal metastasis to around 20% compared to EMILIN1^{Hi} on primary tumours or nevus high that was around 55% and 40% respectively **(Fig.31a,b)**.

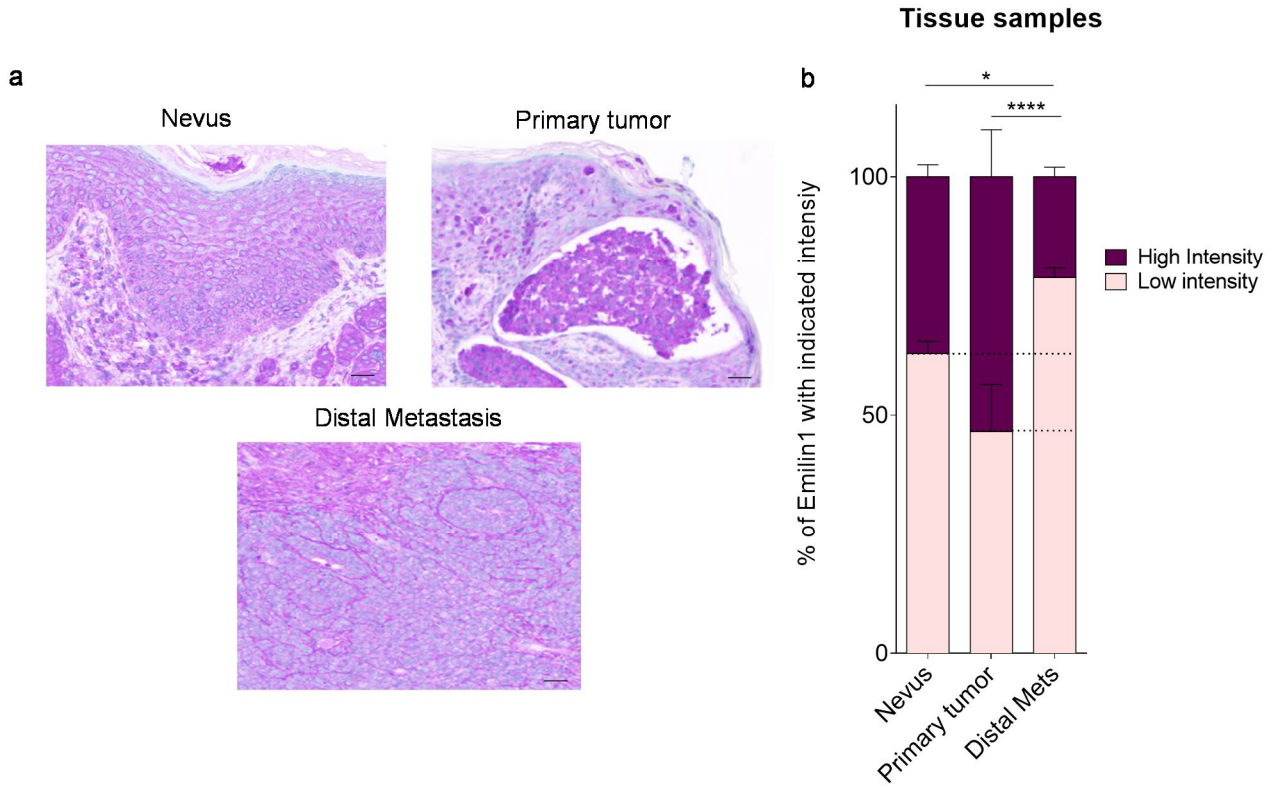

Fig.31 Analysis of Emilin1 expression in human melanomas and metastasis (a) Representative images of nevus, primary melanoma and distal metastasis tissue samples from patients. Scales 40 and 20 μm **(b)** Relative percentage of EMILIN1 expression in human melanoma samples at high and low intensity (n=9 nevus, n=3 primary tumor, n=10 distal metastasis).

Similarly, the analysis of EMILIN1 expression in a another independent cohort formed by 4 skin samples, 9 nevus, 10 primary tumours and 6 lymph node metastasis showed that the percentage of EMILIN1^{Hi} cells was significantly reduced in nevus compared to normal skin from 25% to 15% being around 20% in primary tumour and lymph node metastasis **(Fig.32a,b)**.

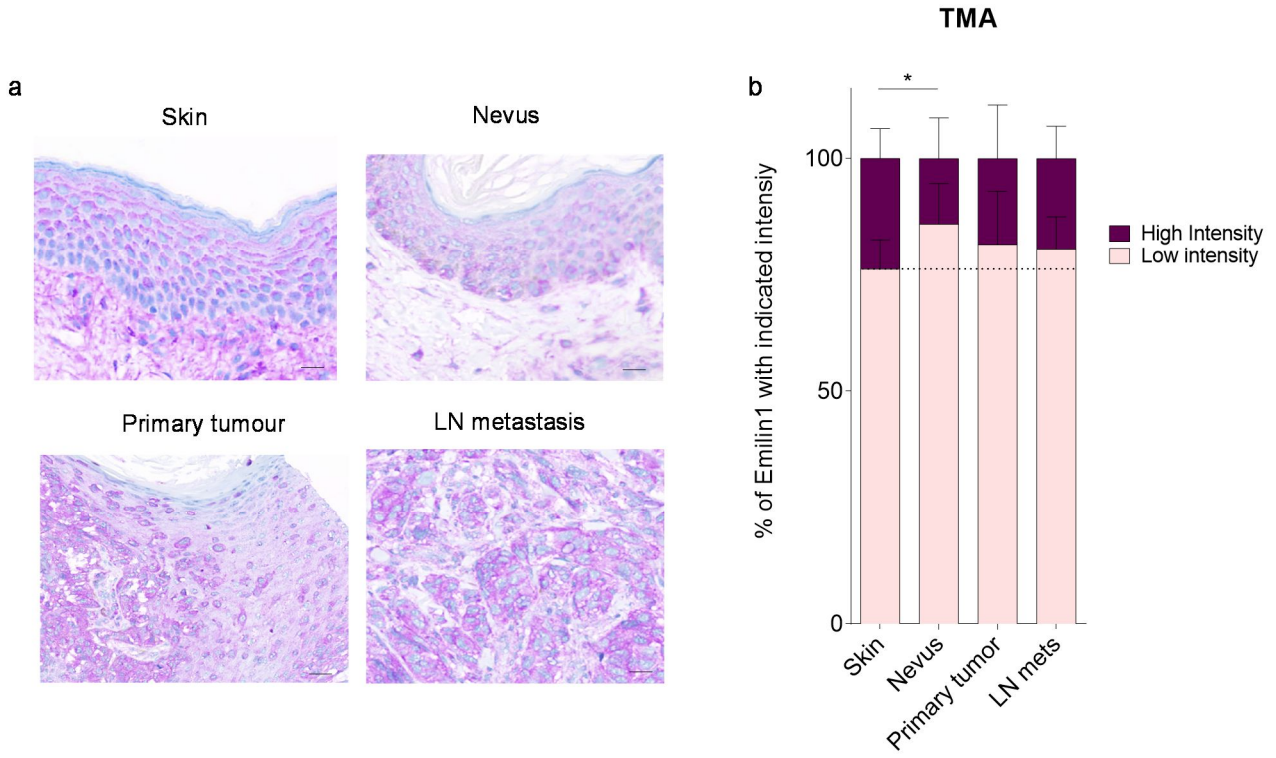

Fig.32 Analysis of Emilin1 expression in human melanomas and metastasis (a) Representative images of skin, nevus, primary melanoma and lymph node metastasis from tissue microarray (TMA) with melanoma samples from patients. Scales 40 μm **(b)** Relative percentage of EMILIN1 expression in human melanoma samples at high and low intensity (n=4 skin, n=9 nevus, n=10 primary tumor, n=6 lymph node metastasis).

Overall, these data suggest that melanoma cells that express high levels of EMILIN1 expression are reduced along tumour progression in human melanoma, however its expression is still observed in all stages. Since this analysis does not allow defining if EMILIN1 expression (either in high or low levels) is functional or degraded, further analyses are needed to define its role in human melanoma.

6. DISCUSSION

During the last years, many studies have demonstrated that EV secretion is a “novel language” of communication between cells actively involved in tumor progression [137]. Data from our laboratory and others support that tumor-derived EVs and, more specifically, exosomes are key players in the formation of pre-metastatic niches at distal sites [14] and metastatic organotropism [32]. Consistent with this, tumor-derived exosomes can reach the sentinel lymph nodes favoring metastatic spread [41, 138, 139]. Indeed, we have recently found that tumour-secreted exosomes are involved in lymph node pre-metastatic niche formation (Garcia-Silva et al. ms. submitted).

It is well known that melanoma and other cancers can induce changes in the microenvironment as lymphangiogenesis in the sentinel lymph nodes [36, 140], the formation of an immunosuppressive environment or/and vascular flow increased [141, 142]. These changes were characterized as processes that contribute to the formation of the PMN in the LNs [140-142], a critical step for metastatic colonization. Nowadays, LN involvement has prognostic significance in melanoma patients [36]. The knowledge of the mechanisms involved in the metastasis of LN, and more importantly, its understanding, is crucial to define the first steps of metastatic spread of melanoma. Importantly, tumor-derived EVs use the lymphatic system to travel to lymph nodes supporting metastasis [41, 138, 139] and lymphangiogenesis [143]. Melanoma-secreted EVs have been described to disseminate via lymphatics and bind subcapsular sinus (SCS) CD169(+)) macrophages in sLNs ensuing enhanced immune responses against cancer cells that tumor growth usually overcome [42]. Recent data from our laboratory demonstrate that tumor-secreted exosomes from high metastatic melanoma cells spread in the lymphatic system [144] (Garcia-Silva et al. ms. submitted). Data support that LECs incorporate tumor-derived exosomes reinforcing lymphangiogenesis and favoring metastasis through specific cargo in exosomes [144] (Garcia-Silva et al. ms. submitted). Moreover, it has been described that tumour cells secrete EVs in the blood stream [25]. Besides plasma, in our laboratory we have recently identified melanoma-secreted EVs in the lymphatic fluid (a.k.a seroma) [144] obtained from the drainage-implanted post-lymphadenectomy as novel surrogate markers of tumor burden [145]. Overall, these data suggest that melanoma-derived EVs use the lymphatic system to spread out favouring lymph node metastasis.

In this thesis we postulated that lymph node microenvironment act as a selective pressure selecting specific phenotypes favored for lymph node metastasis. As such, we wanted to analyze if lymph node metastatic cells present a specific signature that may favor their survival in lymph nodes. For this reason, we have characterized the RNA expression profile and the proteomic signature of secreted exosomes from melanoma lymph node metastatic cell lines.

6.1. Role of melanoma-secreted exosomes in lymph node metastasis

6.1.1. Relevance and biodistribution of exosomes from lymph node metastatic models

It has been previously reported that metastatic melanoma models secrete higher amounts of proteins in exosomes as compared to low metastatic models [30]. In addition, exosome protein concentrations are higher in the plasma and seroma of melanoma subjects with higher stages (III, IV) compared to lower stages (I, II) and subjects without cancer [30, 145]. In agreement with that we observed that exosomes from lymph node metastatic (B16-F1R2) and high metastatic models (B16-F10) secrete higher amounts of protein in the exosomal fraction than poorly metastatic cell line B16-F1. In addition, we observed this behavior in human melanoma lymph node metastatic models. These data suggest that increased protein secretion is an early event observed already in lymph node metastatic models and in stage III melanoma patients [145].

Due to the relevance of exosome secretion in lymph node metastasis we defined the biodistribution *in vivo* of melanoma-derived exosomes through the lymphatic system. It was previously reported that tumor-derived exosomes reach sentinel lymph nodes [41, 139], but never reported using lymph node metastatic models. We observed that melanocyte (melan-a) or low metastatic model (B16-F1)-derived exosomes are mainly detected in the cortical areas of the sentinel lymph node (sLN). However, exosomes derived from the highly metastatic model B16-F10 and the lymph node metastatic model B16-F1R2 was spread out in additional lymph nodes and located in the inner areas of the lymph nodes. Analysis of exosome homing in a short time period showed that B16-F1R2-derived exosomes homed more efficiently in the lymph nodes. All these support that exosome derived from metastatic models have a faster and wider distribution in sentinel lymph nodes in agreement with other results from our laboratory (Garcia-Silva et al. ms. under review).

6.1.2. Lymph node: a selective microenvironment

To investigate if lymph nodes determine the selection of specific phenotypes of melanoma cells, we have characterized the gene expression profile and the proteomic signature associated to exosomes in the lymph node metastatic model B16-F1R2. Previous analysis in this model by

Detmar and colleagues showed that osteopontin was the main protein secreted by tumour cells involved in lymph node lymphangiogenesis [119], however the role of tumour-secreted exosomes has been never analysed.

Analysis of the mRNAs over-expressed in the cells and proteins hyper-secreted in exosomes showed a signature composed by proteins and genes related with extracellular matrix and processes linked to tumour-microenvironment interaction such as ECM-receptor interaction, focal adhesion, laminin interaction and extracellular matrix organization. Among all the proteins observed in the signature, we focused our analysis in Emilin1 due to its relevance in process such as extracellular matrix remodelling, cell adhesion, lymphatic vessel functionality and proliferation [97, 115, 129, 130].

Although LN lymphatic remodeling has been described in pre-clinical tumor models and human cancers [41, 92, 93, 146], an extensive morphological and molecular characterization of this process has been lacking. In a recent study, Detmar and colleagues characterized the expansion of the lymphatic network in tumor-draining LNs over time [66]. Interestingly, Emilin1 was one of the genes hyperexpressed in sentinel lymph nodes in models of melanoma and breast cancer, suggesting the relevance of this protein in lymph node metastasis. Nevertheless, since the analysis was performed at RNA level the authors could not analyze the relevance of this marker of the cell of origin. Therefore, we decided to study the relevance of Emilin1 expression in melanoma cells and its role in lymph node metastasis.

6.2. Defining the role of EMILIN1 in melanoma progression

6.2.1. EMILIN1 secretion and degradation in exosomes, a novel mechanism of inactivation

EMILIN1 has been mainly associated with elastic fibres and microfibrils in blood vessels implicated in elastogenesis and in maintenance of blood and lymphatic vascular cell morphology [103, 104, 147]. *Emilin1(-/-)* mice display elevated systemic blood pressure associated to narrower arteries and defects in lymphatic system [105, 112, 113]. However, it has never been analysed in extracellular vesicles. Our analysis showed for the first time that exosomes derived from the lymph node metastatic model B16-F1R2 were enriched in Emilin1. This fact together with the overexpression at mRNA level suggested that Emilin1 is one of the potential candidates relevant in the survival of B16-F1R2 cells in the lymph node.

Unexpectedly, we found that although Emilin1 was hypersecreted in B16-F1R2-derived exosomes it was degraded and not detected at protein level intracellularly, suggesting somehow that its expression at cellular level was abolished. EMILIN1 accumulation does not acquired the same structural conformation and deposition as in the extracellular matrix of melanocytes. Based on this observation and on the results obtained by Western-blot, in which EMILIN1 was detected in several bands with a lower molecular weight than expected in secreted exosomes, these results therefore suggest a possible degradation and subsequent secretion of EMILIN1 in melanoma progression.

Recently, increasing evidences have started to support other roles of exosomes, not only promoting but also suppressing tumorigenesis. For example, tumor cells have been shown to release exosomes containing tumour antigens that then induce antitumor immune responses representing a promising way of exosome-based tumour vaccine [148-150]. Interestingly, some studies have suggested that expulsion of specific cargo in exosomes may be a way of eliminate tumour suppressor-like cargo (e.g. miRNAs, proteins) from the cell favouring survival of cancer cells [151-153]. So, we wondered if Emilin1 secretion and degradation in exosomes might be a way of eliminate it from melanoma cells as a mechanism involved in melanoma cell survival and metastasis.

Indeed, EMILIN1 has been already described as a *tumour suppressor-like* protein in the microenvironment by its interaction with integrins. For example, it has been shown that the interaction of EMILIN1 in the ECM with the Integrin α4 reduces the activation of the MAPK pathway in epithelial cells [130] or colon cancer models [117]. Also, it has been published that reduction of the interaction between extracellular EMILIN1 with Integrins α4/α9 was accompanied by the activation of PI3K/Akt and Erk1/2 pathways as a result of the reduction of PTEN activity [109]. Another example is that *Ptp4a3* deletion increased the expression of extracellular matrix (ECM) and adhesion genes, including Emilin 1, suggesting again a tumor-supressor like role [154]. Importantly, analysis in *Emilin1* KO showed that its ablation in the microenvironment promoted tumour progression in skin, melanoma and colon cancer models. Similar results were obtained with the E933A EMILIN-1 (E1-E933A) transgenic mouse model, expressing a mutant EMILIN1 unable to interact with α4/α9β1 integrins [117]. These results highlight the important regulatory role of EMILIN1 in the ECM and its interaction with integrins in controlling cell behaviour. However, the intrinsic regulatory mechanisms of Emilin1 protein have been never analysed melanoma. Therefore we decided to focus on: *1) what is the intrinsic role of Emilin1 in melanoma? and 2) what is the extrinsic function of Emilin1 in melanoma-derived exosomes?*

6.2.2. Inhibition of EV secretion accumulate EMILIN1 intracellularly in mouse melanoma cells

Emilin1 degradation is already reported, for example, EMILIN1 degradation by neutrophil elastase (NE) is a specific mechanism leading to the loss of functions disabling its tumor suppressor-like properties [114]. Using a proteomic approaches EMILIN1 has been defined as a potential candidate substrate for MMP-3, -9 and MT1-MMP in the cardiovascular system [155]. However, an exhaustive analysis of EMILIN 1 degradation showed that MMP-3 and MT1-MMP partially cleaved EMILIN1 but without affecting the functional properties, whereas NE was able to fully impair the interaction of gC1q domain with the α4β1 integrin [115]. In the tumor microenvironment, NE is likely secreted by neutrophils, thus impairing its integrity and then its suppressor role. However, more studies are needed to define the specific proteases involved *in vivo* and how they affect metastasis.

In our work we found that EMILIN1 secreted in exosomes is degraded in a similar pattern than previously described [115], however our attempts to inhibit EMILIN1 using NE and MMP inhibitors *in vitro* were unsuccessful (data not shown), suggesting that additional protease activities may be involved in its degradation in melanoma. Defining the Emilin1 "degradome" in melanoma could be crucial to find novel inhibitors that may lead to the reactivation of *tumour suppressor-like* activity *in vivo*.

Since we could not observe an effect by inhibiting the canonical pathways involved in Emilin1 degradation, we decided to test the effect on EMILIN1 expression of 1) the proteasome inhibitor MG-132 and 2) the extracellular vesicle secretion inhibitor GW4869. Out of the two inhibitors, we observed intracellular accumulation of Emilin 1 in B16-F1R2 only after GW4869 treatment. Importantly, we could observe that this treatment does not affect EMILIN1 deposition in the extracellular matrix of the melanocytes. These results suggest that Emilin1 is secreted through extracellular vesicles in melanoma cells and that normal non-tumorigenic cells may use an alternative pathway to deposit Emilin1 in the ECM.

Aberrant secretion, deposition and degradation of ECM components pave the way for invasion of malignant cells, eventually allowing them to reach the vasculature and metastasize [156]. It is still unclear whether physiological deposition of Emilin1 by melanocytes may be affected along melanoma progresion and degradation and secretion in extracellular vesicles might be a pathological pathway involved in metastasis. More studies are needed to define: 1) the mechanisms involved in Emilin 1 secretion by melanocytes, 2) If these mechanisms are affected

along melanoma progression and 3) the impact on tumor microenvironment and metastatic progression.

6.2.3. EMILIN1 impacts negatively on proliferation and migration

The fact that EMILIN1 is lost along melanoma progression, could suggest a potential role as a *tumour suppressor-like* protein. Hence, we studied the intrinsic role of EMILIN1 in melanoma cells by analysing is influence in cell viability and cell cycle assays. EMILIN1 overexpression in B16-F1 cell line reduced cell proliferation. These results are in agreement with published data defining that Emilin1 expression in the ECM reduces cell proliferation in normal and tumour cells [114-116].

Our analysis of cell cycle could not define any effect on it, but rather decrease in cell viability suggesting a metabolic activity. This is the first evidence supporting that overexpression of Emilin1 may lead to metabolic changes in melanoma cells; further analysis is needed to define the specific pathway involved. Other members of the ECM such as Decorin are involved in the internalization of growth factor receptors by endocytosis, which leads to receptor degradation and attenuation of its signaling pathway affecting cancer cell metabolism [157]. It is plausible to speculate that Emilin1 may control the turnover of receptors (e.g. integrins [158], TGFβ-1 receptor [105], importantly related to Emilin1 previously) and regulate indirectly metabolism, nevertheless this hypothesis needs to be tested.

We also analysed the impact of EMILIN1 in cell migration. We observed that cells overexpressing Emilin1 had no directed migration. These data suggest that Emilin1 expression leads to loss of migration directionality. Previous analysis of Emillin1 expression in the skin showed that it locates in the dermis, up to the basement membrane, interacting with components of the extracellular matrix but also with the anchoring complex suggesting an important for cell adhesion, migration, proliferation [159]. Similarly, EMILIN1 promoted cell adhesion and directional haptotaxis (directional cell movement in response to adhesive substrates such as ECM) of trophoblast cells in a gradient-sensitive mechanism [110]. However, in our overexpression models of Emilin1 and stable mutant R914W we could not observe extracellular deposition of Emilin1 being mainly intracellularly. One may think that cells overexpressing Emilin1 are affected in directed migration due to overload on Emilin1 intracelularly affecting the cell migration. Directional cell motility is critical during inflammation, embryogenesis, and cancer metastasis [160-162], therefore defining the role of Emilin1 in this process is worth to study. So far, there is no report of known interacting partners of Emilin1 intracellularly; defining them by specific immunoprecipitation and mass

spectrometry analysis may aid to understand this mechanism. Overall, these data suggest that reduction of Emilin1 levels intracellularly along melanoma progression may aid cells to 1) increased viability 2) effective migration, two of the well-known properties of melanoma cells.

6.2.4. Overexpression of Emilin1 and its secretion in exosomes does not impact on melanoma behaviour

Having in mind that Emilin1 is degraded and secreted in exosomes we wondered what would happen if we overexpress full length Emilin1 in exosomes. We asked these questions: is there any biological explanation on *why melanoma eliminates Emilin1? (besides the intrinsic roles already discussed), Why Emilin1 is not useful in exosomes?.*

EMILIN1 has been described as an important component of the lymphatic perivascular elastic network, lymphatic vessels, as well as in lymphangiogenesis [109, 112, 113, 116]. As previously mentioned, tumor-secreted factors, including exosomes, are key players in lymph node metastasis by influencing and modulating lymphangiogenesis[41, 138, 143, 163-166].

To analyze the role of EMILIN1 in secreted exosomes we overexpressed it in B16-F1 cells, isolated Emilin1-expressing exosomes and injected them in the footpad to analyze their effect in lymphangiogenesis. Importantly, we verified that Emilin1 in exosomes reached sentinel lymph node, after analysis we observed a positive correlation of Emilin1 with Lyve-1 staining althought the increase in lyve-1 staining was not statisticaly significant. We also performed exosome education experiments by conditioning mice with exosomes overexpressing Emilin1 and then analysing tumor cell homing and metastasis. In these experiments, we observed that conditioning mice with exosomes increases melanoma metastasis as previously described in other models [30-32]. However, we could not observe statistical significant differences between B16-F1-derived exosomes or exosomes derived from cells overexpressing Emilin1 (B16-F1-HA-E1)
These results suggest that overexpression of Emilin1 in melanoma derived exosomes, although have a positive influence in lymphangiogenesis and metastasis, it does not offer a significant advantage for B16-F1 cells to metastasize in lymph nodes. Therefore, all these data suggest that EMILIN1 degradation and secretion in exosomes is favouring melanoma progression by 1) inactivating its intrinsic role reducing viability and anti- migratory effects and 2) retaining its metastatic properties **(Fig.1).**

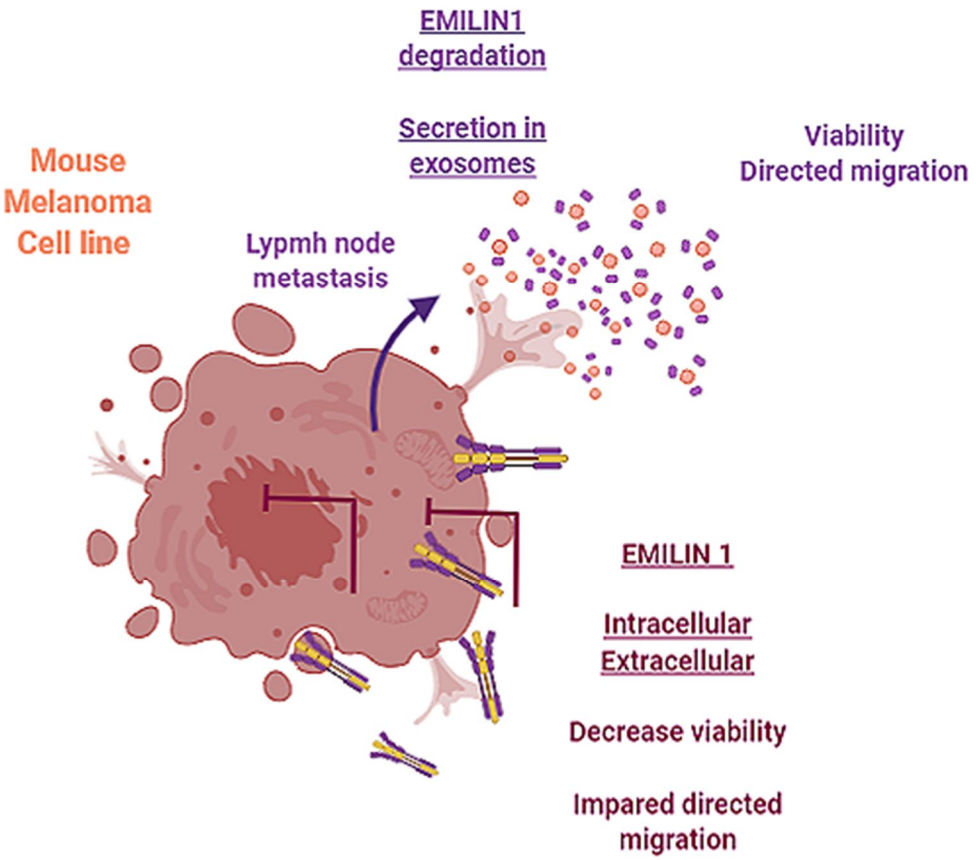

Fig.1 Working model of EMILIN1 in mouse melanoma cell line. EMILIN1 degradation and secretion in exosomes is favouring cell viability, directed migration and enhancing lymph node metastasis.

6.2.5. Emilin1 acts as a *tumour-supressor-like* and *metastasis-supressor like* protein in mouse melanoma models

As previously mentioned, currently Emilin1 is considered as a *tumour-supressor like* protein in skin, cancer and breast cancer [116-118, 143]. Studies with the knock out animal revealed an important role of Emilin1 in the microenvironment to prevent tumour growth and spontaneous metastasis models [117, 143]. Indeed using colitis models, authors showed that *Emilin1* KO mice had increased inflammatory infiltrates, higher colitis scores and more severe mucosal injury respect to the wild type mice [143].

Previous analysis using B16-F10 melanoma models in *Emilin1* KO mice demonstrated that ablation of its expression in the microenvironment favours primary tumour growth and lymph node metastasis [117]. In our analysis we observed a significant reduction in primary tumour growth of

B16-F1R2 tumour cells, however we did not observe any negative impact in lymph node metastasis. This result may be explained because B16-F1R2 cells were isolated from lymph node metastasis [119] and actively degraded and expulsed Emilin1 in exosomes (this thesis); therefore their ability to metastasize in lymph nodes may not be influenced by an *Emilin1* KO microenvironment as compared with B16-F10 that were isolated from lung metastasis. Importantly, we observed a significant decrease in tumour growth with the B16-F1 cells overexpressing Emilin1, suggesting that intrinsic expression of Emilin1 has a similar influence as a *tumour-supressor like* protein as the one observed by the tumour microenvironment. These data support that both intrinsic and extrinsic mechanisms seem to be involved in *tumour-supressor* activity of Emilin1.

On the other hand, experiments with B16-F1R2-R914W mutant cell line, the tumour growth were not influenced in an *Emilin1* KO microenvironment. However, in this model, the effects were observed in lymph node metastasis where we showed a significant decrease. Importantly, analysis of experimental lymph node metastasis after footpad injection showed a significant decrease in both models B16-F1R2-R914W and B16-F1-HA-E1. These data support that besides a *tumour-supressor like* protein, Emilin1 has an important effect reducing lymph node metastasis. Analysis of the main genes affected after Emilin 1 overexpression may be interesting to define the mechanism involved in metastasis suppression.

Moreover, the analysis *in vivo* with the secretome inhibitor GW4869 showed a reduction in primary tumour growth and metastasis. However, in this model we could not rule out the effect of additional factors affected by extracellular vesicle secretion inhibition besides Emilin1. Unfortunately, in this model we could not analyse EMILIN1 levels due to technical issues. An in-deep analysis of EMILIN1 expression after EV inhibition is needed *in vivo* to define its specific role; however it is likely that additional factors are affected. Unfortunately, RNAseq analysis showed a high variability among samples that could not define further pathways involved.

Overall, data support the role of Emilin1 as *tumour suppressor-like* both intrinsically and in the tumour microenvironment. We have defined a novel model of inactivation of Emilin1 by its degradation and secretion in exosomes favouring melanoma proliferation and migration **(Fig.2).** In addition, we observed an important role of Emilin1 as lymph node metastasis *suppressor-like* protein. However there are many questions that remain open, for example *which are the tumour or metastasis suppressor pathways that EMILIN1 influences intrinsically in melanoma? What are the mechanisms of EMILIN1 cleavage and shedding into exosomes? How Emilin1 influences cell proliferation and migration?*

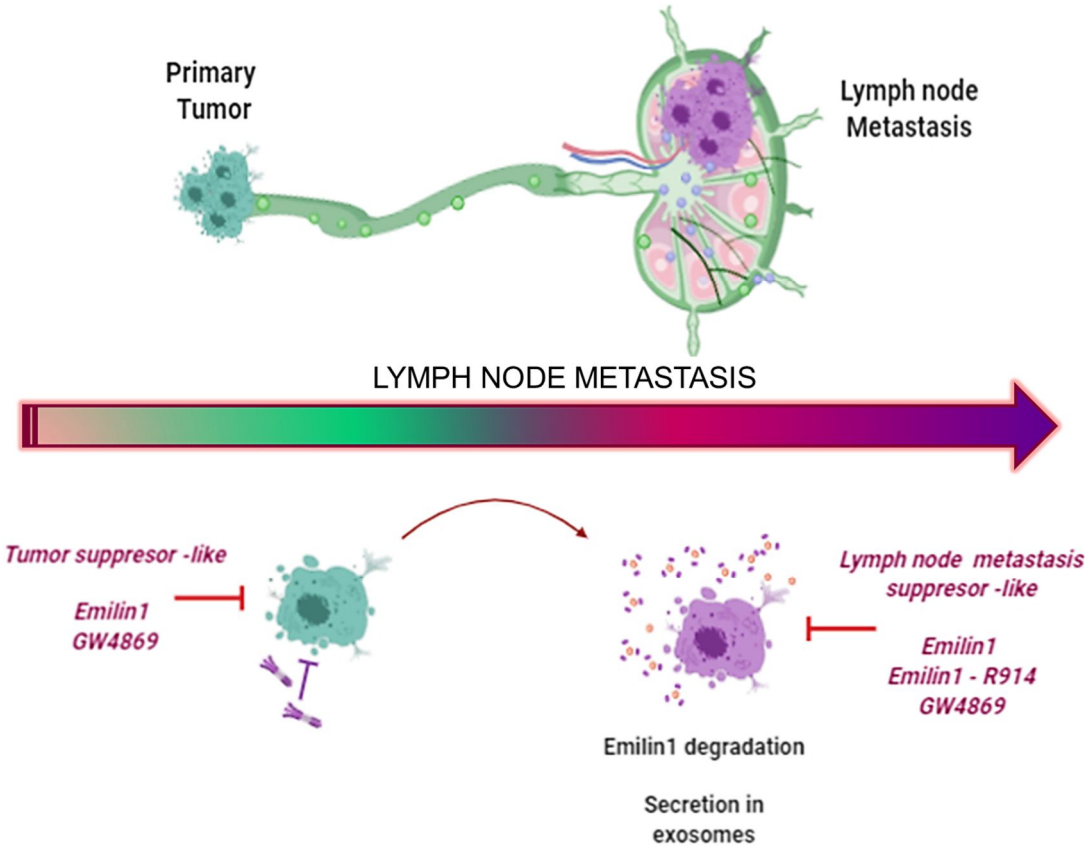

Fig.2 Working model of EMILIN1 along lymph node metastasis. GW4869 inhibition and EMILIN1 or EMILIN1 R914W (stable mutant) levels intracellularly promote not only reduction in primary tumor growth but also in metastasis. Due to that, along lymph node metastasis, EMILIN1 degradation occurs and is secreted in exosomes.

6.2.6. Relevance of EMILIN1 in human melanoma

Currently, there is high controversy about the correlation of EMILIN1 expression with malignancy in human cancer. Studies of EMILIN1 expression in ductal invasive breast cancer carcinoma showed decreased production of Emilin1 mRNA and protein in grade II and III tumours compared to control [118]. The authors found that the suppressive role of EMILIN1 is related to tumor growing, and associated with increased hypoxia, elevated unfolding and degradation of tissue proteins [118]. Similarly, increased expression EMILIN1 among other twelve stromal proteins were associated with low proliferation in non-small cell lung cancer (NSCLC) [167]. These data suggest that decreased production of EMILIN1 in tumors is related with higher proliferation of tumor cells in breast and lung cancer. On the other hand, proteomic analysis identified EMILIN1 overexpressed in osteosarcoma tumours [168]. Similarly, analysis of extracellular matrix proteins in ovarian serous tumours, found that EMILIN1 is overexpressed at mRNA level in comparison with normal ovarian surface epithelium [169].

Our analysis is the first analyzing EMILIN1 expression in human melanoma. The analysis of EMILIN1 expression in the TCGA database showed that *EMILIN1* expression was significantly increased in metastatic tumours and lymph node metastasis at mRNA level, but since EMILIN1 has an important role in the stroma, in this analysis we could not define in which cell type was expressed. To overcome this limitation, we analysed by immunohistochemistry the expression in two independent cohorts of sample. Our data showed that although the total levels of EMILIN1 expression are not affected at protein level, melanoma cells that express high levels of EMILIN1 are reduced significantly in distal metastasis and in nevus compared to skin. Considering the tumour suppressor role previously defined [114, 116, 117, 130] and in this thesis, this may be explained because protein levels are not necessarily related to its functionality in melanoma, a remaining question that needs to be solved. Another explanation could be that a pro- or anti-tumor action could be exerted by EMILIN1 in a tissue-specific manner, as have been described in osteosarcoma [168]. Further analysis determining EMILIN1 stability, degradation and its secretion in circulating exosomes may help in defining these details. Similarly, analysis of EMILIN 1 expression and its correlation with clinical data (e.g mutational status, grade) would be helpful to correlate its expression with outcome, recurrence or response to therapy.

7. CONCLUSIONS

1. Exosomes from metastatic mouse melanoma models (B16-F1R2 and B16-F10) secrete higher amounts of exosomes and protein in the exosomal fraction having a faster and wider distribution in the lymphatic system and lymph nodes than the low metastatic cell line B16-F1.

2. Analysis of gene expression profiles and proteomic cargo in secreted exosomes from B16-F1R2 shown a specific signature of proteins and genes related with extracellular matrix and processes linked to tumour-microenvironment interaction.

3. EMILIN1 is over-expressed and hyper-secreted in exosomes derived from the lymph node metastatic model (B16-F1R2).

4. EMILIN1 is found mostly degraded in exosomes from B16-F1R2 being absent intracellularly. Treatment with GW4869 promote EMILIN1 accumulation in B16-F1R2 reducing primary tumor growth and metastasis *in vivo*.

5. Overexpression EMILIN1 in B16-F1 cells reduce cell viability affecting metabolic balance, does not affect cell cycle and impairs directed migration in melanoma cells.

6. Footpad injection with B16-F1-derived exosomes overexpressing EMILIN 1 correlates positively with lymphangiogenesis and metastasis but does not significantly differ from B16-F1-derived exosomes.

7. Tumour growth of B16-F1R2 is reduced in *Emilin1* knock out animals while lymph node metastases are not affected.

8. Over expression of EMILIN-1 in B16-F1 cells reduces primary tumour growth and lymph node metastasis in experimental metastasis assays.

9. Over expression of EMILIN-1 R914W mutant in B16-F1R2 cells does not affect primary tumour growth but reduces lymph node metastasis in spontaneous and experimental metastasis assay.

10. Analysis of *EMILIN1* expression in TCGA database shows that it is significantly higher in metastatic tumours and lymph node metastasis at mRNA level.

11. Human melanoma tumour cells expressing high levels of EMILIN1 cells are significantly reduced in distal metastasis compared to primary tumour and nevus, and in nevus compared to normal skin in two independent cohorts analysed.

8. CONCLUSIONES

1. Los exosomas derivados de los modelos de melanoma metastásicos de ratón (B16-F1R2 y B16-F10) secretan mayores cantidades de exosomas y proteínas en la fracción exosomal y tienen una distribución más rápida y más amplia en el sistema linfático y ganglios linfáticos, que la línea celular de menor capacidad metastásica B16-F1.

2. El análisis de los perfiles de expresión génica y las proteinas en exosomas secretados por la línea celular B16-F1R2 tienen una firma específica de proteínas y genes relacionados con la matriz extracelular y procesos vinculados a la interacción tumor-microambiente.

3. EMILIN1 está sobreexpresada e hipersecretada en exosomas derivados del modelo metastásico de ganglios linfáticos (B16-F1R2)

4. EMILIN1 se encuentra principalmente degradada en exosomas de B16-F1R2 y no está presente intracelularmente. El tratamiento con GW4869 promueve la acumulación de EMILIN1 en B16-F1R2 reduciendo el crecimiento tumoral primario y la metástasis *in vivo*.

5. La sobre-expresión de EMILIN1 en células B16-F1 reduce la viabilidad celular, viéndose afectado el equilibrio metabólico, y altera la migración dirigida en las células de melanoma, pero no afecta al ciclo celular.

6. La inyección de exosomas derivados de B16-F1 que sobre-expresan EMILIN1 en la almohadilla de la pata promueve se correlaciona positivamente con linfangiogénesis y metástasis, pero no difiere significativamente de la inyección con exosomas derivados de B16-F1.

7. El crecimiento tumoral de la línea celular B16-F1R2 se reduce en los animales KO de *Emilin1*, mientras que las metástasis en los ganglios linfáticos no se ven afectadas.

8. La sobre-expresión de EMILIN1 en células B16-F1 reduce el crecimiento del tumor primario y la metástasis en los ganglios linfáticos en ensayos experimentales de metástasis.

9. La sobre-expresión del mutante EMILIN1 R914W en células B16-F1R2 no afecta al crecimiento primario del tumor, pero reduce la metástasis en los ganglios linfáticos en ensayos de metástasis espontánea y experimental.

10. El análisis de la expresión de EMILIN1 en la base de datos TCGA muestra que es significativamente mayor en tumores metastásicos distales y metástasis a ganglios linfáticos a nivel de ARNm.

11. Las células tumorales de melanoma humano que expresan altos niveles de células EMILIN1 se reducen significativamente en la metástasis distal en comparación con el tumor primario y de los nevus, y en los nevus en comparación con la piel normal en el análisis realizado en dos cohortes independientes.

9. REFERENCES

1. Price, J.E., S.L. Aukerman, and I.J. Fidler, *Evidence that the process of murine melanoma metastasis is sequential and selective and contains stochastic elements.* Cancer Res, 1986. **46**(10): p. 5172-8.
2. Poste, G. and I.J. Fidler, *The pathogenesis of cancer metastasis.* Nature, 1980. **283**(5743): p. 139-46.
3. Talmadge, J.E. and I.J. Fidler, *AACR centennial series: the biology of cancer metastasis: historical perspective.* Cancer Res, 2010. **70**(14): p. 5649-69.
4. Joyce, J.A. and J.W. Pollard, *Microenvironmental regulation of metastasis.* Nat Rev Cancer, 2009. **9**(4): p. 239-52.
5. Poltavets, V., et al., *The Role of the Extracellular Matrix and Its Molecular and Cellular Regulators in Cancer Cell Plasticity.* Front Oncol, 2018. **8**: p. 431.
6. Condeelis, J. and J.E. Segall, *Intravital imaging of cell movement in tumours.* Nat Rev Cancer, 2003. **3**(12): p. 921-30.
7. Wyckoff, J., et al., *A paracrine loop between tumor cells and macrophages is required for tumor cell migration in mammary tumors.* Cancer Res, 2004. **64**(19): p. 7022-9.
8. Wong, S.Y. and R.O. Hynes, *Lymphatic or hematogenous dissemination: how does a metastatic tumor cell decide?* Cell Cycle, 2006. **5**(8): p. 812-7.
9. Chiang, S.P., R.M. Cabrera, and J.E. Segall, *Tumor cell intravasation.* Am J Physiol Cell Physiol, 2016. **311**(1): p. C1-C14.
10. Gupta, G.P. and J. Massague, *Platelets and metastasis revisited: a novel fatty link.* J Clin Invest, 2004. **114**(12): p. 1691-3.
11. Massague, J. and A.C. Obenauf, *Metastatic colonization by circulating tumour cells.* Nature, 2016. **529**(7586): p. 298-306.
12. Paget, S., *The distribution of secondary growths in cancer of the breast. 1889.* Cancer Metastasis Rev, 1989. **8**(2): p. 98-101.
13. Langley, R.R. and I.J. Fidler, *Tumor cell-organ microenvironment interactions in the pathogenesis of cancer metastasis.* Endocr Rev, 2007. **28**(3): p. 297-321.
14. Peinado, H., et al., *Pre-metastatic niches: organ-specific homes for metastases.* Nat Rev Cancer, 2017. **17**(5): p. 302-317.
15. Kaplan, R.N., et al., *VEGFR1-positive haematopoietic bone marrow progenitors initiate the pre-metastatic niche.* Nature, 2005. **438**(7069): p. 820-7.
16. Peinado, H., S. Lavotshkin, and D. Lyden, *The secreted factors responsible for pre-metastatic niche formation: old sayings and new thoughts.* Semin Cancer Biol, 2011. **21**(2): p. 139-46.
17. Psaila, B. and D. Lyden, *The metastatic niche: adapting the foreign soil.* Nat Rev Cancer, 2009. **9**(4): p. 285-93.
18. Salvador, F., et al., *Lysyl Oxidase-like Protein LOXL2 Promotes Lung Metastasis of Breast Cancer.* Cancer Res, 2017. **77**(21): p. 5846-5859.
19. Wang, D., et al., *CXCL1 Is Critical for Premetastatic Niche Formation and Metastasis in Colorectal Cancer.* Cancer Res, 2017. **77**(13): p. 3655-3665.
20. Fong, M.Y., et al., *Breast-cancer-secreted miR-122 reprograms glucose metabolism in premetastatic niche to promote metastasis.* Nat Cell Biol, 2015. **17**(2): p. 183-94.
21. Gomez, D. and G.K. Owens, *Smooth muscle cell phenotypic switching in atherosclerosis.* Cardiovasc Res, 2012. **95**(2): p. 156-64.
22. Murgai, M., et al., *KLF4-dependent perivascular cell plasticity mediates pre-metastatic niche formation and metastasis.* Nat Med, 2017. **23**(10): p. 1176-1190.
23. Colombo, M., G. Raposo, and C. Thery, *Biogenesis, secretion, and intercellular interactions of exosomes and other extracellular vesicles.* Annu Rev Cell Dev Biol, 2014. **30**: p. 255-89.
24. Lane, R.E., et al., *Extracellular vesicles as circulating cancer biomarkers: opportunities and challenges.* Clin Transl Med, 2018. **7**(1): p. 14.
25. Thery, C., L. Zitvogel, and S. Amigorena, *Exosomes: composition, biogenesis and function.* Nat Rev Immunol, 2002. **2**(8): p. 569-79.

26. Raposo, G. and W. Stoorvogel, *Extracellular vesicles: exosomes, microvesicles, and friends.* J Cell Biol, 2013. **200**(4): p. 373-83.
27. Becker, A., et al., *Extracellular Vesicles in Cancer: Cell-to-Cell Mediators of Metastasis.* Cancer Cell, 2016. **30**(6): p. 836-848.
28. Camussi, G., et al., *Exosomes/microvesicles as a mechanism of cell-to-cell communication.* Kidney Int, 2010. **78**(9): p. 838-48.
29. Jung, T., et al., *CD44v6 dependence of premetastatic niche preparation by exosomes.* Neoplasia, 2009. **11**(10): p. 1093-105.
30. Peinado, H., et al., *Melanoma exosomes educate bone marrow progenitor cells toward a pro-metastatic phenotype through MET.* Nat Med, 2012. **18**(6): p. 883-91.
31. Costa-Silva, B., et al., *Pancreatic cancer exosomes initiate pre-metastatic niche formation in the liver.* Nat Cell Biol, 2015. **17**(6): p. 816-26.
32. Hoshino, A., et al., *Tumour exosome integrins determine organotropic metastasis.* Nature, 2015. **527**(7578): p. 329-35.
33. Zomer, A., et al., *In Vivo imaging reveals extracellular vesicle-mediated phenocopying of metastatic behavior.* Cell, 2015. **161**(5): p. 1046-1057.
34. Jones, D., E.R. Pereira, and T.P. Padera, *Growth and Immune Evasion of Lymph Node Metastasis.* Front Oncol, 2018. **8**: p. 36.
35. Friedl, P. and K. Wolf, *Tumour-cell invasion and migration: diversity and escape mechanisms.* Nat Rev Cancer, 2003. **3**(5): p. 362-74.
36. van Akkooi, A.C., C. Verhoef, and A.M. Eggermont, *Importance of tumor load in the sentinel node in melanoma: clinical dilemmas.* Nat Rev Clin Oncol, 2010. **7**(8): p. 446-54.
37. Karaman, S. and M. Detmar, *Mechanisms of lymphatic metastasis.* J Clin Invest, 2014. **124**(3): p. 922-8.
38. Brown, M., et al., *Lymph node blood vessels provide exit routes for metastatic tumor cell dissemination in mice.* Science, 2018. **359**(6382): p. 1408-1411.
39. Pereira, E.R., et al., *Lymph node metastases can invade local blood vessels, exit the node, and colonize distant organs in mice.* Science, 2018. **359**(6382): p. 1403-1407.
40. Nogues, L., et al., *The influence of tumour-derived extracellular vesicles on local and distal metastatic dissemination.* Mol Aspects Med, 2018. **60**: p. 15-26.
41. Hood, J.L., R.S. San, and S.A. Wickline, *Exosomes released by melanoma cells prepare sentinel lymph nodes for tumor metastasis.* Cancer Res, 2011. **71**(11): p. 3792-801.
42. Pucci, F., et al., *SCS macrophages suppress melanoma by restricting tumor-derived vesicle-B cell interactions.* Science, 2016. **352**(6282): p. 242-6.
43. Matthews, N.H., et al., *Epidemiology of Melanoma*, in *Cutaneous Melanoma: Etiology and Therapy*, W.H. Ward and J.M. Farma, Editors. 2017: Brisbane (AU).
44. Miller, A.J. and M.C. Mihm, Jr., *Melanoma.* N Engl J Med, 2006. **355**(1): p. 51-65.
45. Schadendorf, D., et al., *Melanoma.* Nat Rev Dis Primers, 2015. **1**: p. 15003.
46. Chudnovsky, Y., P.A. Khavari, and A.E. Adams, *Melanoma genetics and the development of rational therapeutics.* J Clin Invest, 2005. **115**(4): p. 813-24.
47. Shain, A.H. and B.C. Bastian, *From melanocytes to melanomas.* Nat Rev Cancer, 2016. **16**(6): p. 345-58.
48. Mort, R.L., I.J. Jackson, and E.E. Patton, *The melanocyte lineage in development and disease.* Development, 2015. **142**(4): p. 620-32.
49. Jimbow, K., et al., *Mitotic activity in non-neoplastic melanocytes in vivo as determined by histochemical, autoradiographic, and electron microscope studies.* J Cell Biol, 1975. **66**(3): p. 663-70.
50. Costin, G.E. and V.J. Hearing, *Human skin pigmentation: melanocytes modulate skin color in response to stress.* FASEB J, 2007. **21**(4): p. 976-94.
51. Matama, T., A.C. Gomes, and A. Cavaco-Paulo, *Hair Coloration by Gene Regulation: Fact or Fiction?* Trends Biotechnol, 2015. **33**(12): p. 707-711.

52. Bastian, B.C., *The molecular pathology of melanoma: an integrated taxonomy of melanocytic neoplasia.* Annu Rev Pathol, 2014. **9**: p. 239-71.
53. Fedorenko, I.V., G.T. Gibney, and K.S. Smalley, *NRAS mutant melanoma: biological behavior and future strategies for therapeutic management.* Oncogene, 2013. **32**(25): p. 3009-18.
54. Ilieva, K.M., et al., *Effects of BRAF mutations and BRAF inhibition on immune responses to melanoma.* Mol Cancer Ther, 2014. **13**(12): p. 2769-83.
55. Kwong, L.N. and L. Chin, *The brothers RAF.* Cell, 2010. **140**(2): p. 180-2.
56. Rinderknecht, M. and M. Detmar, *Tumor lymphangiogenesis and melanoma metastasis.* J Cell Physiol, 2008. **216**(2): p. 347-54.
57. Doeden, K., et al., *Lymphatic invasion in cutaneous melanoma is associated with sentinel lymph node metastasis.* J Cutan Pathol, 2009. **36**(7): p. 772-80.
58. Dadras, S.S., et al., *Tumor lymphangiogenesis: a novel prognostic indicator for cutaneous melanoma metastasis and survival.* Am J Pathol, 2003. **162**(6): p. 1951-60.
59. Ji, R.C., *Lymph Nodes and Cancer Metastasis: New Perspectives on the Role of Intranodal Lymphatic Sinuses.* Int J Mol Sci, 2016. **18**(1).
60. Stacker, S.A., et al., *Lymphangiogenesis and lymphatic vessel remodelling in cancer.* Nat Rev Cancer, 2014. **14**(3): p. 159-72.
61. Garnier, L., A.O. Gkountidi, and S. Hugues, *Tumor-Associated Lymphatic Vessel Features and Immunomodulatory Functions.* Front Immunol, 2019. **10**: p. 720.
62. Shayan, R., et al., *Tumor location and nature of lymphatic vessels are key determinants of cancer metastasis.* Clin Exp Metastasis, 2013. **30**(3): p. 345-56.
63. Olmeda, D., et al., *Whole-body imaging of lymphovascular niches identifies pre-metastatic roles of midkine.* Nature, 2017. **546**(7660): p. 676-680.
64. Walker, C., E. Mojares, and A. Del Rio Hernandez, *Role of Extracellular Matrix in Development and Cancer Progression.* Int J Mol Sci, 2018. **19**(10).
65. Sceneay, J., M.J. Smyth, and A. Moller, *The pre-metastatic niche: finding common ground.* Cancer Metastasis Rev, 2013. **32**(3-4): p. 449-64.
66. Commerford, C.D., et al., *Mechanisms of Tumor-Induced Lymphovascular Niche Formation in Draining Lymph Nodes.* Cell Rep, 2018. **25**(13): p. 3554-3563 e4.
67. Palaj, J., et al., *Fibrinogen Levels Are Associated with Lymph Node Involvement and Overall Survival in Gastric Cancer Patients.* Anticancer Res, 2018. **38**(2): p. 1097-1104.
68. Adams, G.N., et al., *Colon Cancer Growth and Dissemination Relies upon Thrombin, Stromal PAR-1, and Fibrinogen.* Cancer Res, 2015. **75**(19): p. 4235-43.
69. Palumbo, J.S., et al., *Spontaneous hematogenous and lymphatic metastasis, but not primary tumor growth or angiogenesis, is diminished in fibrinogen-deficient mice.* Cancer Res, 2002. **62**(23): p. 6966-72.
70. Frantz, C., K.M. Stewart, and V.M. Weaver, *The extracellular matrix at a glance.* J Cell Sci, 2010. **123**(Pt 24): p. 4195-200.
71. Ricard-Blum, S., *The collagen family.* Cold Spring Harb Perspect Biol, 2011. **3**(1): p. a004978.
72. Hamaia, S. and R.W. Farndale, *Integrin recognition motifs in the human collagens.* Adv Exp Med Biol, 2014. **819**: p. 127-42.
73. Sudhakar, A., et al., *Human alpha1 type IV collagen NC1 domain exhibits distinct antiangiogenic activity mediated by alpha1beta1 integrin.* J Clin Invest, 2005. **115**(10): p. 2801-10.
74. Wise, S.G. and A.S. Weiss, *Tropoelastin.* Int J Biochem Cell Biol, 2009. **41**(3): p. 494-7.
75. Pankov, R. and K.M. Yamada, *Fibronectin at a glance.* J Cell Sci, 2002. **115**(Pt 20): p. 3861-3.
76. Sottile, J. and J. Chandler, *Fibronectin matrix turnover occurs through a caveolin-1-dependent process.* Mol Biol Cell, 2005. **16**(2): p. 757-68.
77. Huang, W., et al., *Interference of tenascin-C with syndecan-4 binding to fibronectin blocks cell adhesion and stimulates tumor cell proliferation.* Cancer Res, 2001. **61**(23): p. 8586-94.
78. Bonnans, C., J. Chou, and Z. Werb, *Remodelling the extracellular matrix in development and disease.* Nat Rev Mol Cell Biol, 2014. **15**(12): p. 786-801.

79. Mott, J.D. and Z. Werb, *Regulation of matrix biology by matrix metalloproteinases.* Curr Opin Cell Biol, 2004. **16**(5): p. 558-64.
80. Arpino, V., M. Brock, and S.E. Gill, *The role of TIMPs in regulation of extracellular matrix proteolysis.* Matrix Biol, 2015. **44-46**: p. 247-54.
81. Trackman, P.C., *Functional importance of lysyl oxidase family propeptide regions.* J Cell Commun Signal, 2018. **12**(1): p. 45-53.
82. Peinado, H., et al., *A molecular role for lysyl oxidase-like 2 enzyme in snail regulation and tumor progression.* EMBO J, 2005. **24**(19): p. 3446-58.
83. Socovich, A.M. and A. Naba, *The cancer matrisome: From comprehensive characterization to biomarker discovery.* Semin Cell Dev Biol, 2019. **89**: p. 157-166.
84. Aguado, B.A., et al., *Extracellular matrix mediators of metastatic cell colonization characterized using scaffold mimics of the pre-metastatic niche.* Acta Biomater, 2016. **33**: p. 13-24.
85. Oskarsson, T., et al., *Breast cancer cells produce tenascin C as a metastatic niche component to colonize the lungs.* Nat Med, 2011. **17**(7): p. 867-74.
86. Provenzano, P.P., et al., *Collagen density promotes mammary tumor initiation and progression.* BMC Med, 2008. **6**: p. 11.
87. Hoye, A.M. and J.T. Erler, *Structural ECM components in the premetastatic and metastatic niche.* Am J Physiol Cell Physiol, 2016. **310**(11): p. C955-67.
88. Aguado, B.A., et al., *Engineering the pre-metastatic niche.* Nat Biomed Eng, 2017. **1**.
89. Rana, S., K. Malinowska, and M. Zoller, *Exosomal tumor microRNA modulates premetastatic organ cells.* Neoplasia, 2013. **15**(3): p. 281-95.
90. Liu, Y., et al., *Tumor Exosomal RNAs Promote Lung Pre-metastatic Niche Formation by Activating Alveolar Epithelial TLR3 to Recruit Neutrophils.* Cancer Cell, 2016. **30**(2): p. 243-256.
91. Achen, M.G. and S.A. Stacker, *Exit Stage Left: A Tumor Cell's Journey from Lymph Node to Beyond.* Trends Cancer, 2018. **4**(8): p. 519-522.
92. Kanady, J.D., et al., *Connexin37 and Connexin43 deficiencies in mice disrupt lymphatic valve development and result in lymphatic disorders including lymphedema and chylothorax.* Dev Biol, 2011. **354**(2): p. 253-66.
93. Lutter, S., et al., *Smooth muscle-endothelial cell communication activates Reelin signaling and regulates lymphatic vessel formation.* J Cell Biol, 2012. **197**(6): p. 837-49.
94. Jurisic, G., et al., *An unexpected role of semaphorin3a-neuropilin-1 signaling in lymphatic vessel maturation and valve formation.* Circ Res, 2012. **111**(4): p. 426-36.
95. Bouvree, K., et al., *Semaphorin3A, Neuropilin-1, and PlexinA1 are required for lymphatic valve formation.* Circ Res, 2012. **111**(4): p. 437-45.
96. James, J.M., A. Nalbandian, and Y.S. Mukouyama, *TGFbeta signaling is required for sprouting lymphangiogenesis during lymphatic network development in the skin.* Development, 2013. **140**(18): p. 3903-14.
97. Colombatti, A., et al., *The EMILIN/Multimerin family.* Front Immunol, 2011. **2**: p. 93.
98. Doliana, R., et al., *EMI, a novel cysteine-rich domain of EMILINs and other extracellular proteins, interacts with the gC1q domains and participates in multimerization.* FEBS Lett, 2000. **484**(2): p. 164-8.
99. Ghai, R., et al., *C1q and its growing family.* Immunobiology, 2007. **212**(4-5): p. 253-66.
100. Tom Tang, Y., et al., *The complete complement of C1q-domain-containing proteins in Homo sapiens.* Genomics, 2005. **86**(1): p. 100-11.
101. Mei, J. and J. Gui, *Bioinformatic identification of genes encoding C1q-domain-containing proteins in zebrafish.* J Genet Genomics, 2008. **35**(1): p. 17-24.
102. Milanetto, M., et al., *Emilin genes are duplicated and dynamically expressed during zebrafish embryonic development.* Dev Dyn, 2008. **237**(1): p. 222-32.
103. Colombatti, A., et al., *Glycoprotein 115, a glycoprotein isolated from chick blood vessels, is widely distributed in connective tissue.* J Cell Biol, 1985. **100**(1): p. 18-26.
104. Colombatti, A., et al., *The EMILIN protein family.* Matrix Biol, 2000. **19**(4): p. 289-301.

105. Zacchigna, L., et al., *Emilin1 links TGF-beta maturation to blood pressure homeostasis.* Cell, 2006. **124**(5): p. 929-42.
106. Hamann, A., et al., *Role of alpha 4-integrins in lymphocyte homing to mucosal tissues in vivo.* J Immunol, 1994. **152**(7): p. 3282-93.
107. Komoriya, A., et al., *The minimal essential sequence for a major cell type-specific adhesion site (CS1) within the alternatively spliced type III connecting segment domain of fibronectin is leucine-aspartic acid-valine.* J Biol Chem, 1991. **266**(23): p. 15075-9.
108. Verdone, G., et al., *The solution structure of EMILIN1 globular C1q domain reveals a disordered insertion necessary for interaction with the alpha4beta1 integrin.* J Biol Chem, 2008. **283**(27): p. 18947-56.
109. Danussi, C., et al., *EMILIN1-alpha4/alpha9 integrin interaction inhibits dermal fibroblast and keratinocyte proliferation.* J Cell Biol, 2011. **195**(1): p. 131-45.
110. Spessotto, P., et al., *EMILIN1 represents a major stromal element determining human trophoblast invasion of the uterine wall.* J Cell Sci, 2006. **119**(Pt 21): p. 4574-84.
111. Danussi, C., et al., *EMILIN1/alpha9beta1 integrin interaction is crucial in lymphatic valve formation and maintenance.* Mol Cell Biol, 2013. **33**(22): p. 4381-94.
112. Danussi, C., et al., *Emilin1 deficiency causes structural and functional defects of lymphatic vasculature.* Mol Cell Biol, 2008. **28**(12): p. 4026-39.
113. Capuano, A., et al., *Integrin binding site within the gC1q domain orchestrates EMILIN-1-induced lymphangiogenesis.* Matrix Biol, 2019. **81**: p. 34-49.
114. Pivetta, E., et al., *Neutrophil elastase-dependent cleavage compromises the tumor suppressor role of EMILIN1.* Matrix Biol, 2014. **34**: p. 22-32.
115. Maiorani, O., et al., *Neutrophil elastase cleavage of the gC1q domain impairs the EMILIN1-alpha4beta1 integrin interaction, cell adhesion and anti-proliferative activity.* Sci Rep, 2017. **7**: p. 39974.
116. Danussi, C., et al., *An EMILIN1-negative microenvironment promotes tumor cell proliferation and lymph node invasion.* Cancer Prev Res (Phila), 2012. **5**(9): p. 1131-43.
117. Capuano, A., et al., *Abrogation of EMILIN1-beta1 integrin interaction promotes experimental colitis and colon carcinogenesis.* Matrix Biol, 2019.
118. Rabajdova, M., et al., *The crucial role of emilin 1 gene expression during progression of tumor growth.* J Cancer Res Clin Oncol, 2016. **142**(11): p. 2397-402.
119. Liersch, R., et al., *Analysis of a novel highly metastatic melanoma cell line identifies osteopontin as a new lymphangiogenic factor.* Int J Oncol, 2012. **41**(4): p. 1455-63.
120. Vizoso, M., et al., *Epigenetic activation of a cryptic TBC1D16 transcript enhances melanoma progression by targeting EGFR.* Nat Med, 2015. **21**(7): p. 741-50.
121. Wisniewski, J.R., et al., *Universal sample preparation method for proteome analysis.* Nat Methods, 2009. **6**(5): p. 359-62.
122. Trapnell, C., et al., *Differential gene and transcript expression analysis of RNA-seq experiments with TopHat and Cufflinks.* Nat Protoc, 2012. **7**(3): p. 562-78.
123. Langmead, B., et al., *Ultrafast and memory-efficient alignment of short DNA sequences to the human genome.* Genome Biol, 2009. **10**(3): p. R25.
124. Li, H., et al., *The Sequence Alignment/Map format and SAMtools.* Bioinformatics, 2009. **25**(16): p. 2078-9.
125. Love, M.I., W. Huber, and S. Anders, *Moderated estimation of fold change and dispersion for RNA-seq data with DESeq2.* Genome Biol, 2014. **15**(12): p. 550.
126. Subramanian, A., et al., *Gene set enrichment analysis: a knowledge-based approach for interpreting genome-wide expression profiles.* Proc Natl Acad Sci U S A, 2005. **102**(43): p. 15545-50.
127. Zanetti, M., et al., *EMILIN-1 deficiency induces elastogenesis and vascular cell defects.* Mol Cell Biol, 2004. **24**(2): p. 638-50.
128. Bindea, G., et al., *ClueGO: a Cytoscape plug-in to decipher functionally grouped gene ontology and pathway annotation networks.* Bioinformatics, 2009. **25**(8): p. 1091-3.

129. Pivetta, E., et al., *Local inhibition of elastase reduces EMILIN1 cleavage reactivating lymphatic vessel function in a mouse lymphoedema model.* Clin Sci (Lond), 2016. **130**(14): p. 1221-36.
130. Modica, T.M.E., et al., *The extracellular matrix protein EMILIN1 silences the RAS-ERK pathway via alpha4beta1 integrin and decreases tumor cell growth.* Oncotarget, 2017. **8**(16): p. 27034-27046.
131. Moro, N., C. Mauch, and P. Zigrino, *Metalloproteinases in melanoma.* Eur J Cell Biol, 2014. **93**(1-2): p. 23-9.
132. Hofmann, U.B., et al., *Matrix metalloproteinases in human melanoma.* J Invest Dermatol, 2000. **115**(3): p. 337-44.
133. Kavanagh, E.L., et al., *Protein and chemotherapy profiling of extracellular vesicles harvested from therapeutic induced senescent triple negative breast cancer cells.* Oncogenesis, 2017. **6**(10): p. e388.
134. Vader, P., X.O. Breakefield, and M.J. Wood, *Extracellular vesicles: emerging targets for cancer therapy.* Trends Mol Med, 2014. **20**(7): p. 385-93.
135. de Groot, A.C., *Kathon CG and cosmetic products.* Contact Dermatitis, 1990. **23**(3): p. 206-7.
136. Schwager, S. and M. Detmar, *Inflammation and Lymphatic Function.* Front Immunol, 2019. **10**: p. 308.
137. Tkach, M. and C. Thery, *Communication by Extracellular Vesicles: Where We Are and Where We Need to Go.* Cell, 2016. **164**(6): p. 1226-1232.
138. Srinivasan, S., F.O. Vannberg, and J.B. Dixon, *Lymphatic transport of exosomes as a rapid route of information dissemination to the lymph node.* Sci Rep, 2016. **6**: p. 24436.
139. Hood, J.L., *The association of exosomes with lymph nodes.* Semin Cell Dev Biol, 2017. **67**: p. 29-38.
140. Sleeman, J.P., *The lymph node pre-metastatic niche.* J Mol Med (Berl), 2015. **93**(11): p. 1173-84.
141. Eccles, S., L. Paon, and J. Sleeman, *Lymphatic metastasis in breast cancer: importance and new insights into cellular and molecular mechanisms.* Clin Exp Metastasis, 2007. **24**(8): p. 619-36.
142. Sleeman, J.P. and N. Cremers, *New concepts in breast cancer metastasis: tumor initiating cells and the microenvironment.* Clin Exp Metastasis, 2007. **24**(8): p. 707-15.
143. Sun, B., et al., *Colorectal cancer exosomes induce lymphatic network remodeling in lymph nodes.* Int J Cancer, 2019. **145**(6): p. 1648-1659.
144. Broggi, M.A.S., et al., *Tumor-associated factors are enriched in lymphatic exudate compared to plasma in metastatic melanoma patients.* J Exp Med, 2019. **216**(5): p. 1091-1107.
145. Garcia-Silva, S., et al., *Use of extracellular vesicles from lymphatic drainage as surrogate markers of melanoma progression and BRAF (V600E) mutation.* J Exp Med, 2019. **216**(5): p. 1061-1070.
146. Achen, M.G. and S.A. Stacker, *Molecular control of lymphatic metastasis.* Ann N Y Acad Sci, 2008. **1131**: p. 225-34.
147. Randell, A. and N. Daneshtalab, *Elastin microfibril interface-located protein 1, transforming growth factor beta, and implications on cardiovascular complications.* J Am Soc Hypertens, 2017. **11**(7): p. 437-448.
148. Yang, Y., et al., *Increased induction of antitumor response by exosomes derived from interleukin-2 gene-modified tumor cells.* J Cancer Res Clin Oncol, 2007. **133**(6): p. 389-99.
149. Wolfers, J., et al., *Tumor-derived exosomes are a source of shared tumor rejection antigens for CTL cross-priming.* Nat Med, 2001. **7**(3): p. 297-303.
150. Lee, E.Y., et al., *Therapeutic effects of autologous tumor-derived nanovesicles on melanoma growth and metastasis.* PLoS One, 2012. **7**(3): p. e33330.
151. Kanlikilicer, P., et al., *Ubiquitous Release of Exosomal Tumor Suppressor miR-6126 from Ovarian Cancer Cells.* Cancer Res, 2016. **76**(24): p. 7194-7207.
152. Dean, I., et al., *The secretion and biological function of tumor suppressor maspin as an exosome cargo protein.* Oncotarget, 2017. **8**(5): p. 8043-8056.
153. Gabriel, K., et al., *Regulation of the tumor suppressor PTEN through exosomes: a diagnostic potential for prostate cancer.* PLoS One, 2013. **8**(7): p. e70047.
154. McQueeney, K.E., et al., *A chemical genetics approach identifies PTP4A3 as a regulator of colon cancer cell adhesion.* FASEB J, 2018. **32**(10): p. 5661-5673.

155. Stegemann, C., et al., *Proteomic identification of matrix metalloproteinase substrates in the human vasculature.* Circ Cardiovasc Genet, 2013. **6**(1): p. 106-17
156. Yuzhalin, A.E., et al., *Dynamic matrisome: ECM remodeling factors licensing cancer progression and metastasis.* Biochim Biophys Acta Rev Cancer, 2018. **1870**(2): p. 207-228.
157. Seidler, D.G., et al., *Decorin protein core inhibits in vivo cancer growth and metabolism by hindering epidermal growth factor receptor function and triggering apoptosis via caspase-3 activation.* J Biol Chem, 2006. **281**(36): p. 26408-18.
158. Capuano, A., et al., *The alpha4beta1/EMILIN1 interaction discloses a novel and unique integrin-ligand type of engagement.* Matrix Biol, 2018. **66**: p. 50-66.
159. Fitoussi, R., et al., *Localization, fate and interactions of Emilin-1 in human skin.* Int J Cosmet Sci, 2019. **41**(2): p. 183-193.
160. Roussos, E.T., J.S. Condeelis, and A. Patsialou, *Chemotaxis in cancer.* Nat Rev Cancer, 2011. **11**(8): p. 573-87.
161. Sung, B.H. and A.M. Weaver, *Exosome secretion promotes chemotaxis of cancer cells.* Cell Adh Migr, 2017. **11**(2): p. 187-195.
162. Jacquemet, G., H. Hamidi, and J. Ivaska, *Filopodia in cell adhesion, 3D migration and cancer cell invasion.* Curr Opin Cell Biol, 2015. **36**: p. 23-31.
163. Zhou, C.F., et al., *Cervical squamous cell carcinoma-secreted exosomal miR-221-3p promotes lymphangiogenesis and lymphatic metastasis by targeting VASH1.* Oncogene, 2019. **38**(8): p. 1256-1268.
164. Li, M., et al., *Horizontal transfer of exosomal CXCR4 promotes murine hepatocarcinoma cell migration, invasion and lymphangiogenesis.* Gene, 2018. **676**: p. 101-109.
165. Carrasco-Ramirez, P., et al., *Podoplanin is a component of extracellular vesicles that reprograms cell-derived exosomal proteins and modulates lymphatic vessel formation.* Oncotarget, 2016. **7**(13): p. 16070-89.
166. Chen, C., et al., *Exosomal long noncoding RNA LNMAT2 promotes lymphatic metastasis in bladder cancer.* J Clin Invest, 2019.
167. Edlund, K., et al., *CD99 is a novel prognostic stromal marker in non-small cell lung cancer.* Int J Cancer, 2012. **131**(10): p. 2264-73.
168. Rao, U.N., et al., *Distinct profiles of oxidative stress-related and matrix proteins in adult bone and soft tissue osteosarcoma and desmoid tumors: a proteomics study.* Hum Pathol, 2013. **44**(5): p. 725-33.
169. Salani, R., et al., *Expression of extracellular matrix proteins in ovarian serous tumors.* Int J Gynecol Pathol, 2007. **26**(2): p. 141-6.

10. APPENDIX

Table 1. Analysis by mass spectrometry of exosomes secreted by mouse cell lines to define exosomal signatures associated to lymph node metastasis.

Gene names	PROT log2 (R2 / F1)	Gene names	PROT log2 (R2 / F1)	Gene names	PROT log2 (R2 / F1)
Casq1	6,81	Gm15800	2,82	Rpl4	2,27
Clu	6,76	Mbp	2,79	Ubash3b	2,26
Acsbg1	6,20	Rpl17	2,79	Arhgdib	2,26
Dip2b	5,63	Rplp1	2,78	Rpl5	2,26
Rpl32	4,97	Dlst	2,75	Apaf1	2,26
Hist1h1c	4,69	Tinagl1	2,73	Rpl13a	2,25
Cd37	4,65	Anxa11	2,72	Rpl18a	2,25
Mitd1	4,30	Xylt1	2,69	Dstn	2,24
Chmp1b1	4,25	Taok1	2,68	Prpf8	2,24
Asb2	4,20	Mybbp1a	2,66	Fmnl2	2,23
Gdf15	4,14	Gns	2,64	Capn7	2,23
Emilin1	4,00	Capn6	2,63	Rps24	2,22
Mdk	3,88	Rpl21	2,60	Rpl18	2,18
Rps27a	3,85	*Agrn*	2,60	Rpl24	2,18
Hic2	3,80	Fam129a	2,59	Ist1	2,17
Cpne2	3,78	Rpl36	2,58	Dip2b	2,17
Pef1	3,69	Prkcq	2,53	Ipo4	2,17
Ccdc50	3,65	*Hspg2*	2,52	Pfkp	2,16
Rpl30	3,63	Rpl27a	2,52	Anxa7	2,15
Col5a1	3,61	Rpl35a	2,50	Mink1	2,14
Rpl34	3,54	Rpl26	2,47	Aprt	2,13
Fau	3,54	Mcm7	2,46	*Nid1*	2,12
Nid2	3,42	Rpl15	2,45	Map4k4	2,10
Ulbp1	3,34	Rhoc	2,42	Rpl14	2,09
Tnik	3,33	Ulk3	2,41	Cpne3	2,08
Peli1	3,32	Rpl8	2,41	Cnn3	2,07
Hapln1	3,30	Lamb2	2,40	Tubgcp3	2,06
Tubb3	3,28	Rpl13	2,38	Cobll1	2,06
Rps8	3,24	H2afy	2,38	Dip2c	2,05
Icam2	3,20	Eef1d	2,37	Naalad2	2,03
Spast	3,04	Pcdh1	2,37	Tubb6	2,03
Rap1a	3,01	Rpl7	2,34	Mdh1	2,03
Rps27	2,96	Rpl28	2,34	Akr1b1/3	2,02
Rps6	2,94	Rps11	2,31	Rpl10	2,02
Pdgfrb	2,91	Anxa6	2,31	Nmt1	2,02
Rpl3	2,88	Picalm	2,31	Rpl27	2,01
Rpl19	2,85	Hist1h1e	2,30	Clic4	2,00
Gpc1	2,82	Snf8	2,29	Abcf2	2,00

Table 2. Correlation of proteomic and transcriptomic data.

Gene names	PROT log2 (R2 / F1)	RNA SEQ log2 (R2 / F1)
Clu	6,76	6,02
Acsbg1	6,20	5,62
Mdk	3,88	4,95
Gdf15	4,14	4,39
Hapln1	3,30	4,36
Slc40a1	1,73	4,23
Cd37	4,65	4,17
Slc12a8	1,34	4,12
Icam2	3,20	3,27
Casq1	6,81	3,22
Emilin1	4,00	2,92
Igf2bp3	1,32	2,86
Mbp	2,79	2,54
Slc38a3	1,77	2,49
Col5a1	3,61	2,39
Pdgfrb	2,91	2,24
Glipr2	1,77	2,19
Rab17	1,51	2,13
Crmp1	1,99	2,05